CREWES

CONSORTIUM FOR RESEARCH IN ELASTIC WAVE EXPLORATION SEISMOLOGY

2020 Sponsors Meeting

Online

December 2nd - December 4th

Providing Advanced Seismic Imaging to the Geophysics Community for 32 years

UNIVERSITY OF CALGARY
FACULTY OF SCIENCE
Department of Geoscience

CREWES

Research Report 2020
Volume 32

In this volume…

Report Summaries

For ***Complete Reports*** *and* ***Student Theses*** *please visit:*

https://www.crewes.org

(Sign in/password required)

UNIVERSITY OF CALGARY
FACULTY OF SCIENCE
Department of Geoscience

Notice of Intent to Publish

Please note that the authors of the research in this 32nd Volume of the Abstract Book intend to publish or otherwise publically disseminate their full research papers in the coming calendar year. According to the contracts between the University of Calgary (CREWES) and each Sponsor, the University will make available to the Sponsor a copy of the proposed publication resulting from the CREWES Project prior to submission for publication. In the event that the Sponsor determines that Research Results within the proposed publication contain Sponsor Confidential Information, the Sponsor shall have thirty (30) days to notify the University in writing and the University shall remove Sponsor Confidential information prior to publication. This 30 day period shall be considered to have started at the end of this meeting (December 4, 2020). These full research reports are available on the CREWES website to all Sponsors and their employees.

CREWES in 2020

It is a pleasure and a privilege to welcome you to the 2020 CREWES Annual Sponsors' Meeting and technical review. It has, of course, been a year dominated by the global pandemic, a year marked by uncertainty across almost all of our personal and professional networks, our family, friends, coworkers and colleagues. So, first and foremost my task here is to express, on behalf of our group, the profound hope that you and yours are safe and healthy.

Our team has been impacted by the pandemic in ways familiar to everyone. In early March, a COVID-19 case was reported in the Earth Sciences building on the University of Calgary campus, not far from the main CREWES offices, and the decision was made to send staff and students to work at home for the week. By the end of that week, the world was entering lockdown, and… well, we all know the story. By April, CREWES was setting itself up to carry out our spring/summer semester work in the new at-home format; students, postdocs and faculty were collaborating online, and our weekly research meetings moved to Zoom. One positive feature of this was that the technical presentations could easily be recorded, and those presentations are available to any interested sponsor on our webpage now. By July some degree of relaxation of restrictions was occurring, and with carefully vetted safety plans, we were able to jump in to some of our high-priority laboratory and field work. I hope you'll take the time to read the summaries of the progress in this report.

The stress of isolation has not been negligible. I want to make particular mention of the CREWES postdoctoral fellows and graduate students, many of whom experienced the pandemic living in quite close quarters with roommates, often far from their families. The resilience with which they faced these challenges, progressing their degrees and their research in 2020, is inspiring. I can see the evidence of that throughout these pages, and I believe you'll be able to also.

The year has seen some good news also. I am delighted to report that our application for a Collaborative Research and Development (CRD) grant from the Canadian government was successful, and will, over the course of its 5 year term, bring approximately $1.5 million dollars directly to bear on the science and technology we are carrying out at CREWES. These are matched dollars, and are here for us because, and only because, of your support as industry partners.

In fact, all work at CREWES relies critically on your continued support. We realize all too well how much work you do to keep that support in place, especially in a year like this one. So let me end this introduction with a huge, and heartfelt, thanks. We take the responsibility of living up to that effort extremely serious, and we look forward to continuing to do so into 2021 and beyond.

Calgary, Alberta
December, 2020

Kristopher Innanen
CREWES Director

Table of Contents

* Video Presenter

2020 CREWES Sponsors

Acceleware	Aramco Services Company
CGG	Chevron Corporation
CNOOC International	Devon Energy Corporation
INOVA Geophysical	Petrobras
Petronas Carigali SDN BHD	PTTEP
Sinopec	TGS

Natural Sciences and Engineering Research Council of Canada (NSERC) - Collaborative Research and Development Grant

NSERC CRSNG

Additional funding provided by:

CANADA FIRST RESEARCH EXCELLENCE FUND

CREWES Personnel 2020

LEADERSHIP

Kristopher A. Innanen, Director
Professor, Department of Geoscience, University of Calgary

B.Sc. Physics and Earth Science, 1996, York University
M.Sc. Physics, 1998, York University
Ph.D. Geophysics, 2003, University of British Columbia

- Work Experience: University of Houston

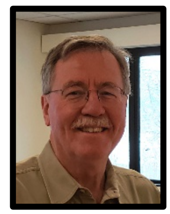

Don C. Lawton, Associate Director
Director for Containment and Monitoring Institute (CaMI)

Faculty Professor, Department of Geoscience, University of Calgary

B.Sc. (Hons. Class I) Geology, 1973, University of Auckland
Ph.D. Geophysics, 1979, University of Auckland

- Work Experience: New Zealand Steel Mining Ltd., Amoco Minerals (N.Z.) Ltd., Carbon Management Canada

Daniel Trad, Associate Director
Associate Professor, Department of Geoscience, University of Calgary

Licenciatura in Geophysics, 1994, Universidad Nacional de San Juan, Argentina
Ph.D Geophysics, 2001, University of British Columbia

- Work Experience: Electromagnetic Methods (Argentina and Brazil), Seismic Research and development (Veritas, CGG, Techco, in Calgary and France)

Michael P. Lamoureux
Professor, Department of Mathematics and Statistics, University of Calgary

Adjunct Professor, Department of Geoscience, University of Calgary

B.Sc. Mathematics, 1982, University of Alberta
M.Sc. Mathematics, 1983, Stanford University
Ph.D. Mathematics, 1988, University of California, Berkeley

- Work Experience: Farallon Computing, NSERC Canada

Kevin W. Hall, Technical Manager

B.Sc. Geophysics, 1992, University of Calgary
M.Sc. Geophysics, 1996, University of Calgary

- Work Experience: Lithoprobe Seismic Processing Facility at the University of Calgary

Gary F. Margrave, Emeritus Director

Emeritus Professor, Faculty Professor, Department of Geoscience, University of Calgary

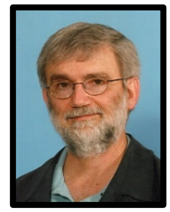

B.Sc. Physics, 1975, University of Utah
M.Sc. Physics, 1977, University of Utah
Ph.D. Geophysics, 1981, University of Alberta

- Work Experience: Chevron Canada Resources, Chevron Geoscience Company, Devon Canada, TGS Canada

RESEARCH STAFF, POST DOCS AND VISITING SCHOLARS

Kevin L. Bertram

Electronics Technician Certificate, 2005, Southern Alberta Institute of Technology
- Work Experience: Aram Systems Ltd.

Malcolm B. Bertram

B.Sc. Geology, Auckland, New Zealand
- Work Experience: GSI (Western Australia), Western Geophysics (Western Australia), Auckland University, University of Calgary

Ali Fathalian

B.Sc. Applied Physics, 2001, University of Razi, Iran
M.Sc. Condensed Matter Physics, 2003, University of Razi, Iran
Ph.D. Condensed Matter Physics, 2007, University of Razi, Iran
Ph.D. Geophysics, 2019, University of Calgary

Marcelo Guarido de Andrade

B.Sc. Physics, 2006, University of São Paulo, Brazil
M.Sc. Geophysics, 2008, University of São Paulo, Brazil
Ph.D. Geophysics, 2017, University of Calgary
- Work Experience: Verdazo Analytics, Schlumberger (Houston), PGS (Rio de Janeiro, Brazil), Orthogonal Geophysics, Husky Energy

David C. Henley

B.Sc. Physics, 1967, Colorado State University
M.Sc. Physics, 1968, University of Michigan
- Work Experience: Shell Oil Co., Shell Canada Ltd.

Helen Isaac

B.Sc. Mathematics, 1973, Imperial College, London
M.Sc. Geophysics, 1974, Imperial College, London
Ph.D. Geophysics, 1996, University of Calgary
- Work Experience: Phillips Petroleum Company, Hudson's Bay Oil and Gas, Canterra Energy, Husky, Fold-Fault Research Project at the University of Calgary

Scott Keating

B.Sc. with Honours in Physics 2014, University of Alberta
Ph.D. Geophysics, 2020, University of Calgary

- Work Experience: CNOOC International

Marie Macquet

B.Sc. Earth Science, 2009, University of Nantes (France)
M.Sc. Planetology, 2011, University of Nantes (France)
Ph.D. Geophysics, 2014, Isterre, University of Grenoble (France)

Joe Wong

B.Sc. Physics/Mathematics, 1971, Queen's University
M.Sc. Applied Geophysics, 1973, University of Toronto
Ph.D. Applied Geophysics, 1979, University of Toronto

- Work Experience: Ontario Ministry of the Environment, University of Toronto, JODEX Applied Geoscience Limited, CREWES

Hongliang Zhang

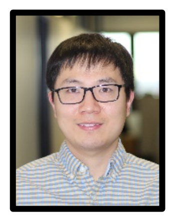

B.Sc. Geophysics, 2010, China University of Geosciences, Wuhan, China
M.Sc. Petroleum Geology, 2013, Peking University, Beijing, China
Ph.D. Geophysics, 2019, University of Calgary

Work Experience: Institute of Geology and Geophysics, Chinese Academy of Sciences, Beijing, China

GRADUATE STUDENTS

Ninoska Amundaray

B.Sc. Geophysical Engineering, 2016, Simon Bolivar University, Venezuela
- Work experience: PDVSA, Venezuela

Farzaneh Bayati

B.Sc. Physics, 2008, University of Science and Technology
M.Sc. Geophysics Exploration, 2012, University of Tehran
- Work experience: Tehran Energy Consultants company (TEC), Tehran, Iran

Matt Eaid

B.Sc. (First Class Honours) Geophysics, 2015, University of Calgary
- Work experience: Shell Canada Ltd., Husky Energy, Chevron Energy Technology Company

Xin Fu

B.Sc. Geophysics, 2015, China University of Petroleum (East China)
M.Sc. Geophysics, 2018, China University of Petroleum(Beijing)

Qi Hu

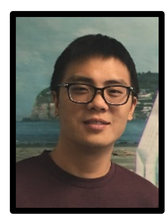

B.Sc. Geophysics, 2011, Yangtze University, Hubei, China
M.Sc. Geophysics, 2014, China University of Petroleum, China
- Work Experience: Sinopec Geophysical Research Institute

Shang Huang

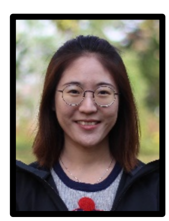

B.Eng. Geophysics, 2017, China University of Petroleum, China
M.Sc. Geophysics, 2018, University of Calgary

Andy Iverson

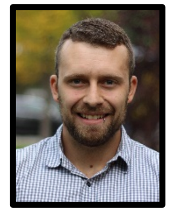

B.Sc. Geophysics (First Class Honours), 2012, University of Calgary

- Work Experience: Apache Canada Ltd, Nexen Energy ULC, Velvet Energy Ltd.

Brendan Kolkman-Quinn

B.Sc. with Honours in Physics, 2009, University of Alberta
B.Sc. Geophysics, 2014, University of Calgary

- Work Experience: ConocoPhillips Canada

Bernie Law

B.Sc. Geological Engineering (Geophysics), 1982, University of Saskatchewan

- Work Experience: Key Seismic Solutions Ltd., Precision Seismic, Veritas Software, SDP

Arthur Lee

B.Sc. in Electrical Engineering (minor in Computer Engineering), 1988, University of Calgary

- Work Experience: Hampson-Russell GeoSoftware CGG Calgary

Da Li

B.Sc. Geophysics, 2012, China University of Geosciences (Beijing)
M.Sc. Geophysics, 2016, China University of Geosciences (Beijing)

He Liu

B.Sc. Prospecting Technology and Engineering, 2012, China University of Petroleum (Beijing)
M.Sc. Geophysics, 2014, China University of Petroleum (Beijing)
Ph.D. Geophysics, 2019, China University of Petroleum (Beijing)

Ellen Liu

B.Sc. Chemical Engineering, 2014, University of Alberta

- Work Experience: ConocoPhillips Canada

Mariana Lume

B.Sc. Geophysical Engineering, 2019, Simon Bolivar University, Venezuela

- Work Experience: PDVSA Intevep

Jorge Monsegny

B.Sc. Computer Science, 2003, National University of Colombia
M.Sc. Mathematics, 2007, National University of Colombia

- Work Experience: Santander Industrial University, Ecopetrol ICP, National University of Colombia

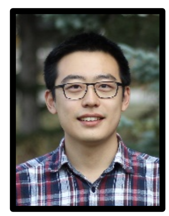

Zhan Niu

B.Sc. Geophysics (First Class Honours with minor in geology), 2017, University of Calgary

- Work Experience: CGG Crawley

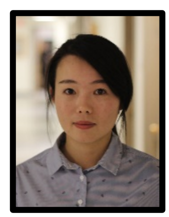

Luping Qu

B.Sc. Geophysics, 2014, China University of Petroleum (East China)
M.Sc. Geophysics, 2017, China University of Petroleum (Beijing)

Ziguang Su

B.Eng. Exploration Geophysics, 2017, China University of Petroleum, China
B.A. English, 2017, China University of Petroleum
M.Sc. Geophysics, 2018, University of Calgary

Ron Weir

B.Sc. Geophysics, 1978, University of Alberta

- Work Experience: Harvest Operations Corp/KNOC

Tianze Zhang

B.Sc. Applied Geophysics, 2015, Jilin University, China
M.Sc. Geological Engineering, 2018, Jilin University, China

Kai Zhuang

B.Sc. Geophysics, 2018, University of Calgary

ASSOCIATED FACULTY and SCIENTISTS

Huaizhen Chen
Research Fellow, Tongji University, Shanghai, China
Adjunct Researcher, CREWES, University of Calgary

Ph.D. Geophysics, 2015, China University of Petroleum
B.Sc. Geophysics, 2010, China University of Petroleum

Andreas Cordsen
Technical Advisor, CREWES, University of Calgary

M.Sc. Geology, 1975, Queen's University, Kingston
M.Sc. Geophysics, 1980, Dalhousie University, Halifax

- Work Experience: BEB, Esso Resources, Norcen Energy, GEDCO, Schlumberger, CHAD Data Ltd.
-

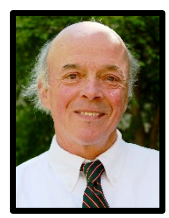

Sam Gray
Technical Advisor, CREWES, University of Calgary

B.S. Math, 1970, Georgetown University
Ph.D. Math, 1978, University of Denver

- Work experience: U.S. Naval Research Lab, General Motors Institute, Amoco, BP, Veritas, CGG

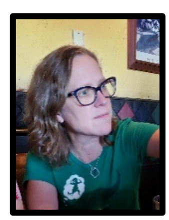

Rachel Lauer
Assistant Professor, University of Calgary

B.Sc. Psychology, Bryn Mawr College
M.Sc. Environmental Engineering Geoscience, Radford University
Ph.D. Geoscience, Pennsylvania State University

- Work Experience: Consultant at NAEVA Geophysics

Faranak Mahmoudian

Technical Advisor, CREWES, University of Calgary

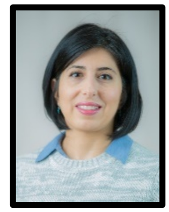

B.Sc. Applied Physics, 2000, K. N. Toosi University of Technology, Iran
M.Sc. Geophysics, 2006, University of Calgary
Ph.D. Geophysics, 2013, University of Calgary

- Work Experience: Shell Canada, Earth Signal Processing

Brian H. Russell

Adjunct Professor, Department of Geoscience, University of Calgary

B.Sc. Physics, 1972, University of Saskatchewan
Honours Certificate in Geophysics, 1975, University of Saskatchewan
M.Sc. Geophysics, 1978, University of Durham
Ph.D. Geophysics, 2004, University of Calgary

- Work Experience: Chevron Geoscience Company, Teknica Resource Development, Veritas Software Ltd., Hampson-Russell Software Ltd, CGG GeoSoftware

Roman Shor

Assistant Professor, Department of Chemical and Petroleum Engineering, University of Calgary

Associate Head (Undergraduate Studies), Department of Chemical and Petroleum Engineering, University of Calgary

B.Sc. Computer Science, 2009, University of Pennsylvania
M.Sc. Computer Science, 2010, University of Pennsylvania
M.Sc. Petroleum Engineering, 2014, University of Texas at Austin
Ph.D. Petroleum Engineering, 2016, University of Texas at Austin

- Work Experience: Shell, Merck, Lehman Brothers

Robert R. Stewart
Cullen Chair in Exploration Geophysics, University of Houston

Adjunct Professor, Department of Geoscience, University of Calgary

B.Sc. Physics and Mathematics, 1978, University of Toronto
Ph.D. Geophysics, 1983, Massachusetts Institute of Technology

- Work Experience: Veritas Software Ltd., Gennix Technology Corp., University of Calgary

Xiucheng Wei
Technical Advisor, CREWES, University of Calgary

B.Sc. Geophysics, 1982, China University of Petroleum
M.Sc. Geophysics, 1992, China University of Petroleum
Ph.D. Geophysics, 1995, China University of Petroleum

- Work Experience: China National Petroleum Company (CNPC), China University of Petroleum (CUP), British Geological Survey (BGS), China Petroleum & Chemical Corporation (Sinopec), International Research Coordinator with the Faculty of Science at the University of Calgary

Matt Yedlin
Associate Professor, Department of Electrical and Computer Engineering, University of British Columbia

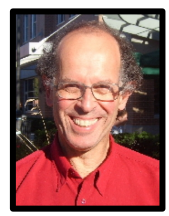

B.Sc. Honours Physics, 1971, University of Alberta
M.Sc. Physiology, 1973, University of Toronto
Ph.D. Geophysics, 1978, University of British Columbia

- Work Experience: Conoco

Student Theses

The following theses were completed with CREWES in 2020:

M.Sc.	Andrew Scott Iverson	Refining the amplitude of inverse scattering series internal multiple predictions
Ph.D.	Scott Douglas Keating	Viscoelastic full-waveform inversion: treating attenuation uncertainty, characterizing cross-talk, and quantifying confidence in inversion results
Ph.D.	Ronald McKenzie Weir	New technologies for unconventional reservoir characterization: Seismic inversion, focal-time estimation, and signal processing to improve reservoir imaging

FWI time-lapse monitoring of CO2 injection using VSP at CaMI FRS: a feasibility study

Ninoska Amundaray*, Kris Innanen, Marie Macquet, and Don Lawton

ABSTRACT

Full waveform inversion (FWI) holds a strong potential for reservoir monitoring due to its proven capabilities to determine high-resolution subsurface models. An expanding branch of reservoir monitoring, seismic time-lapse, aims to image variations in the elastic properties of selected formations due to carbon dioxide (CO_2) storage. Several datasets and technologies are being assessed to verify secured containment of the gas, among others, vertical seismic profiles (VSP). Previous investigations for the Containment and Monitoring Institute Field Research Station (CaMI FRS) suggest changes in the bulk and shear moduli in shallow reservoir for a CO_2 injection program of a maximum 1664 tons. In this paper, we modeled two sensor dispositions with two different source arrangements of VSP, to evaluate the performance of an FWI algorithm at this geological setting. A multiscale approach with nine frequency bands (4-8 Hz, 4-12 Hz, 4-16 Hz, 4-20 Hz, 4-24 Hz, 4-28 Hz, 4-32 Hz, 4-36 Hz and 4-40 Hz) was utilized to evaluate three stages of gas injection from a baseline to a five-year period. Inverted models converged towards the true solution suggested from previous projections. Time-lapse results reproduce a reduction of P-wave velocity for near and far offsets, registering a maximum 17% decrease at reservoir levels. At these depths, model resolution does not appear to be particularly influenced by the amount and distribution of receivers, as much as it is controlled by number of modeled sources.

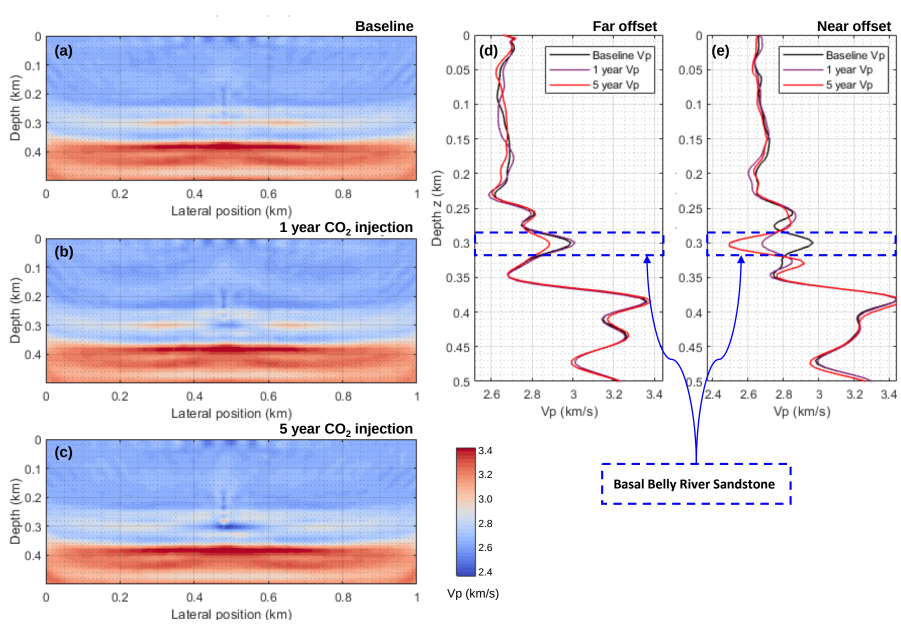

FIG. 1. Inversion results modeled with the permanent VSP experiment design at the FRS with sensors deployed between 190 to 305 m and a source distribution spaced every 60 m. Inverted models at (a) baseline stage, (b) after one year of CO_2 injection, and (c) after five years of CO_2 injection. Comparison of inverted models at reservoir levels for (d) far offset location, and (e) near offset location.

Time domain FWI in Matlab with applications to inversion of simulated VSP data

Ninoska Amundaray and Kris Innanen

ABSTRACT

The optimization function in a full waveform inversion (FWI) iterative scheme is given by the difference between observed and synthetic data. Initial difficulties are traceable to the environment and design of seismic acquisition, which are more complex in land datasets. Recent applications of FWI using vertical seismic profiles (VSP) demonstrate suitable features of these surveys to overcome some inversion challenges. In this report, we analyzed the performance of a standard FWI algorithm with simulated VSP data in Matlab, as a preparatory step to use it with real data. Inverted models converged towards the optimal solution, illustrating how the resolution is controlled by the disposition of sources and receivers in an acquisition survey. Multiscale approaches tested emphasize the usage of frequency bands to reconcile model features with the frequency spectrum of the dataset. Fast convergence of the algorithm is achieved utilizing a reverse time migration (RTM) of the residuals constructed using a crosscorrelation imaging condition, equivalent to the FWI gradient.

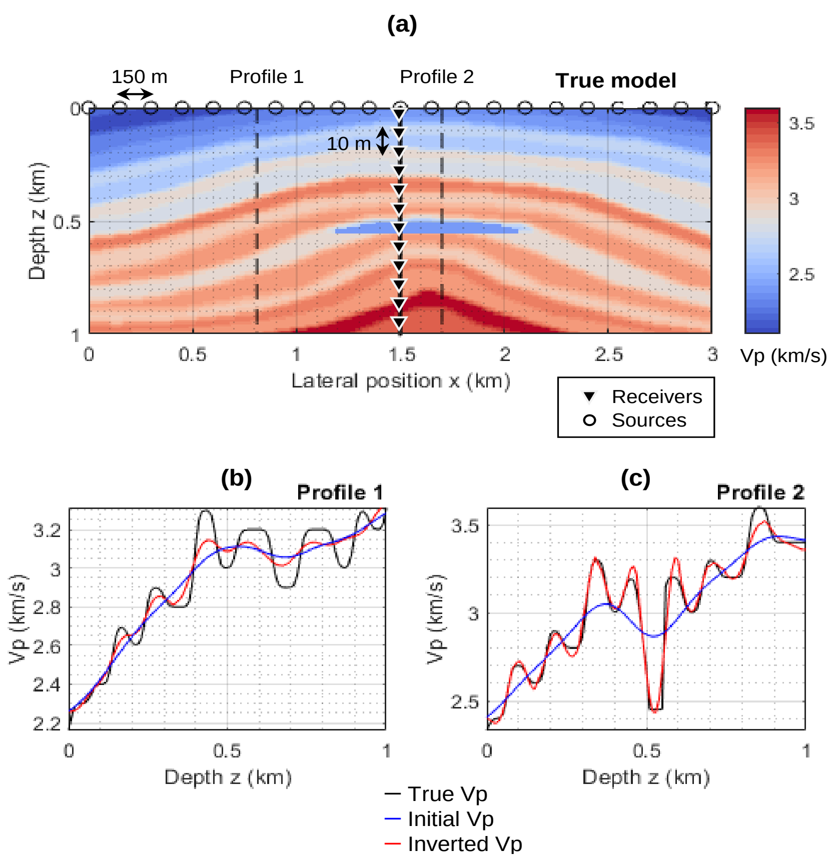

FIG. 1. (a) True P-wave velocity model overlain by the acquisition design for the simulated VSP survey. Comparison of P-wave velocity at (b) profile location 1 distanced 690 m from the receivers, and (c) profile location 2 distanced 200 m from the receivers.

3D data interpolation using adaptive rank reduction method

Farzaneh Bayati and Daniel Trad

ABSTRACT

Seismic data reconstruction is an important step in seismic data processing that affects the whole processing sequence because many tools for noise attenuation or imaging require the input data to be sampled regularly in space to work properly. It is also important for data acquired on difficult terrain with natural or cultural obstacles which may be missing a large portion of the surface shots and receivers. For plane waves or data with small curvatures, the rank reduction method is a very effective signal reconstructing method One of the advantages of rank reduction methods is simultaneous random noise attenuation and data interpolation. One of its limitations, on the other hand, is that it needs to satisfy the plane wave assumption. To satisfy the plane wave assumption the rank reduction methods need to be applied to local windows. Most of the time it is not easy to find the proper window size because it is hard to decide whether the structure in the local window is linear or not. Moreover, it is hard to approximate the rank of each window. Choosing the wrong rank will lead to a failure because the overestimation of rank remains a significant residual and underestimation of it will cause random noise and distort the signal. In this report, we will apply a method that selects rank automatically for each local window, and then apply the method on a global window.

In the adaptive rank reduction method, we want to find the cutoff number that indicates when the contribution from the signal becomes much less than the contribution of the missing traces or random noise. This cutoff number happens at the point where the ratio of two consecutive singular values becomes the largest.

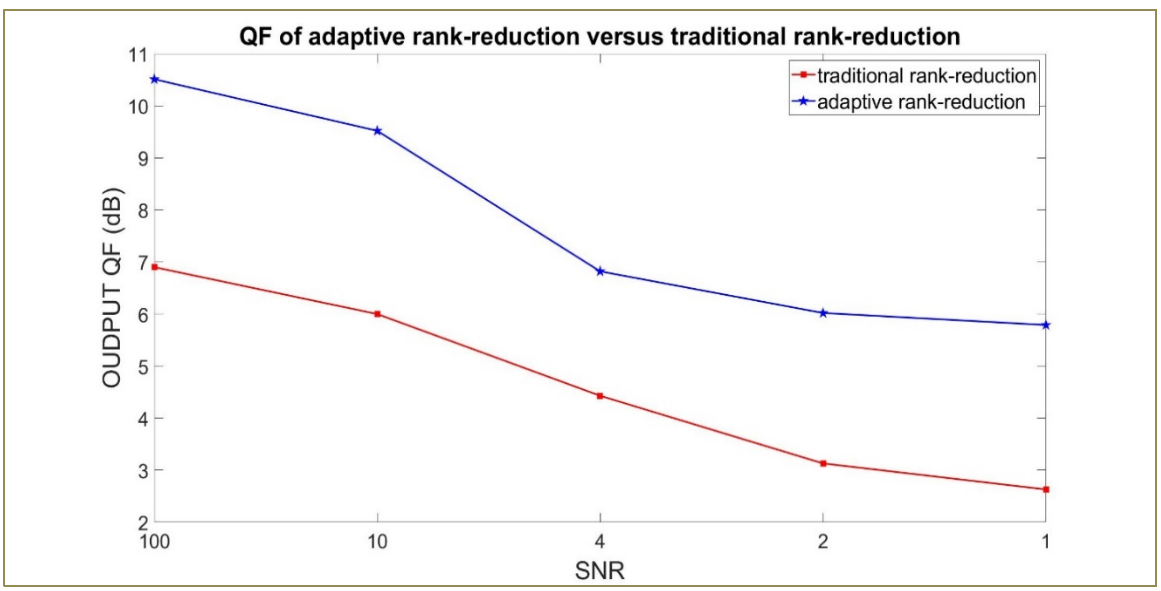

FIG. 1. Comparison of the output quality factor of the adaptive rank-reduction method with the traditional rank-reduction method for a 3D data set with 51% missing traces contaminating with different level of random noise on the global window.

Adaptations for working in the year 2020

Kevin L. Bertram

ABSTRACT

There is no question that the COVID-19 pandemic has changed the day to day lives of everybody. As with the rest of the world, CREWES has had to adapt and change not only how research projects are carried out, but the day to day operations in the office as well. Work must now be carried out in a way that meets the restrictions imposed by the Alberta government and the governing body of the University of Calgary.

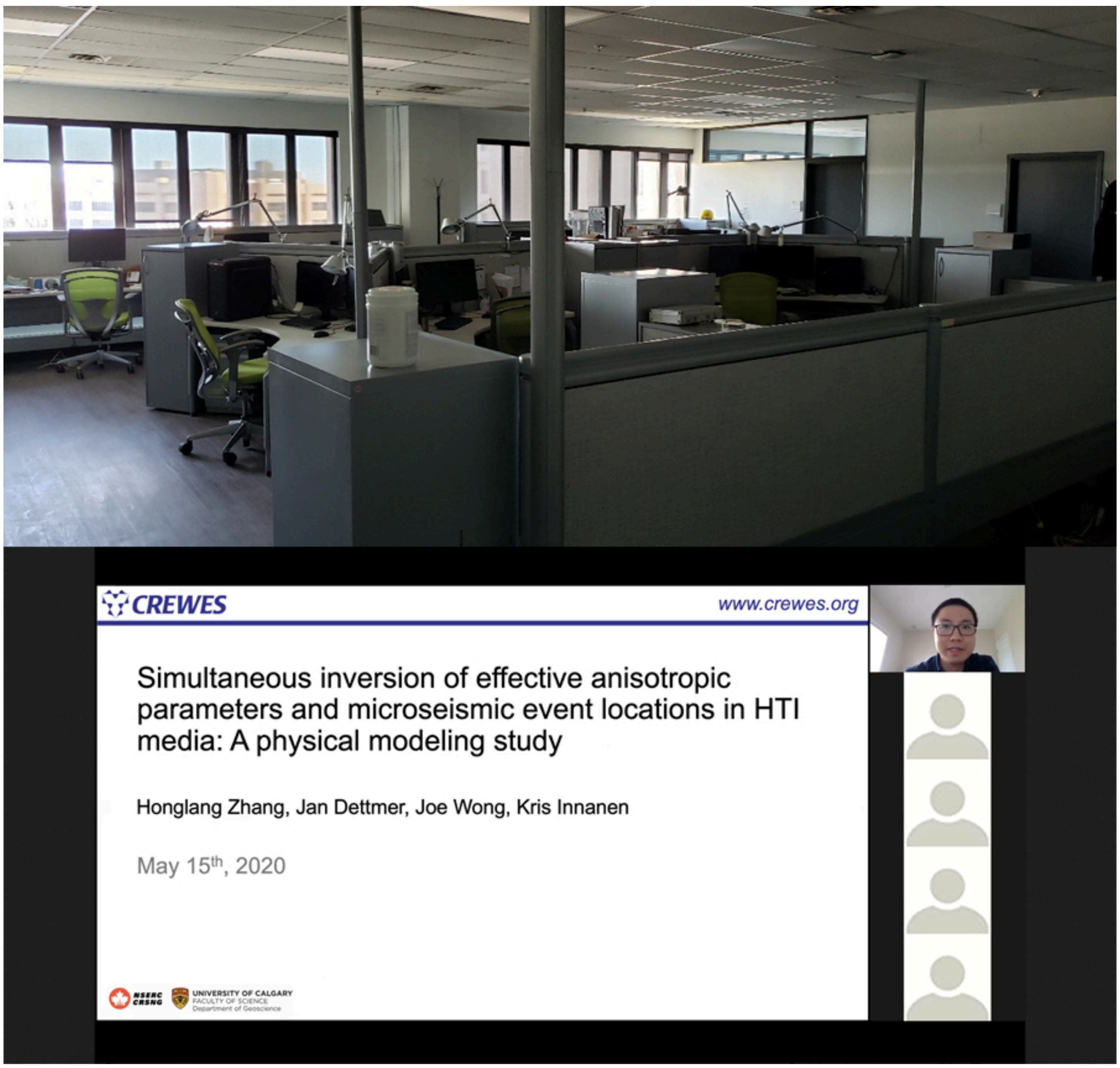

FIG. 1. The CREWES student area on the sixth floor of the Geosciences building remains empty, but weekly meetings and collaboration continues online.

A brief overview of CREWES field work in 2020

Kevin L. Bertram, Thomas Wilson, Kevin W. Hall, Malcolm Bertram, and Rachel Lauer

ABSTRACT

CREWES tries to get as much real-world data from field work as possible. This year is obviously different with the current pandemic restricting travel and keeping people at home. The number of times that CREWES made it to the field has been greatly diminished. CREWES has been involved in only two surveys for a total of three days in the field so far.

The first survey was carried out to provide data for Dr. Rachel Lauer's student Tom Wilson.

The second survey was a repeat of walk away VSP at the CaMI FRS.

FIG. 1. Equipment and data from field surveys conducted by members of CREWES.

Enhanced receiver hardware for physical modeling

Kevin L. Bertram and Joe Wong

ABSTRACT

With the expectation of increasing the amount that the physical modeling system will be used in the coming years there are efforts to improve efficiency and create a more customizable setup. This upgrade will cover both the input and output aspects of the physical modeling system. This report covers upgrades to the number of receiver channels that can be used simultaneously to record data.

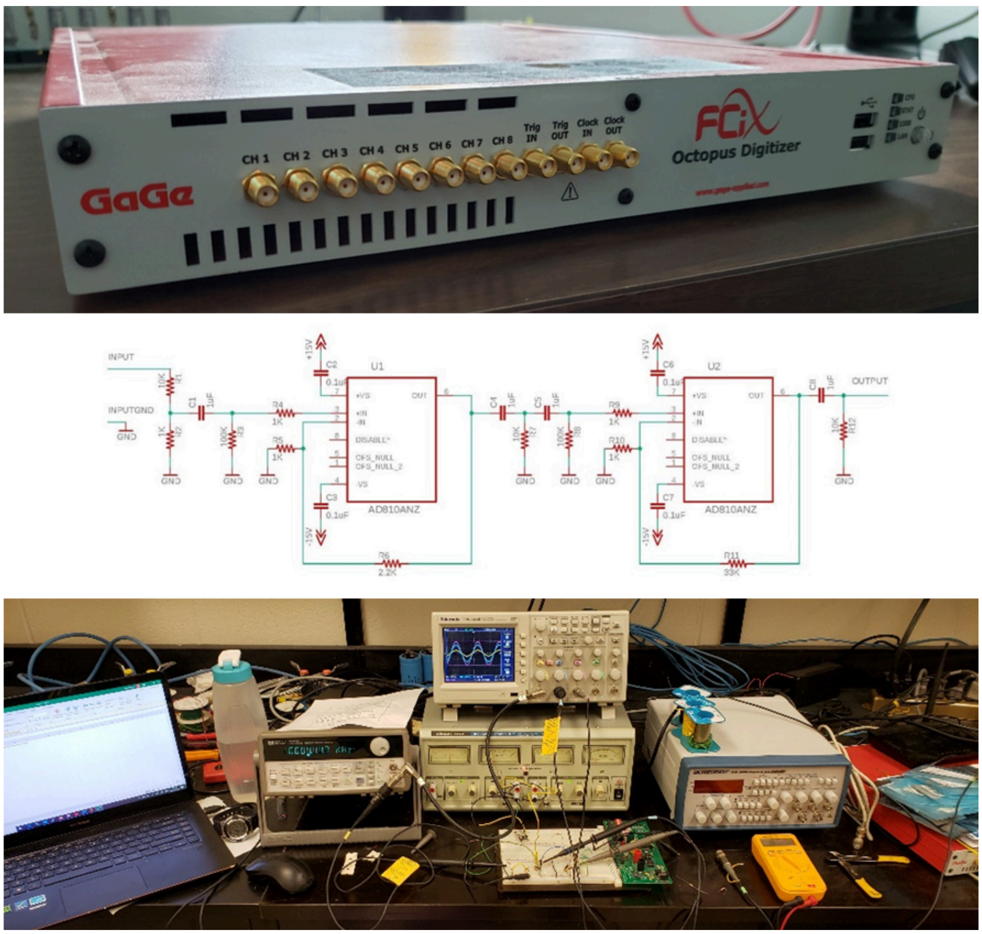

FIG. 1. Testing prototype receiver stages for the physical modeling system.

Azimuthal PP and PS seismic amplitude variation with angle inversion for orthogonal fracture weaknesses

Huaizhen Chen* and Kris Innanen

ABSTRACT

Characterization of fracture connectivity is an important task in detection of fractures in hydrocarbon reservoirs. The current reflection coefficients are mainly derived under the assumption of horizontal or tilted transversely isotropic (HTI or TTI) media for a rock containing a single set of aligned fractures. Driven by an effective model for the case of two sets of orthogonal fractures in an isotropic background, we first express and simplify stiffness parameters in terms of two sets of normal and tangential fracture weaknesses. In the case of a reflection interface separating an isotropic medium and a medium that contains two sets of orthogonal fractures, we present the approximate perturbations in stiffness parameters, which are utilized for the derivation of PP- and PS-wave linearized reflection coefficients. Using the derived PP- and PS-wave reflection coefficients, we establish an inversion approach of joint azimuthal PP- and PS-wave amplitudes variation with incidence angle (AVA) to estimate the normal and tangential fracture weaknesses. In the inversion approach, the least-squares algorithm and Bayesian Markov chain Monte Carlo (MCMC) method are combined, and initial models of fracture weaknesses are built using results of anisotropic AVA gradient. We apply the proposed inversion approach to synthetic seismic data of different signal-to-noise ratios (SNR), and the established inversion approach can provide more accurate normal and tangential fracture weaknesses than the conventional least-squares algorithm even in the case of SNR of 2. Applying the inversion approach to real datasets of PP and PS waves, we obtain reliable results of fracture weaknesses that can match well log curve of velocity and anisotropic AVA gradient, which may provide the possibility to characterize how fractures distribute and to estimate fracture connectivity in hydrocarbon reservoirs.

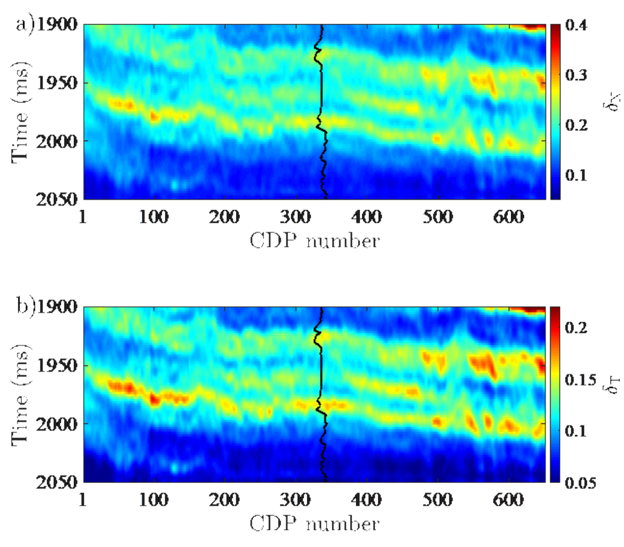

FIG. 1. a) Inversion results of the normal fracture weakness δ_N, and b) Inversion results of the tangential fracture weakness δ_T. The curve is P-wave velocity.

Bayesian inversion of azimuthal seismic amplitude data for indicators of interconnected aligned cracks

Huaizhen Chen and Kris Innanen

ABSTRACT

Detection of natural fractures and identification of infilling fluids in fractures are important objectives in exploration and characterization of unconventional reservoirs (e.g. shale or tight sand reservoirs). In the case of rocks containing interconnected aligned fractures, both anisotropy and attenuation appears in reflected amplitudes of seismic wave. Starting with an effective model of interconnected aligned fractures in an elastic and isotropic background, we first present simplified complex stiffness parameters as a function of attenuation factor 1/Q in an attenuative anisotropic medium, and perturbations in stiffness parameters across an interface separating two attenuative anisotropic media. Using an approximate relationship between reflection coefficient and scattering potentials, we derive a linearized complex PP-wave reflection coefficient in terms of reflectivities of P- and S-wave moduli and density and changes in the tangential fracture weakness δ_T and attenuation factor 1/Q, which provides a possibility to estimate fracture weakness and attenuation factor from reflection amplitudes. Based on the derived reflection coefficient, we propose an inversion approach of employing real and imaginary parts of complex seismic data in frequency domain for estimating unknown parameters following a Bayesian framework. Applying the inversion approach to frequency-dependent synthetic seismic datasets of different incidence and azimuthal angles, we may obtain the inverted tangential fracture weakness that can match the true value, and the attenuation factor can be estimated reliably even though the estimation should be improved at the location of fractured reservoir. Future work should focus on the illustration of stability and robustness of the proposed inversion approach and the verification of reliability of the approach using real datasets.

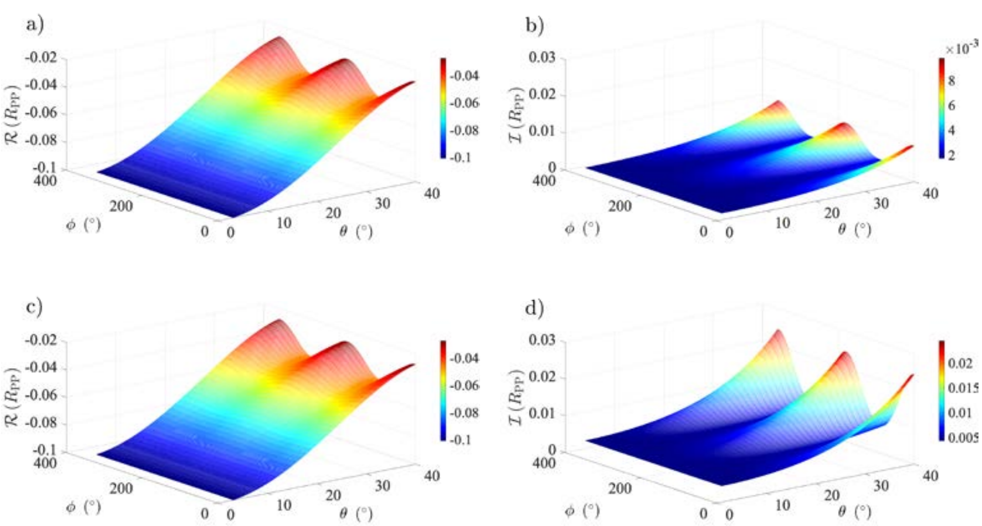

FIG. 1. a) and b) Real and imaginary parts of reflection coefficients of frequency 20 Hz; and c) and d) Real and imaginary parts of reflection coefficient of frequency 50 Hz.

Analytic and finite-difference modeling of DAS fiber data from moment tensor sources

Matthew Eaid and Kris Innanen

ABSTRACT

Distributed acoustic sensing has become a prevalent technology for reservoir monitoring and has potential for applications in earthquake seismology. In preparation for advanced applications of these datasets such as imaging and inversion, we develop two methods for forward modeling DAS datasets generated by moment tensor type sources. The first is an efficient analytic modeling algorithm well-suited to modeling large datasets of DAS-microseismic direct arrivals. Another paper in this issue uses this algorithm for generation of a datasets used as input for a machine learning study for source mechanism estimation. The second method we develop is a full 3D finite-difference method based on the velocity-stress method.

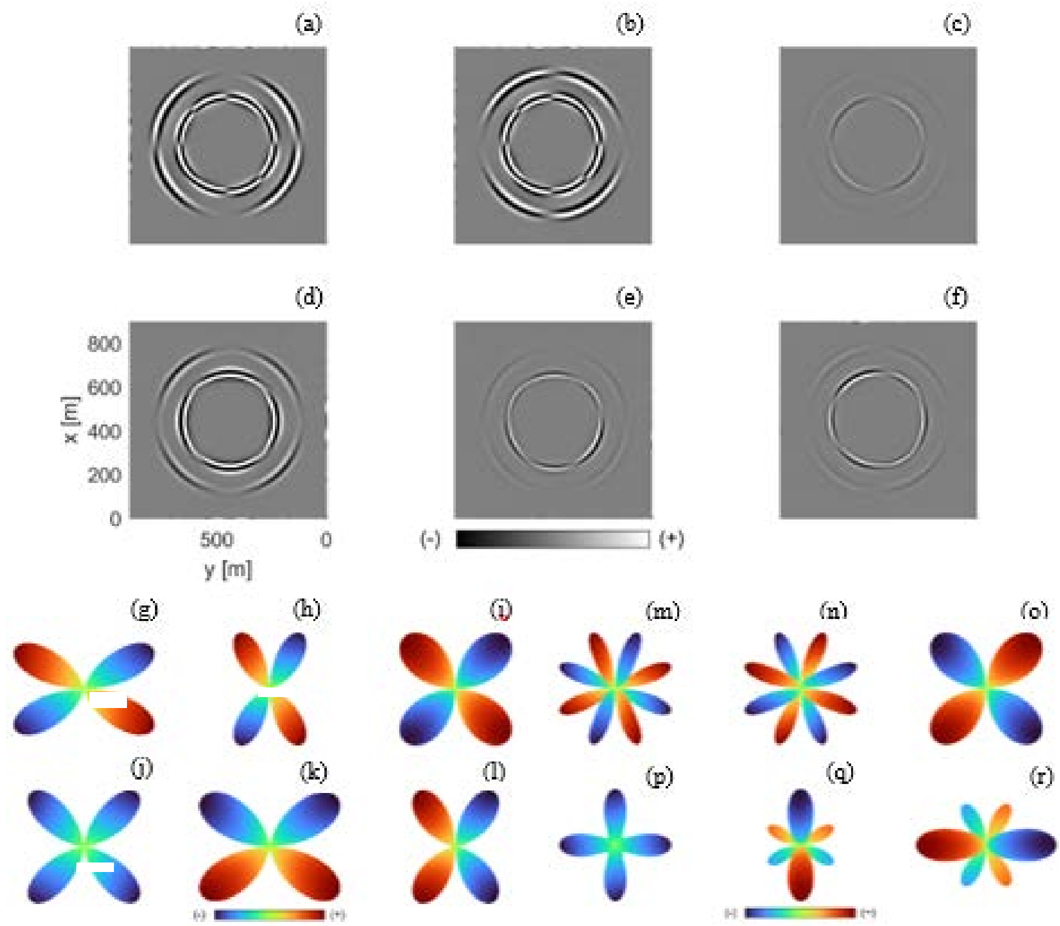

FIG. 1. (a)-(f) Snapshot of numerically modelled wavefield using velocity-stress finite difference method for (a) ϵ_{xx}, (b) ϵ_{yy}, (c) ϵ_{zz}, (d) ϵ_{xy}, (e) ϵ_{xz}, (f) ϵ_{yz}. Corresponding radiation patterns from analytic modelling for the P-wave components (g) ϵ_{xx}, (h) ϵ_{yy}, (i) ϵ_{zz}, (j) ϵ_{xy}, (k) ϵ_{xz}, (l) ϵ_{yz}, and S-wave components (m) ϵ_{xx}, (n) ϵ_{yy}, (o) ϵ_{zz}, (p) ϵ_{xy}, (q) ϵ_{xz}, (r) ϵ_{yz}.

Elastic FWI of the CAMI FRS 3D walkaway-walkaround VSP fiber survey: A synthetic case study

Matthew Eaid, Scott Keating, Marie Macquet, and Kris Innanen

ABSTRACT

Distributed acoustic sensing could further enable reservoir monitoring by providing a means of acquiring repeatable seismic surveys. Monitoring during CO_2 sequestration is a key area where advancements in DAS monitoring will be beneficial. The containment and monitoring institute (CaMI) has a Field Research Station designed to explore technologies for this very purpose. In 2018 a baseline 3D walkaway-walkaround VSP was acquired with geophones, straight DAS fiber, and helical DAS fiber. In preparation for inverting this dataset and computing a baseline model for future time-lapse surveys, we examine the inversion of simulated datasets from synthetic models computed from field site well logs. A key component of this study is examination of various elastic model parameterizations and the effect they have on the quality of the inversions. Through our analysis we determine that all of the parameterizations tested produce reasonable inversion results, but a $I_p - I_s - \rho$ parameterization appears to be the most robust and is most successful in mitigating cross talk. These baseline inverted models are then used as starting models in an inversion from simulated data from models after 5 years of CO_2 injection. Using data from all three sensors types we are able to invert for the V_p anomaly induced by injection but struggle to invert for the V_s and ρ anomalies.

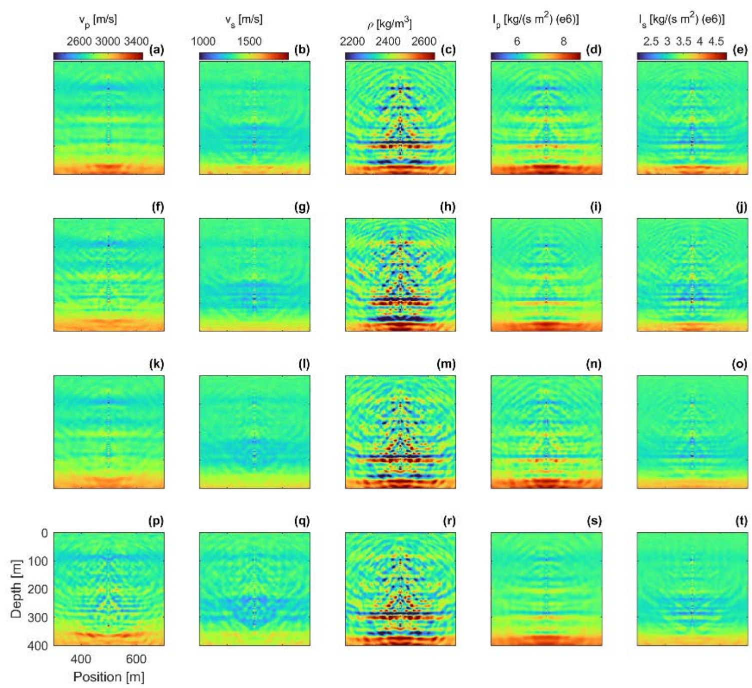

FIG. 1. Inversions from helical fiber data for $\mathrm{V_p}, \mathrm{V_s}, \rho, \mathrm{I_p}$, and $\mathrm{I_s}$ for the $V_p - V_s - \rho$ parameterization (a)-(e), $V_p - V_s - I_p$ parameterization (f)-(j), $V_p - V_s - I_p$ parameterization (k)-(o), and $I_p - I_s - \rho$ parameterization (p)-(t).

Estimation of DAS-microseismic source mechanisms using unsupervised deep learning

Matthew Eaid*, Chaoshun Hu, Lin Zhang, Scott Keating, and Kris Innanen

ABSTRACT

Distributed acoustic sensing (DAS) is an increasingly prevalent technology for seismic acquisition, especially in reservoir monitoring settings. Recently, it has attracted interest for microseismic monitoring during hydraulic fracturing and as a complement to broadband seismometers for measuring teleseismic waves generated by earthquakes. A key component of these data is the source mechanism information encoded in the direct arrivals and how to best utilize this data to make inferences about the source mechanism, given DAS measurements of the direct arrivals is an open question. DAS is a relatively new technology, providing very large datasets of different physical aspects of the wavefield than geophones or seismometers. Consequently, conventional moment tensor inversion is challenging to transfer directly to DAS data. Instead, we turn our attention to deep learning algorithms for estimating these source mechanisms. Viewing our seismic data as containing diagnostic features of the source mechanism, we reduce the data to only those features most pertinent to moment tensor inversion by training a convolutional auto-encoder. The extracted features are then analyzed using clustering and generative adversarial networks (GAN). Clustering based on source mechanism is observed, confirming the extracted features contain important source mechanism information. Furthermore, we develop a trained GAN that provides an accurate mapping from feature space to moment tensor estimate, which shows promise when applied to a field DAS-microseismic dataset collected during hydraulic fracturing. Data modeled with the predicted source mechanism shows a strong correlation to the field data event.

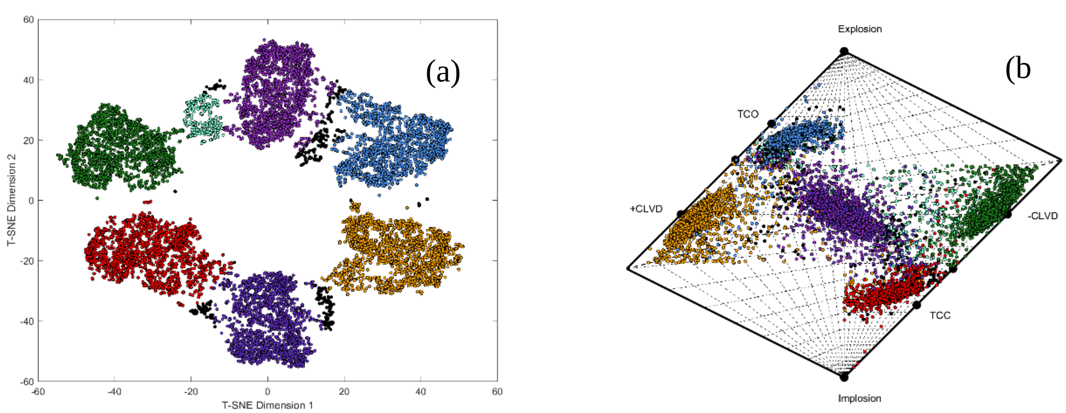

FIG 1. (a) Seven clusters in T-SNE space identified using the DBSCAN algorithm where each dot represents one of 10,000 input images. (b) Hudson space representation of each images source mechanism colored by the cluster to which is belongs.

The role of fiber gauge lengths in elastic FWI of data from coiled DAS fibers

Matthew Eaid*, Scott Keating, and Kris Innanen

ABSTRACT

Distributed acoustic sensing is an important technology that offers distinct benefits for reservoir monitoring. The increased access they provide to borehole acquisition geometries, has the potential to supply transmission data crucial to successful applications of full waveform inversion on land data. The properties of the fiber such as its geometric shape, and the its gauge length, especially in relation to the geometry, are expected to have implications for parameter resolution in FWI. In this paper we explore the role of the fiber gauge length in FWI, by examining (1) how it affects a given fibers sensitivity to each component of the strain field, and (2) how the relative sensitivity to these strain components affects parameter resolution. This explored through numerical simulations on a simple model on both clean and noisy data, as well as a more complex, and geologically reasonable model.

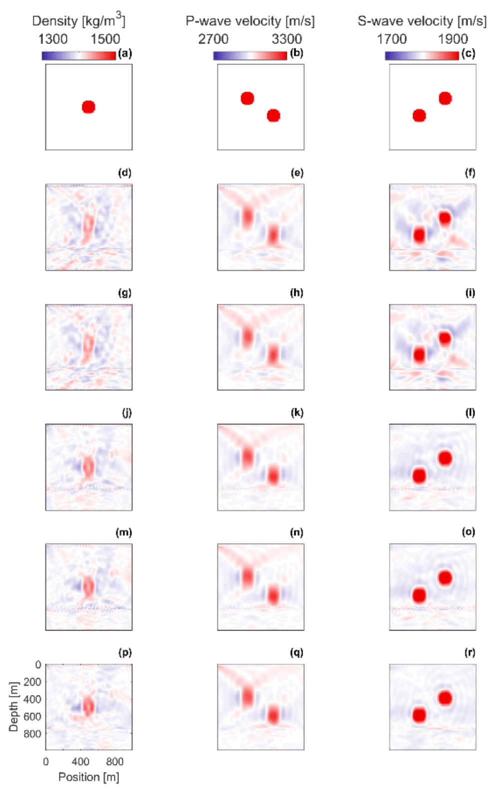

FIG. 1. (a)-(c) True models for density, P-wave velocity, and S-wave velocity. Inversions for density (column 1), P-wave velocity (column 2), and S-wave velocity (column 3), (d)-(f) for a gauge length of 10.08 m, (g)-(i) for a gauge length of 24 cm, (j)-(l) for a gauge length of 18 cm, (m)-(o) for a gauge length of 3 cm, and (p)-(r) for geophones.

Deep learning for 3D fault detection within virtual reality visualization seismic volumes

Ali Fathalian, Marcelo Guarido, Daniel Trad, and Kris Innanen

ABSTRACT

An important key for seismic structural interpretation and reservoir characterization is the delineating faults that are considered as seismic reflection discontinuities in conventional methods. Fault detection considers as a binary image segmentation problem of labeling a seismic image with ones on faults and zeros on non-faults using a fully supervised convolutional neural network. The network is trained by using 3D synthetic seismic images and their corresponding binary labels images. The network learns to calculate features that are important for fault detection after training with a synthetic data set. We apply this method to a migrated 3D volume from Australia. In this paper, the seismic information extended reality analytics (SIERA) presents a seismic data visualization in an extended reality environment. Because it is highly customizable, it provides an effective way to interact with seismic data and machine learning results.

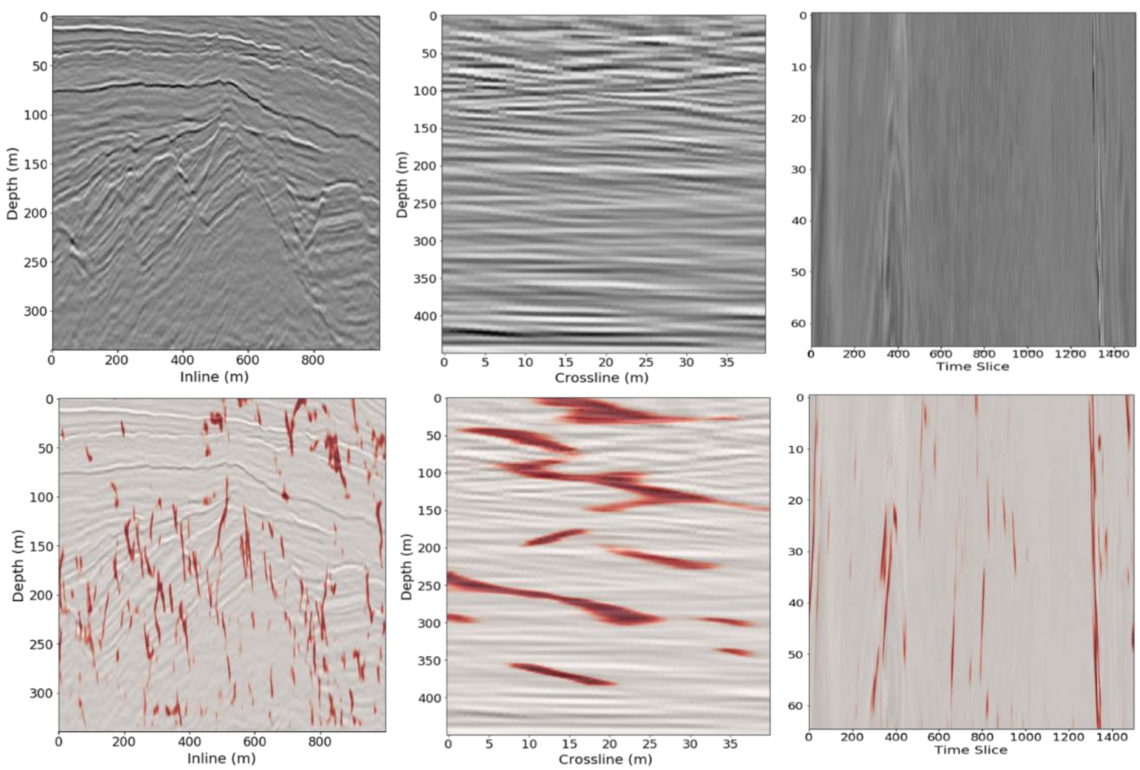

FIG. 1. The crossline, inline, and time slice of 3D Australian's Offshore seismic image are displayed with faults that are detected by using the trained CNN model.

Numerical simulation of seismic wave propagation in attenuative transversely isotropic media

Ali Fathalian, Daniel Trad, and Kris Innanen

ABSTRACT

Simulation of wave propagation in a TTI viscoacoustic medium is an important problem. We have developed a derivation of a system of equations for viscoacoustic waves in a medium with transverse isotropy (TI) in velocity and attenuation based on a standard linear solid model. The resulting system of equations is first order in time for the stress-strain relationship. The numerical implementation of this system determines with the finite-difference method, with second-order accuracy in time and fourth-order accuracy in space. Our results show that the proposed approach for modeling is able of capturing TI effects in attenuation and illustrating the efficiency of this system of equations for applications in seismic imaging and inversion.

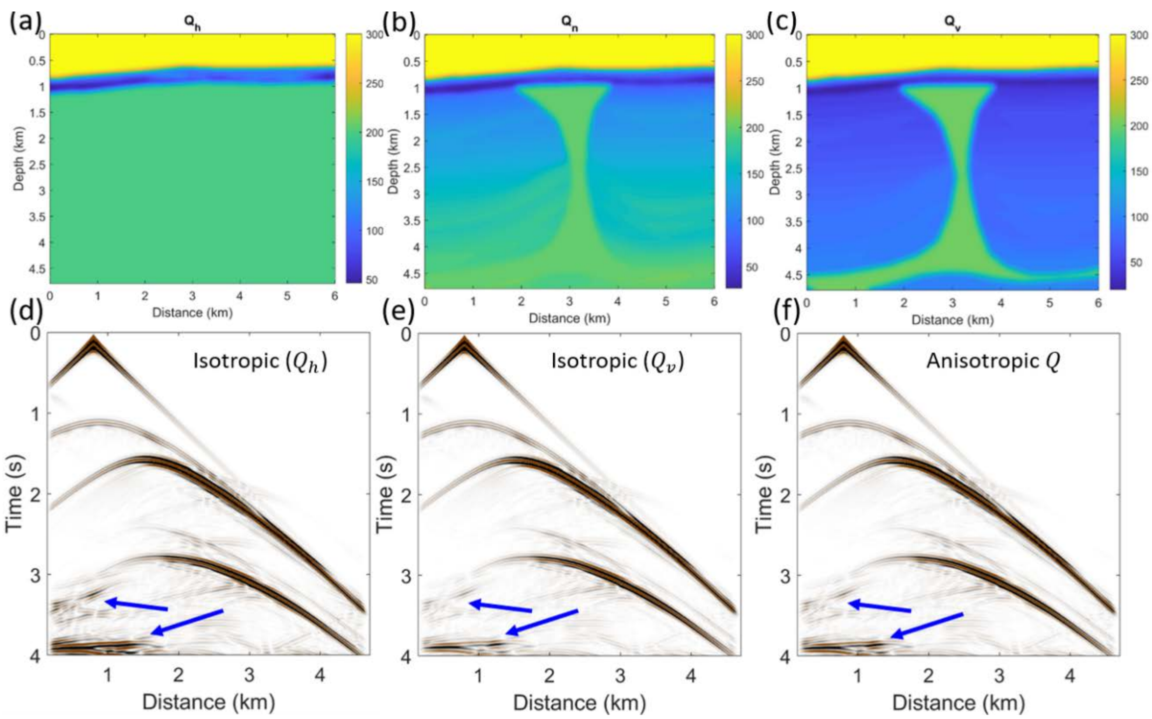

FIG. 1. (a-c) Quality factors of horizontal, vertical, and normal components. Shot gather computed with (c) isotropic attenuation with $Q = Q_h$, (d) isotropic model of attenuation with $Q = Q_v$, and (c) anisotropic model of attenuation.

Double-wavelet Double-difference elastic full-waveform inversion

Xin Fu, Scott Keating, Kris Innanen, and Qi Hu

ABSTRACT

Full-wave inversion (FWI) based on the wave equation has been employed extensively in geophysics. Time-lapse FWI that can detect time-lapse property changes of the subsurface with a high resolution has become an important tool. As a popular inversion time-lapse strategy, double-difference FWI (DDFWI) contains twice inversions, the first inversion is the baseline inversion, in which the input elements are the baseline data and a reasonable initial model, in the second monitoring inversion, DDFWI uses the starting model of the inverted baseline model and a composited data as an alternative of the monitoring data, that is, the difference data (the difference between the monitoring data and the baseline data) plus the synthetic data of the inverted baseline model. Since DDFWI is using the difference data, which helps it to focus on the target time-lapse area, thus DDFWI has fewer coherent errors in the inverted time-lapse model. But DDFWI also is of the shortcoming of requiring good repeatability of baseline and monitoring surveys, especially, when the wavelets of baseline data and monitoring data are different, the coherent errors are very heavy. To solve this problem, Fu et al. (2020) have developed a double-wavelet DDFWI method and implemented for the acoustic FWI. In this study, we will expand the double-wavelet method to the elastic FWI.

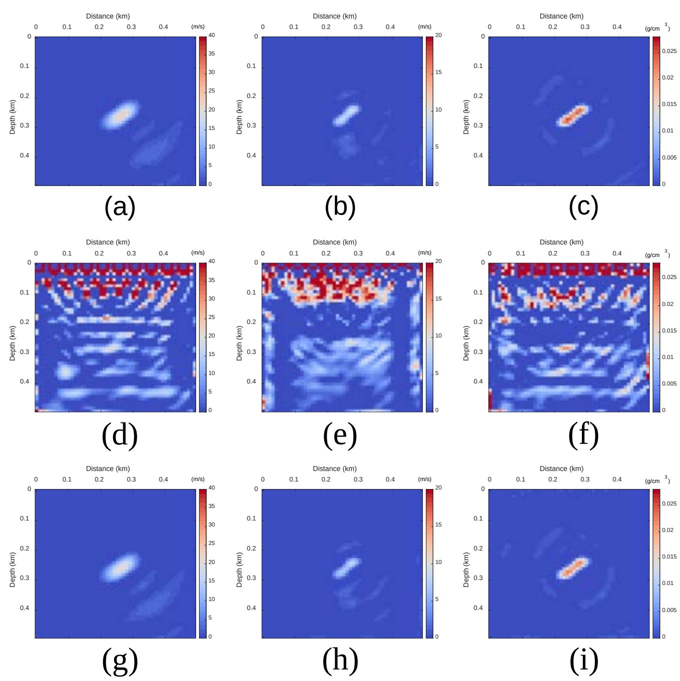

FIG. 1. The inverted time-lapse models of DDFWI in the case of baseline and monitoring wavelets are identical, (a) P-wave velocity, (b) S-wave velocity, and (c) density. The inverted time-lapse models of DDFWI in the case of baseline and monitoring wavelets are not identical, (d) P-wave velocity, (e) S-wave velocity, and (f) density. The inverted time-lapse models of DWDDFWI in the case of baseline and monitoring wavelets are not identical, (g) P-wave velocity, (h) S-wave velocity, and (i) density.

MCMC-based time-lapse full-waveform inversion

Xin Fu* and Kris Innanen

ABSTRACT

In this study, we have proposed a Bayesian time-lapse full-waveform inversion (FWI) based on the Markov chain Monte Carlo (MCMC) algorithm and a new method to estimate the data error standard deviation for the time-lapse data according to its feature. To achieve the MCMC-based time-lapse FWI, we have employed the inversion strategies including the double-difference time-lapse FWI (DDFWI), the time-domain multisource data, the local-updating target-oriented inversion, calculating model covariance with the adaptive Metropolis algorithm, and the new data error standard deviation estimation method. The MCMC algorithm applied is a random walk Metropolis-Hastings MCMC, a typical stochastic global optimization method. In the conventional deterministic optimization (DO) DDFWI containing a baseline inversion for the baseline model and a monitoring inversion for the monitoring model, both inversions are performed by the DO FWI. In the MCMC DDFWI proposed in this work, we keep the DO FWI for the baseline inversion but employ the MCMC algorithm for the monitoring inversion. And the final time-lapse model is the difference between the inverted monitoring model and the baseline model. Synthetic data tests using a 2D acoustic model have demonstrated the feasibility of MCMC DDFWI on both time-lapse model inversion and uncertainty qualification. We also have compared the MCMC DDFWI with the conventional DO DDFWI, which shows that the inverted average time-lapse model of MCMC DDFWI can provide the results with clearer edges of the nonzero time-lapse model change and fewer coherent errors.

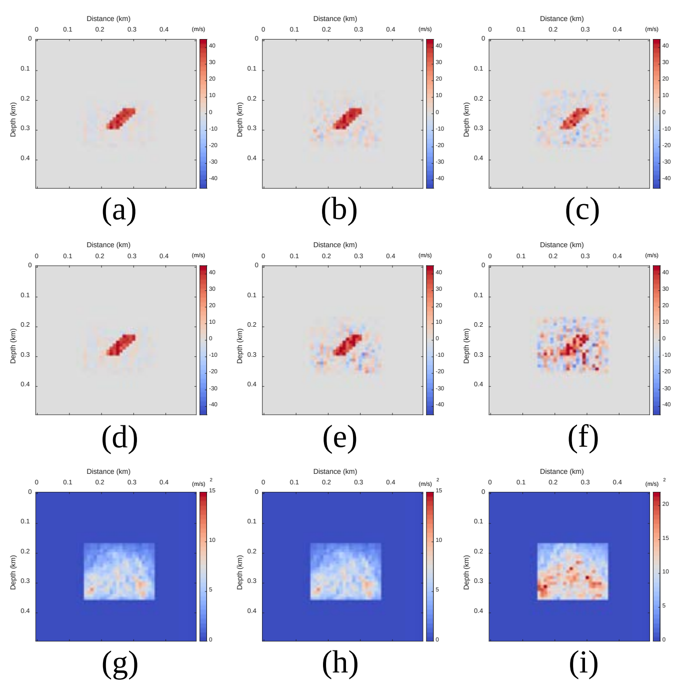

FIG. 1. The inverted average time-lapse models (a)-(c), maximum probability (MAP) models (d)-(f), and posterior model standard deviations (g)-(i) of noisy data with different noise levels. From the first column to the third column, the corresponding data noise becomes stronger.

A new parallel simulated annealing algorithm for 1.5D acoustic full-waveform inversion

Xin Fu and Kris Innanen

ABSTRACT

Full-wave inversion (FWI) based on deterministic optimization (DO) methods is an appealing tool to detect the physical properties of the subsurface media, and increasing successful examples have been reported. However, the DO FWI is highly model-dependent, its success relies on a good starting model. To solve this problem, some researchers resort to the stochastic global optimization (SGO) methods that have shown the potential to alleviate the suffering of the model-dependent problem in FWI. Whereas, the SGO methods also have their own drawback that it needs to solve a great number of forward problems This is dramatically computationally expensive for the wave-equation-based FWI. In our study, we use a heuristic SGO algorithm, the very fast simulated annealing (VFSA) algorithm, to implement the constant-density acoustic FWI. To save computational time, we develop a new parallelization VFSA, in which the serial structure of VFSA is changed to some degree. Instead of updating the model parameter one by one in the same thread in a conventional serial VFSA, the parallel VFSA updates the N model parameter separately on N threads, in which the maximum efficient processor number is N. Since performing a 2D VFSA FWI directly without using any parameterization to reduce parameter number (dimension) is still prohibitive, we test the different FWIs (the DO FWI, the conventional serial VFSA FWI, and the new parallel VFSA FWI) on a 1.5D model, and for both VSP (vertical seismic profile) and surface seismic data. For each data, we use both an unbiased starting model crossing the true model and a biased starting model far away from the true model with the depth increase to investigate how the different FWIs rely on the starting model. The tests show that all FWIs for VSP seismic data are not too model-dependent, but the DO FWI for surface seismic data is mode-dependent and the VFSA FWIs can solve this problem well. Furthermore, to further save the computational cost, the data used for VFSA FWIs are multisource shot gathers. And all seismic data used are in time domain.

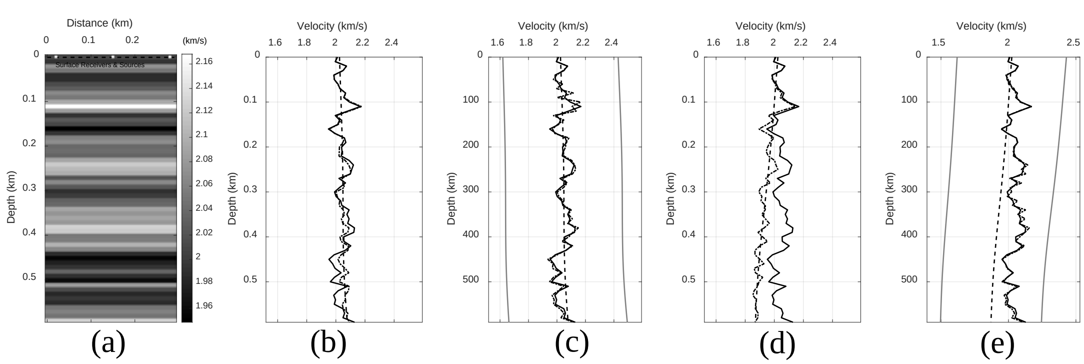

FIG. 1. (a) True model and acquisition geometry. Inverted results of DO FWI (b) and the parallel VFSA FWI (c) with an unbiased initial model. Inverted results of DO FWI (d) and the parallel VFSA FWI (e) with a biased initial model.

Application of machine learning to the analysis of pipeline incidents in Canada

Marcelo Guarido*, Daniel Trad, and Kris Innanen

ABSTRACT

Analyzing pipelines incidents in Canada is important to understand their impact on the environment and workers' safety. Data provided by the Government of Canada is confusing and incomplete but contains useful information that can be analyzed and modeled to mitigate future incidents. Most of the reports come from the province of Alberta, which contains most of the pipelines in Canada, and are mainly related to 4 companies. We could notice a correlation between the number of incidents per year with the price of the WTI crude oil price, as well as weekend effects. No seasonality is observed in the data, but we noticed some outliers - months with a larger number of reports than the average - and they are related to a single company. Clustering for dimensionality reduction and cluster analysis, applied on pipeline and maintenance information, showed 4 main clusters, each associated with different insights, such as the average volume of substance released, how long took for the occurrences discovering, and emergency level.

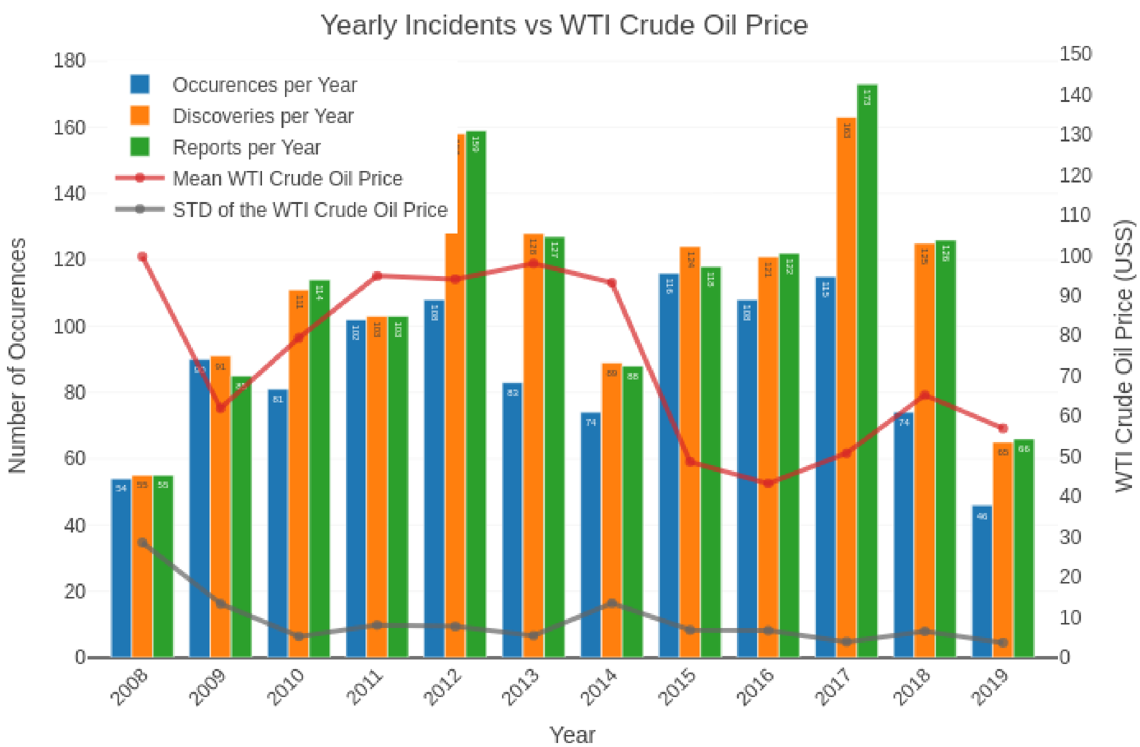

FIG. 1. Comparing the yearly number of incidents with the WTI crude oil price.

The effect of the COVID-19 pandemic to the WTI crude oil price using forecasting models

Marcelo Guarido, Daniel Trad, and Kris Innanen

ABSTRACT

Accurately forecasting the price of oil can be considered a Holy Grail in the petroleum industry, and even more important to take business decisions during a crisis, like the COVID-19 pandemic. For that, we are proposing the use of an ensemble of powerful forecasting methods to do an impact analysis of the pandemic to the oil and gas industry. By forecasting the prices with models trained with oil prices prior to 2020, we created a baseline of what the price of the WTI crude oil should have been without the pandemic and, with the information of the US production, we estimated that, in 6 months of the pandemic, a loss of around 60 billion USD in the US alone. We also estimate that, if the scenario of the pandemic does not change, the price of the oil for the 12 months after October 2020 will stay on a stable low level around 37 USD per barrel.

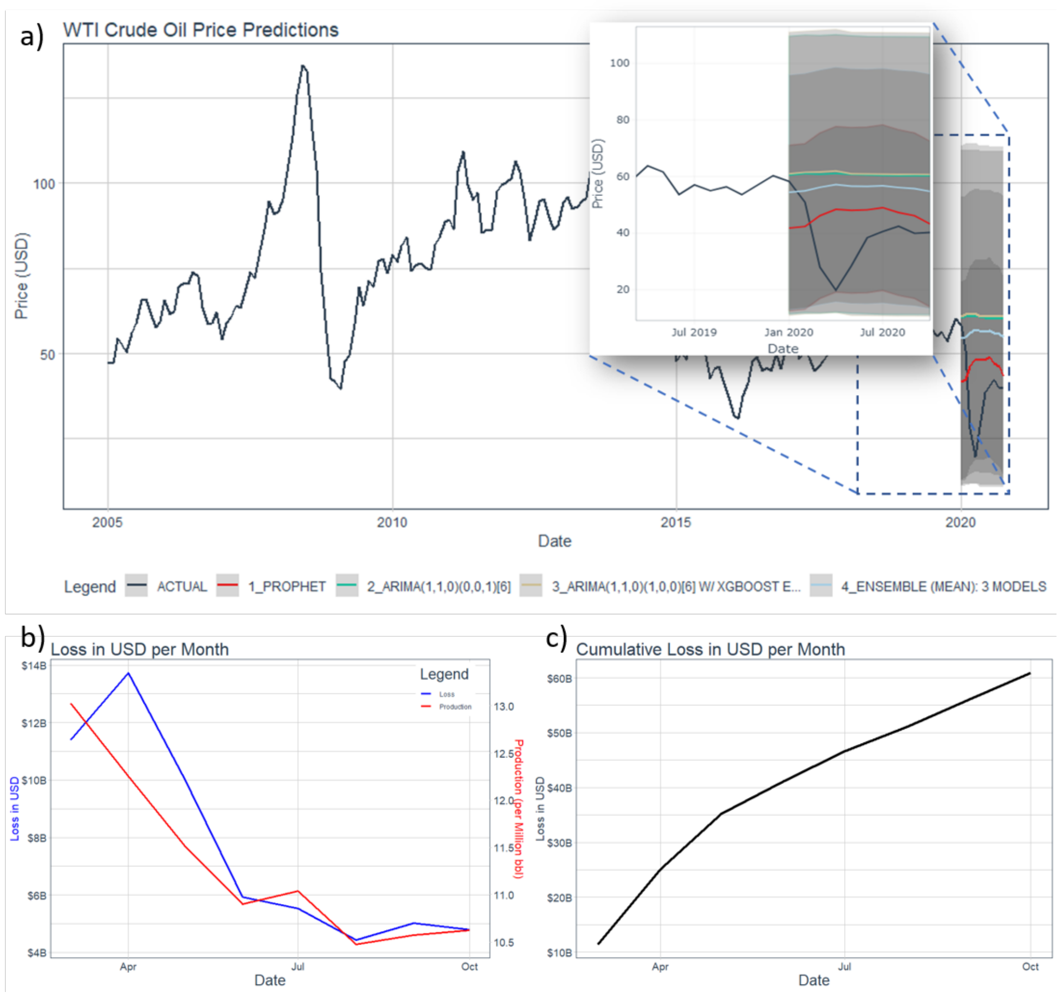

FIG. 1. a) Monthly WTI crude oil price from 2005/01 to 2020/10 compared with the forecasting models, b) monthly loss (blue) and production (red) and c) cumulative monthly loss.

The Pitfalls and Insights of Log Facies Classification for a Machine Learning Contest

Marcelo Guarido, David J. Emery, Marie Macquet, Daniel Trad, and Kris Innanen

ABSTRACT

FORCE: Machine Predicted Lithology was a classification contest using well logs from the Norwegian coast of the North Sea. While lithology is the general physical characteristics of rocks our Machine Learn approaches concentrated on the petrology or composition of rocks sample by sample. We used different solutions for the provided data set and created workflows that clean and complete the data. An additional problem was that the training data was not balanced with 1 class making up 62% of the training data and 7 of the classes less than 4%. We built two different models, one for balanced predictions using a gradient boosting algorithm, and another focusing on the common classes using a model that stacks gradient boosting and random forest probability predictions. The primary Machine Learning pitfall was to balance the petrophysical analysis with the lithofacies associated training classes. The FORCE label training classes also contain a mixture of lithofacies within each class and thus a high degree of mineralogy variation or crosstalk in the confusion matrix. A second pitfall was how the Machine Learning contest was scored used a penalty matrix metric that did not compensate for the imbalance of the input data. The first of our approaches had a great balanced accuracy score of 0.561, but with a poor score for the contest metric, scoring −1.35. The second model scored −0.58 on the contest metric, with a trade-off on the balanced accuracy score, which reduced to 0.41.

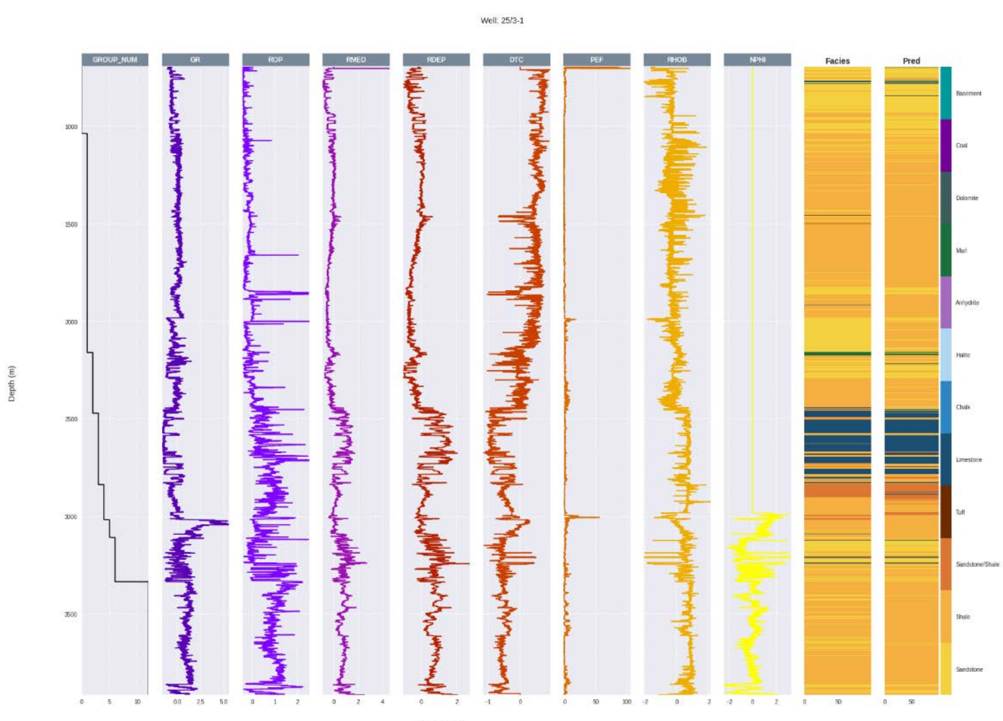

FIG. 1. Lithofacies predictions with imbalanced models.

Field testing of multicomponent DAS sensing

Kevin W. Hall*, Kris Innanen and Don C. Lawton

ABSTRACT

We constructed an experimental directional DAS sensor (DDS) at the Containment and Monitoring Institutes Field Research Station (CaMI.FRS) in 2018. The sensor consists of two buried 10x10 m squares of straight and helically wound fibre, with the second square rotated forty-five degrees relative to the first. Three-component geophones were planted on the surface just outside of the corners of the DDS, and four source locations (Vibe Points) were acquired using a 5 m gauge length in the DAS interrogator.

Building on work reported last year, where horizontal components of the geophone data were converted to strain-rate traces and visually compared to fibre strain-rate traces, we use directional strain-rate traces to estimate time-series of strain-rate-tensors for the DDS and surface geophones for the first direct ground-roll arrival across the DDS.

The estimated tensors are almost identical for the straight and helically wound fibre after trace scaling, but the amplitudes of the geophone strain-rate tensors are higher than seen for the fibre results in some cases. We speculate this is because the geophones and the fibre are not co-located.

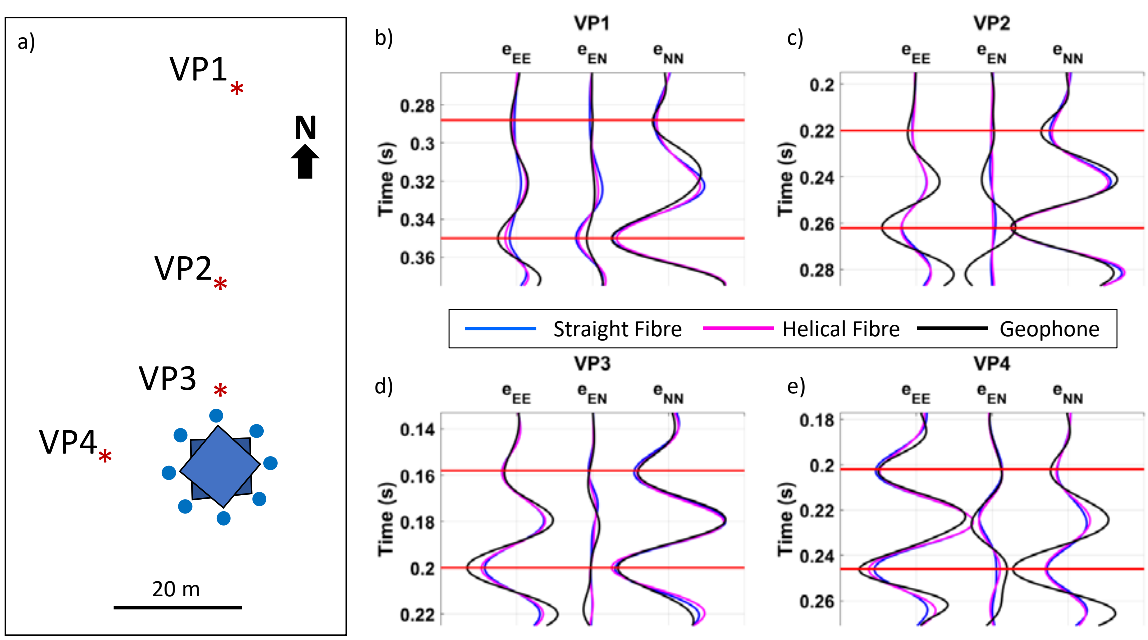

FIG. 9. Map showing four Vibe points, DDS, and geophone locations (a), and strain-rate tensors estimated for the first identifiable ground-roll peak for VP1 (b), VP2 (c), VP3 (d), and VP4 (e).

Non-impulsive source waveforms for physical modelling

Kevin W. Hall, Joe Wong, Kevin L. Bertram, and Kris Innanen

ABSTRACT

The physical modelling system is being upgraded with an arbitrary waveform generator (AWG), that will allow us to use non-impulsive source waveforms including sinusoidal frequency sweeps, square-wave frequency sweeps, and m-sequences (pseudorandom binary sequences). Some of these waveforms, such as constant amplitude mono-frequency square waves or mono-frequency spike series can be run without an AWG. Square wave signals and spike series have only two normalized values: +1 and -1. Therefore, they are called binary-valued sequences, and are much more easily generated by electronic circuits for practical usage than are sinusoidal signals.

This report examines the theoretical effect of running a variety of source waveforms, including Vibroseis sweeps, through our system, and predicts our future results if we use a pair of millimeter-sized source transducers, which have a characteristic impulse response. We also show actual data resulting from a spike series run through 37 mm buzzers. Of interest for all source waveforms is the expected amplitude at the receiver for 10 kHz (equivalent to 1 Hz after scaling by 10000 to real-world seismic exploration frequencies), which we need if we wish to run full-waveform inversions (FWI) on physically modeled data. Our results show that running a frequency sweep that spends proportionately more time near 1 Hz (scaled) can improve our recorded amplitudes at that frequency, but enhancing this signal will require further processing.

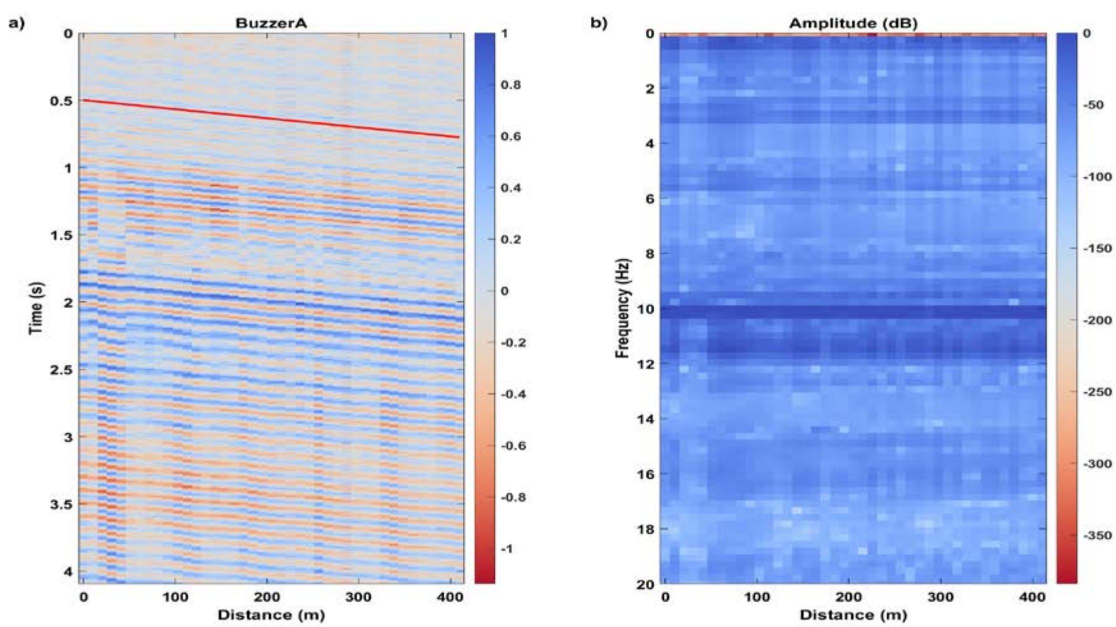

FIG. 1. Walk-away data for 37 mm buzzers in water after subtracting the mean and applying a linear detrend to each trace. No filters or AGC. The red reference line plotted over top of 13a was calculated using 1485 m/s (water velocity) and arbitrarily positioned to begin at 0.5 s.

A tale of two realities: reconciling physical and numerical modeling via ‘bootstrap’ processing

David C. Henley

ABSTRACT

Seismic physical modeling is the process of conducting seismic surveys on laboratory scale models of earth structures, using ultrasonic transducers, to simulate the expected seismic response to similar structures in the earth. From modeling results, we improve our understanding of the generation and propagation of various elastic and acoustic wave modes in the real earth. Because of the similarity to seismic field surveying, physical model results can be considered a form of ‘ground truth’ for geology accurately represented by the model.

Numerical modeling, on the other hand, creates a simulated seismic response to a digital representation of a physical earth structure. It is useful not only for evaluating how well a digital model represents the earth, but also for verifying the modeling process itself. Numerical modeling plays a significant role in Full Waveform Inversion, since a modeling algorithm is used to compute a seismic response to the most current earth model to compare with the most current processed input data, in order to update the model.

Using a scale model constructed and surveyed in the CREWES physical modeling lab, we have the unique opportunity to compare images obtained from the physical model survey data with images produced by the data from numerical modeling of a digital representation of the laboratory scale model. We initially have only a schematic of the laboratory physical model, however, so we first use the schematic, along with an image from the physical survey itself, to create the digital model for input to the numerical modeling algorithm. The physical model data are then re-imaged using this estimated digital model velocity field, and the model itself updated--a ‘bootstrap’ approach. We then use a finite difference acoustic numerical modeling algorithm to create a CMP survey of the digital model, emulating the acquisition geometry of the actual survey. The numerical data are processed identically to the physical model data. We compare the physical and numerical model images. We compare the physical and numerical model images in Figure 1.

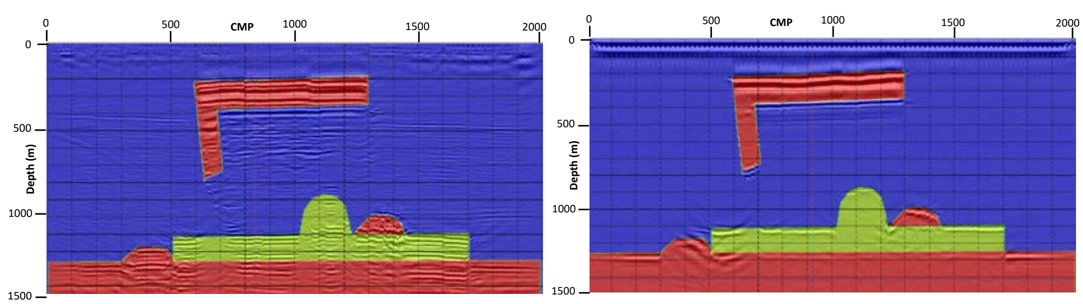

FIG. 1. Pre-stack Kirchhoff depth migration of physical model survey (left) vs. pre-stack Kirchhoff depth migration of finite difference acoustic numerical model (right). Both are overlaid with the digital representation of the physical model.

Elastic FWI with rock physics constraints

Qi Hu* and Kris Innanen

ABSTRACT

Current efforts to use elastic full waveform inversion (EFWI) go beyond imaging of complex structures and aim at determination of reservoir-scale rock physics properties. However, the nonlinearity of EFWI and parameter crosstalk can prevent its convergence toward the actual model. Parameters such as density and fluid saturation are more difficult to retrieve because of their limited contributions to seismic data. We develop a method for EFWI that uses rock physics constraints to mitigate such limited sensitivity. These constraints are in the form of explicit velocity-density relations for different lithologic facies as a function of position, and are imposed through a model regularization term in the objective function. We implement two different workflows of constraining EFWI for elastic and rock physics properties. One is a sequential approach that consists of first inverting for velocity and density through EFWI and then transforming the elastic attributes to rock physics properties. The other is a joint approach where we parameterize EFWI with rock physics properties, allowing elastic and rock physics properties to be simultaneously updated. Constraining each workflow helps improve density and saturation recoveries. We also illustrate that the joint approach is superior to the sequential inversion in terms of computational cost and the ability to ensure consistency between elastic and rock physics properties.

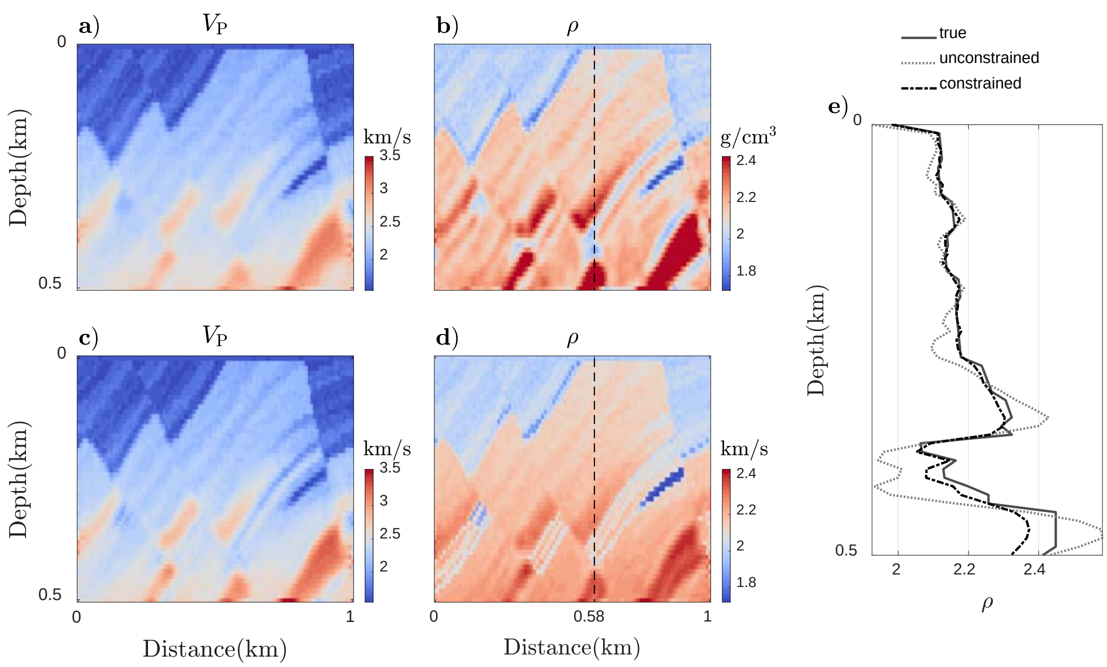

FIG. 1. (a, b) Recovered velocity and density models using the unconstrained inversion. (c, d) Recovered velocity and density models using the constrained inversion. e) Model profiles of density at x=0.58km.

Rock physics properties from seismic attributes with global optimization methods

Qi Hu* and Kris Innanen

ABSTRACT

The estimation of rock physics properties from seismic attributes is a nonlinear inverse problem. We investigate three global optimization methods: simulated annealing, genetic algorithm, and neighborhood algorithm for solving this problem. The input data are P-wave velocity, S- wave velocity, and density, and the rock physics properties to estimate are porosity, clay content, and water saturation. The two parameter sets are connected by an assumed rock physics model. Numerical examples are suggestive that the neighborhood algorithm is most efficient for improving data fit for the experiment we set up; porosity and clay content can be accurately estimated, whereas the water saturation estimate is prone to large errors. We explain this as a consequence of the low sensitivity of velocities and density to this property. However, simultaneous inversion for the whole set of the rock physics properties is problematic if the input data are erroneous. Consequently, we restrict the inversion to porosity and clay content only and assume a priori information of the exact water saturation. This makes the inversion stable with noisy data. Finally, we illustrate the application of the proposed global optimization method using the high-resolution results of elastic full waveform inversion (EFWI).

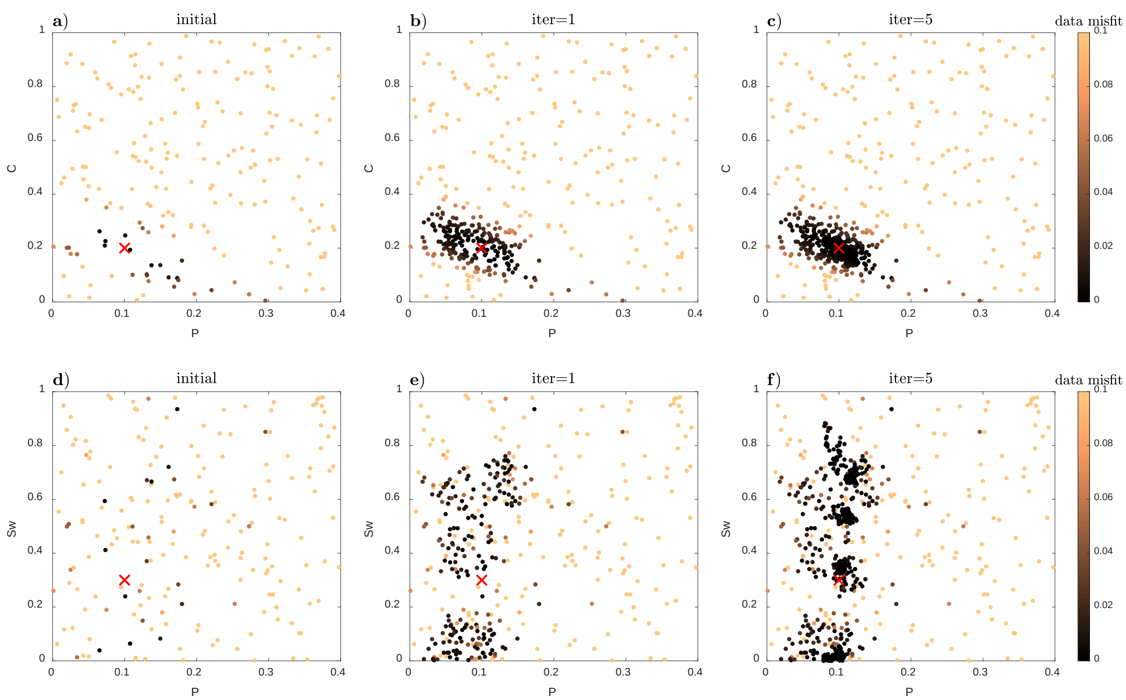

FIG. 1. Simulation results using the neighborhood algorithm. The dots represent the generated models at different iterations and are color-coded by data misfit. The true model is denoted by the red cross. As the algorithm proceeds, the information in the misfit-surface is exploited to concentrate sampling in the regions where the misfit is low.

Full-wavefield migration in the frequency-wavenumber domain

Shang Huang* and Daniel Trad

ABSTRACT

Full wavefield migration (FWM) is an inversion-based migration method that can handle total wavefields, including primary reflections, surface-related multiples and internal multiples. Additional multiple energy can help with improving the subsurface imaging illumination. Previous work focuses on applying full wavefield forward modelling and imaging in the frequency-space domain. In this paper, full wavefield modelling and migration are performed in the frequency-wavenumber (FK) domain, since data in the FK domain is more straightforward to be extrapolated and processed. Phase shift plus interpolation is also combined in the forward modelling to simulate the complex wavefields generated from lateral velocity variations. A deconvolution imaging condition is considered in the imaging procedure to compute more accurate updated model perturbation. The result derived from using full wavefield migration in the frequency-wavenumber domain shows improved reflection response and amplitude spectrum compared with applying primary wavefield migration. This algorithm using multiple reflections provides higher frequency results and better lateral continuity.

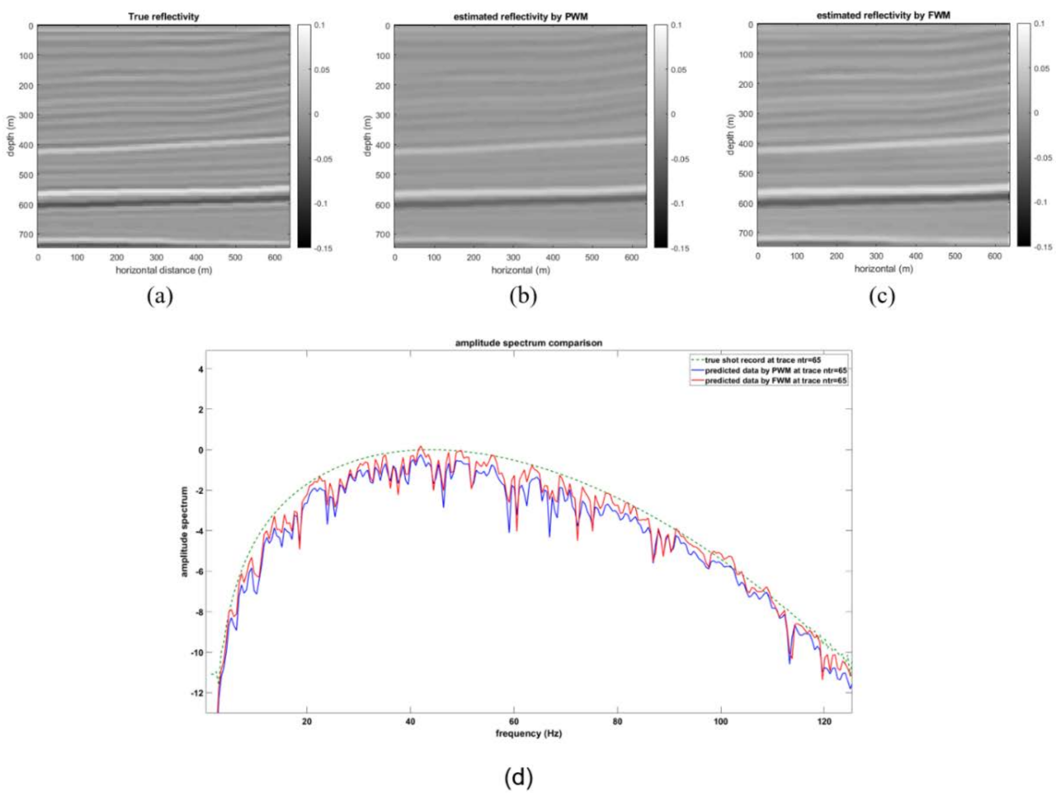

FIG. 1. Example for showing the comparison between full wavefield migration (FWM) and primary wavefield migration (PWM). (a) True reflectivity which is extracted from the left part of the Marmousi model. (b) Estimation of reflectivity by using PWM after 5 iterations. (c) Estimation of reflectivity by using FWM after 5 iterations. (d) Amplitude spectrum comparison between the forward modelling of FWM and PWM.

Application of misfit-based model space coordinate system design to seismic AVO inversion

Kris Innanen*

ABSTRACT

The standard re-expressions used in AVO analysis and inversion (e.g., from velocity-density to modulus-density, or from the Aki-Richards approximation to the Shuey approximation, etc.) are formally coordinate transforms between oblique-rectilinear (i.e., non-Cartesian) coordinate systems. This means alternative re-expressions can be found with favourable updating properties. In a low-dimensional model space like that of AVO (which involves dimensionalities in the low single digits), analytic forms for transformation matrices to systems in which the Hessian operator is an identity matrix can be found. These imply new AVO approximations, within which updates in AVO inversion require no 2nd order objective function information. This may have consequences both for iterative linear AVO inversion algorithms and "weighted stack" algorithms, the latter of which can be based on much simpler weights.

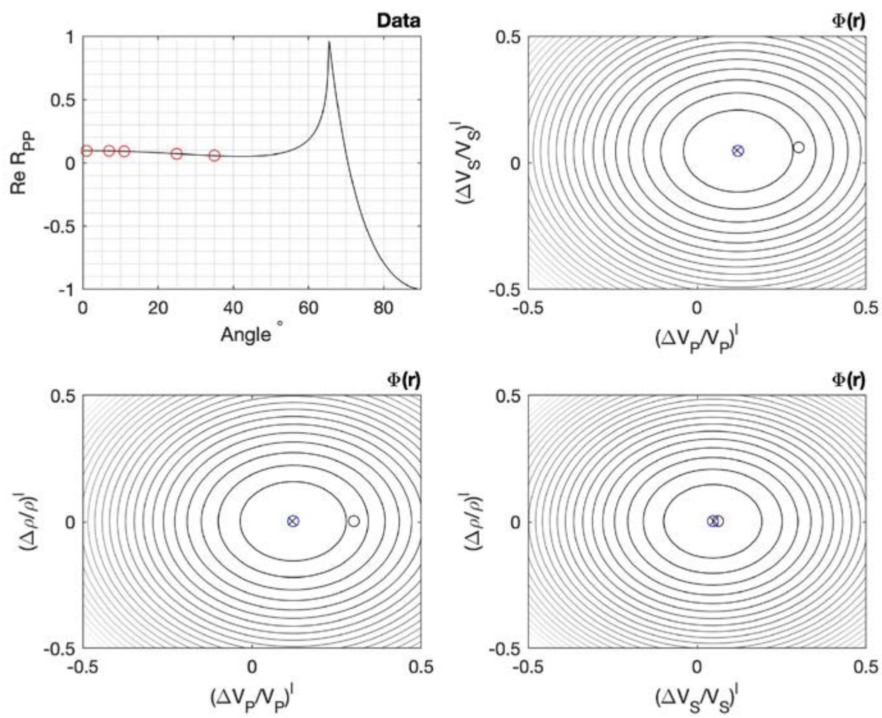

FIG. 1. A simulated AVO inverse problem. Top left: five low- to moderate-angle data are extracted, and used in a single update in the new transformed system. Top right/bottom: Slices through the 3D objective function after transformation with an example starting model and an update constructed through only 1st order misfit information.

Application of misfit-based model space coordinate system design to seismic full waveform inversion

Kris Innanen*

ABSTRACT

The re-parameterizations we encounter regularly in seismic full waveform inversion can all be formally identified as coordinate transforms between suitably general coordinate systems. For instance, changes-of-variable between elastic/acoustic parameter classes, and the variable changes underlying the model space pre-conditioning methods of Harlan, Claerbout and Fomel, can both be shown to be transforms between oblique-rectilinear coordinate systems when covariant notation is employed. With transformation rules in place for updates and displacements (contravariant vectors), and sensitivities and gradients (covariant vectors), as well as objective functions (scalars) and Hessian operators (2nd rank covariant tensors), we may then seek new and potentially useful re-parameterizations. Coordinate systems within which the Hessian is close to the identity have vastly improved optimization properties. Using a newly-derived numerical procedure for designing transformation matrices mapping to such systems, we provide an early examination of re-parameterized FWI.

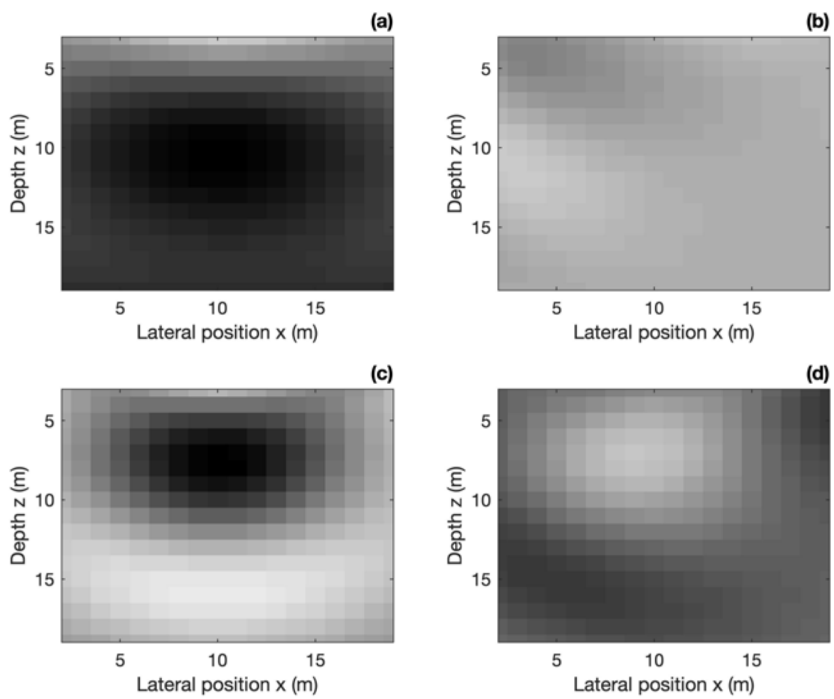

FIG. 1. Acoustic 1-parameter frequency domain full waveform inversion in a small volume: (a) model prior to updating at iteration 6 of 20; (b) model in (a) transformed as a contravariant vector to a system in which the Hessian is the identity; (c) gradient at iteration 6 of 20; (d) gradient in (c) transformed as a covariant vector to the same system.

Model re-parameterization via misfit-based coordinate transforms

Kris Innanen

ABSTRACT

Re-parameterizations of model space, which are widely applied in seismic inverse problems, are coordinate transforms between non-Cartesian systems. To develop this we identify objective functions as scalar functions of the model vectors, which themselves are contravariant vectors; gradients of the objective function are covariant vectors. A procedure for general transformation to a pre-defined coordinate system and optimization within that system is set out. We argue that a under a class of transformations constrained by the Hessian operator in the reference system, steepest-descent updates are precisely parallel to Gauss-Newton updates, and, provided the transform can be efficiently determined, optimization within the transformed system should have favourable convergence properties. This class of transforms includes an infinite number of variants, and seeking examples from within this class with other, additional, favourable features appears warranted.

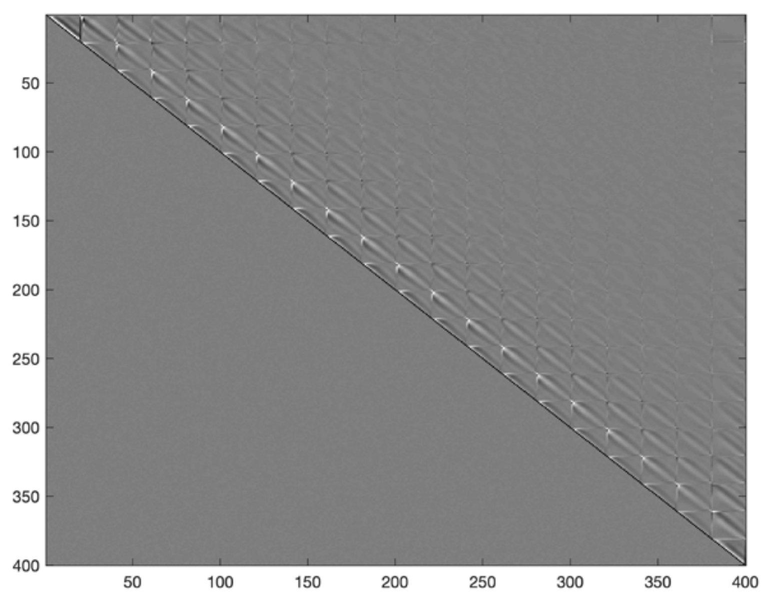

FIG. 1. An example transformation matrix taking an FWI model space parameterization to a new domain in which the Hessian operator is a unit identity matrix.

Numerical procedures for computing constrained coordinate transforms

Kris Innanen

ABSTRACT

In other papers published in this report, general numerical procedures for determining NxN transformation matrices **T**, which satisfy constraints involving the action of **T** on a given symmetric NxN matrix **Φ**, are assumed available. Here procedures of this kind are presented. Remarks on their development, and versions of the procedure that are efficient in that they do not duplicate any large-scale calculation, are included.

$$\Phi = \begin{bmatrix} \phi_{1,1} & \phi_{1,2} & \phi_{1,3} & \cdots & \phi_{1,N} \\ \phi_{1,2} & \phi_{2,2} & \phi_{2,3} & \cdots & \phi_{2,N} \\ \phi_{1,3} & \phi_{2,3} & \phi_{3,3} & \cdots & \phi_{3,N} \\ & & \vdots & \ddots & \\ \phi_{1,N} & \phi_{2,N} & \phi_{3,N} & \cdots & \phi_{N,N} \end{bmatrix}, \mathbf{T} = \begin{bmatrix} t_{1,1} & t_{1,2} & t_{1,3} & \cdots & t_{1,N} \\ t^*_{2,1} & t_{2,2} & t_{2,3} & \cdots & t_{2,N} \\ t^*_{3,1} & t^*_{3,2} & t_{3,3} & \cdots & t_{3,N} \\ \vdots & \vdots & \vdots & \ddots & \\ t^*_{N,1} & t^*_{N,2} & t^*_{N,3} & \cdots & t_{N,N} \end{bmatrix}, \mathbf{T}^T \Phi \mathbf{T} = \mathbf{I}$$

FIG. 1. Variations in the diagonal elements of Hessian operators **Φ**, and non-zero off-diagonal elements, produce convergence problems in optimization. Transformation matrices T with pre-selected lower-triangular values can be determined such that the transformed Hessian is the identity.

A review of tensors in non-Cartesian coordinate systems

Kris Innanen

ABSTRACT

This is a brief review of some of the ideas of tensor mathematics in non-Cartesian coordinate systems. There is no new material here, only a particular selection and arrangement of theory available in many good textbooks. The mathematics is needed in order to discuss model space re-parameterizations as transformations between coordinate systems, and to develop the new re-parameterizations we attempt elsewhere. The document ends with a listing of transformation rules we will use repeatedly elsewhere.

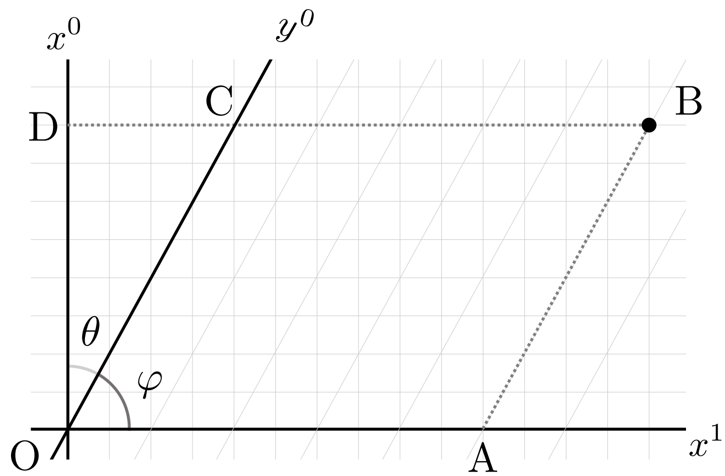

FIG. 1. A diagram to support determining coordinate values of a point B in the orthogonal x system and the oblique y system.

Simultaneous full waveform inversion for sources and anelastic models

Scott Keating* and Kris Innanen

ABSTRACT

Full waveform inversion (FWI) can provide accurate estimates of a variety of mechanical properties in the subsurface. Very often, FWI is used to recover subsurface properties in situations where source properties are well understood. Other seismic inversion strategies exist for the recovery of unknown source properties, and these typically assume a known, simple model of subsurface mechanical properties. In practice, there exist many situations in which a better understanding of both the subsurface model and the seismic sources is desirable. As each of these properties can influence our estimate of the other, it may sometimes be necessary to simultaneously recover both a subsurface model and a characterization of sources. In this report, we propose such a simultaneous inversion, using a FWI approach. We show in a simple synthetic example that this approach can be effective in recovering sources and subsurface models, though some results suggest that sequential inversion approaches may be similarly effective in many settings.

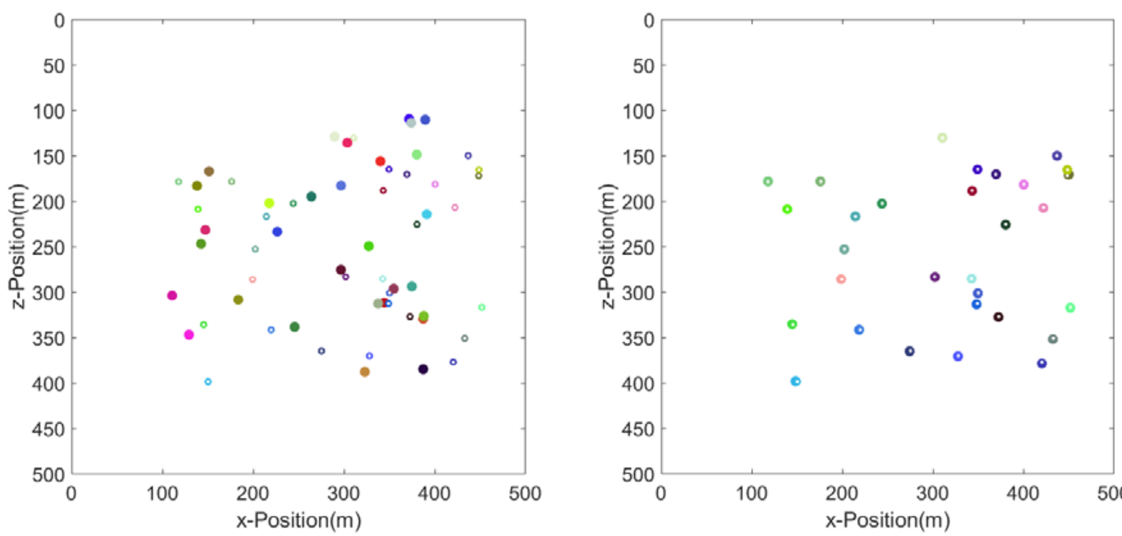

FIG. 1. Source estimates in both position (point location in graph) and 2D moment tensor (M_{zz}, M_{xz}, and M_{xx} correspond to red, green and blue values). Left: true sources (hollow circles) and initial estimates of sources (solid circles). Right: true sources (hollow circles) and final estimates of sources (solid circles). After the simultaneous inversion, both source and model estimates are substantially improved.

A tunneling approach to regularized full waveform inversion

Scott Keating* and Kris Innanen

ABSTRACT

Prior information can be a powerful tool in seismic inversion that can substantially improve on the results that seismic data alone can provide. Knowledge about clustering of rock physics properties may be especially significant, but this type of information is problematic in full waveform inversion due to the local optimization methods which are typically used. Here, we propose a regularization tunneling strategy for full waveform inversion, in which global regularization information is partially accounted for. By introducing the potential for elements of the subsurface model to tunnel between clusters, this approach is able to overcome obstacles associated with local minima in regularization terms from a priori data. We test a tunneling inversion approach on a simple synthetic problem, and find that when information about rock physics clustering is available, the proposed technique has the potential to better use this information than a conventional inversion strategy.

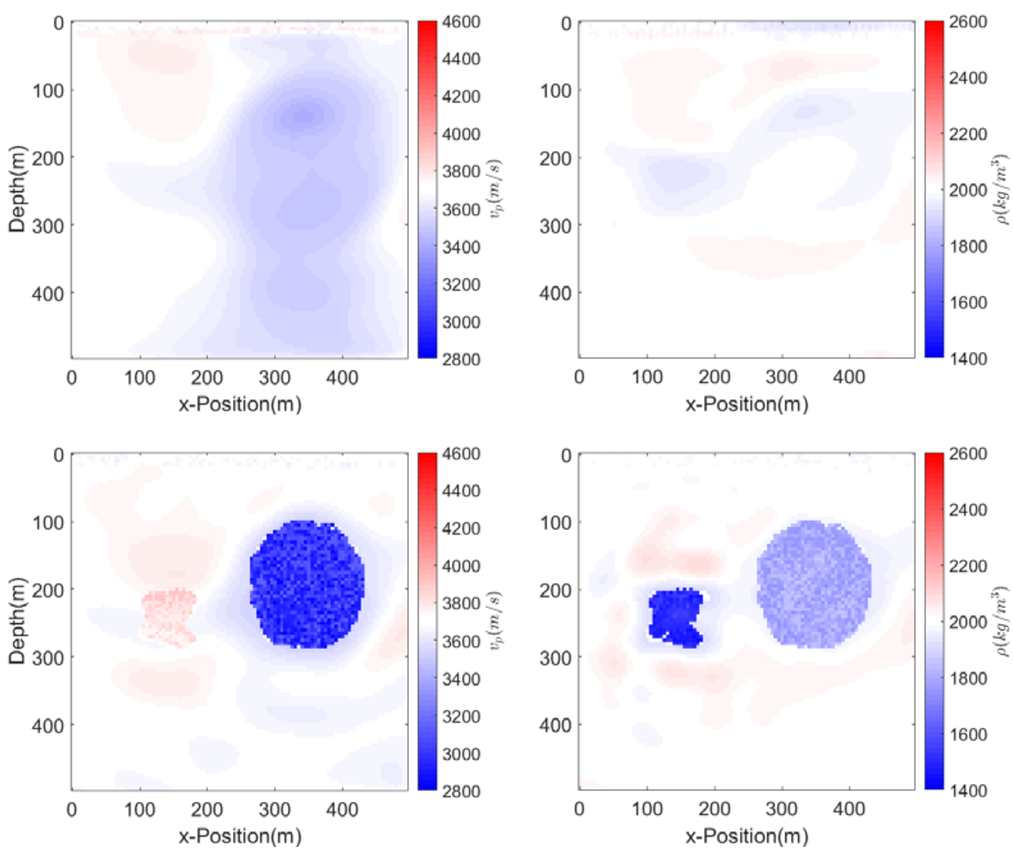

FIG. 1. Synthetic test results in P-wave velocity (left column) and density (right column), where information about rock-types in the inversion is given. Conventional FWI (top row) relies on local optimization and struggles to move model elements between property clusters. The tunneling approach (bottom row) uses nonlocal prior information to allow tunneling between rock physics clusters, improving results.

Time-lapse VSP results from the CaMI Field Research Station

Brendan J. Kolkman-Quinn* and Don Lawton

ABSTRACT

The Containment and Monitoring Institute operates a carbon sequestration Field Research Station (CaMI.FRS) where 15 tonnes of CO_2 have been injected between 2017 and 2019. Walk-away vertical seismic profiles (VSP) were collected in 2017, 2018, and 2019, for the purpose of time-lapse monitoring of the CO_2 plume. Two geophone and three straight-fiber DAS walk-away VSP datasets were processed. The repeatability of the time-lapse data was measured by comparing the normalized-root-mean-square and predictability values of the various datasets. High amplitude, near-offset shots resulted in large residual amplitudes and were excluded from the time-lapse results. The geophone data was found to have significantly better repeatability than the DAS data. NRMS values as low as 8%-12% were obtained for the geophone data, compared to lowest values of 21% to 29% for the DAS data. The 18m offset of the 2019-2017 geophone datasets showed a negative amplitude anomaly with positive side-lobes. This anomaly was broadly consistent with expectations of the CO_2 plume's effect on reflection amplitudes. Confidence in this interpretation was low. The anomaly was confined to one 3m binned trace in one dataset, and not far above the background residual amplitudes. No anomaly was evident in the 2019-2018 time-lapse, between which 7t of CO_2 had been injected. Applying a time-variant inverse-Q filter to the data improved vertical resolution but exacerbated amplitude residuals, worsening the repeatability metrics. Confident interpretation and characterization of the CO_2 plume will require more repeatable, consistent time-lapse results. The cause of low repeatability was attributed mainly to scaling issues between time-lapse surveys, as opposed to specific processing steps in the standard VSP workflow. Better matching of amplitudes between baseline and monitor shot gathers is critical to reducing background residual amplitudes in the time-lapse results.

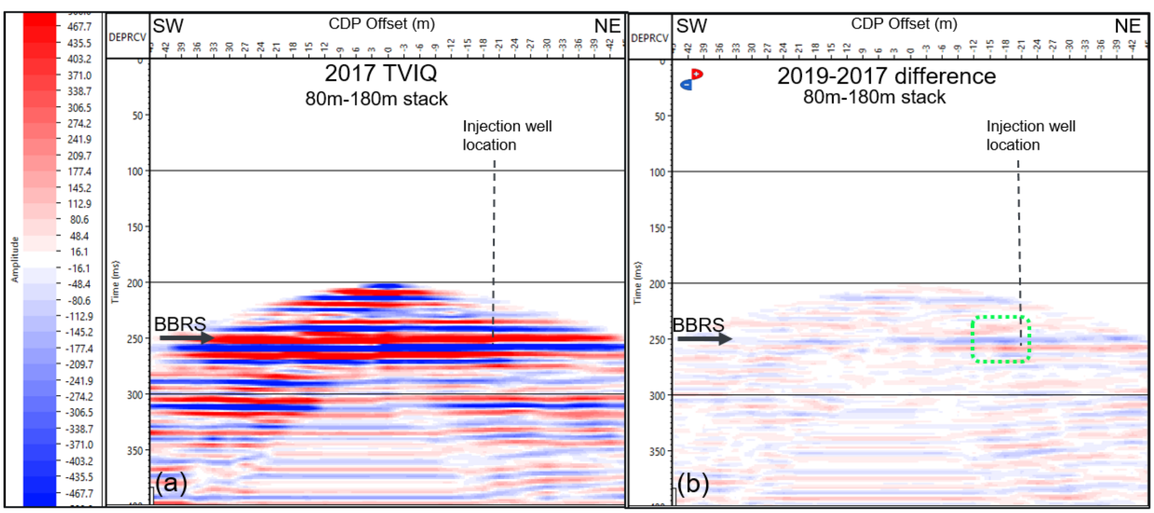

FIG. 1. (a) Geophone 2017 baseline 80m-180m stack with time-variant inverse Q filter applied, and 2019-2017 time-lapse difference (b). Green box indicates negative amplitude anomaly.

GPU tools for seismic wave modelling

Michael P. Lamoureux, Da Li, and RJ Vestrum

ABSTRACT

Current computer desktops and laptops host dedicated graphics processing units (GPUs) which are typically used to speed up computations related to video display on the device. We can take advantage of the integrated GPU to speed up numerical calculations, making effective of parallel processing form of this architecture for raw code acceleration. This article summaries our experience in creating a teaching tool that demonstrates the use of the GPU to model seismic wave propagation in two dimensions, which runs sufficiently fast in real time to make it an enjoyable instructional device. The code is written in a Jupyter notebook, which is a computation tool that has been described in the journal **Nature** as *"the data scientists' computational notebook of choice."* Links are provide to run the demo on your own machine, via a virtual machine hosted online.

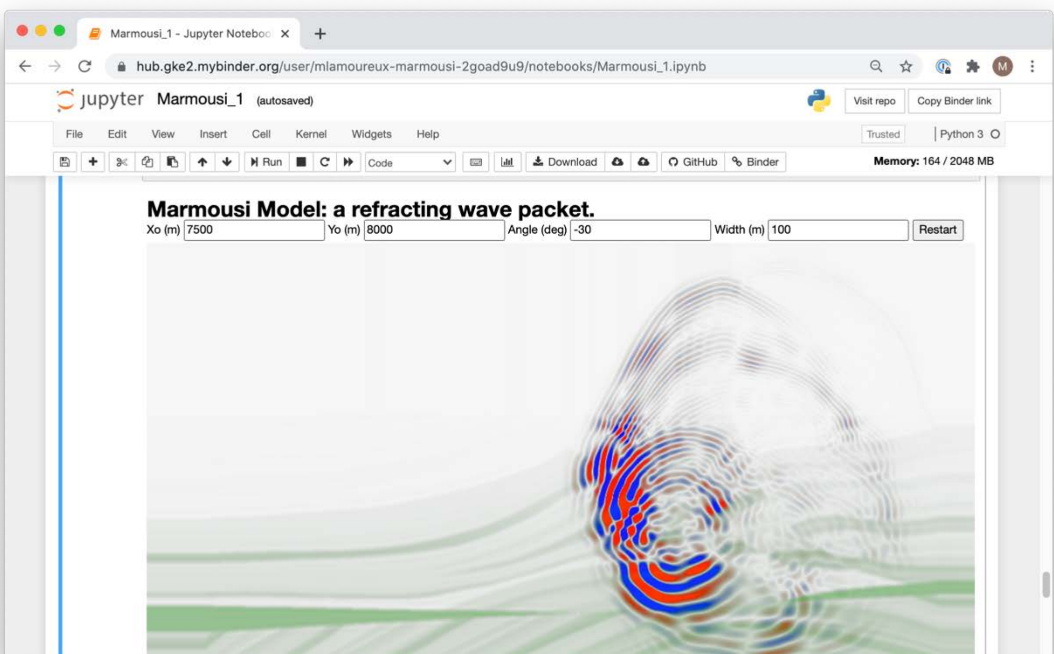

FIG. 1. GPU demo of seismic wave propagation in Marmousi, using a Jupypter notebook.

The application of stereotomography to the Hussar 2D survey

Bernard Law* and Daniel Trad

ABSTRACT

The advantages of stereotomography (Sword 1987, Billette 1998) over classical reflection tomography (Bishop et al.1985; Chiu and Steward,1987) include the additional data measurements of shot and receiver ray parameters and the elimination of the requirement to pick continuous reflection events on pre-stack data. We use the Marmousi model to demonstrate the accuracy of stereotomography. We also use the Hussar data set and well logs to demonstrate the data preparation, the picking procedure and the quality of the stereotomography solution.

Stereotomography

Stereotomography estimates the velocity model and ray path parameters by minimizing the differences between the observed and modelled measurements in the data space.

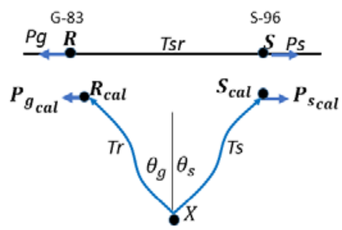

Model space: $\mathbf{m} = [(X, \Theta_s, \Theta_r, T_s, T_r)_{i1=1,N}], [V]_{i2=1,M}]$

Data space : $\mathbf{d} = \left[S, R, P_s, P_g, T_{sr}\ \right]_{j=1,N}$

Fréchet derivative: $A_{ij} = \frac{\partial(S,R,P_s,P_g,T_{sr})}{\partial(X,\Theta_s,\Theta_r,T_s,T_r,V)}$

Inversion: $\mathbf{A}\,\Delta\mathbf{m} = \Delta\mathbf{d}$

Billette and Lambaré 1998

Marmousi model

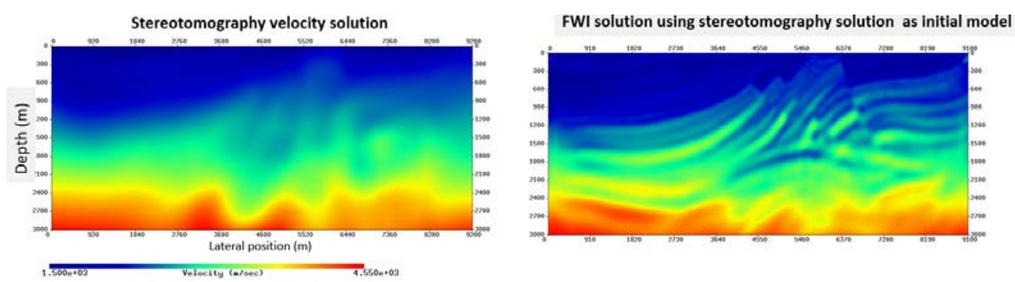

Hussar vertical component data

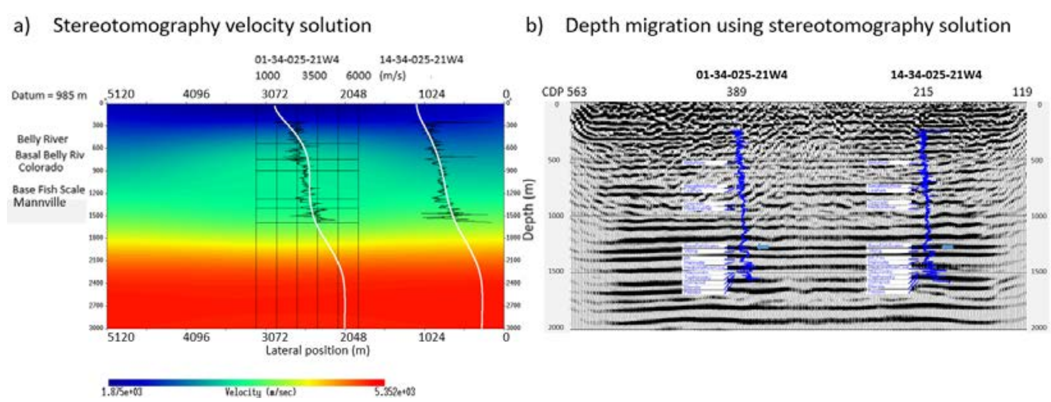

Squid: An innovative new ground-coupled electric seismic source for seismic monitoring

Don Lawton*[11], Trent Hunter[2], Brendan J. Kolkman-Quinn[1], Malcolm Bertram[1], and Greg Maidment[3]

ABSTRACT

A new seismic source has been tested at the Containment and Monitoring Institute Field Research Station (CaMI.FRS) in Newell County, Alberta. The 'Squid' source is a patent pending surface source leveraging the dynamics of an atmospheric plasma discharge in a water filled reactor. The reactor is configured to convert the internal acoustic dynamics into a high-power vertical force output. The system is a fully electric, single channel, low discharge energy, fast repeating impulse generator that can be grid, generator or solar powered.

At the FRS the source was coupled to the ground by bolting it to a thick steel plate at the top of a helical pile that had been screwed into the ground to a depth of 24.7 m. The Squid source triggered a Geode seismic system that recorded vertical seismic profile data from 24 3-component geophones in an observation well over a depth range from 191 m to 306 m below surface, with a geophone interval of 5 m. Good quality data were acquired with a single shot (3.6 kJ energy). The SNR improved significantly after a 50-shot stack. Figure 1a shows a cartoon of the source coupling to bedrock and Figure 1b shows a flattened prestack VSP gather from a source point that is 62 m offset from the observation well. The data exhibit a frequency band from 10 to 180 Hz. The travel times of the downward propagating wavefield indicates that the Squid source is coupling well to the subsurface bedrock through the base of the pedestal.

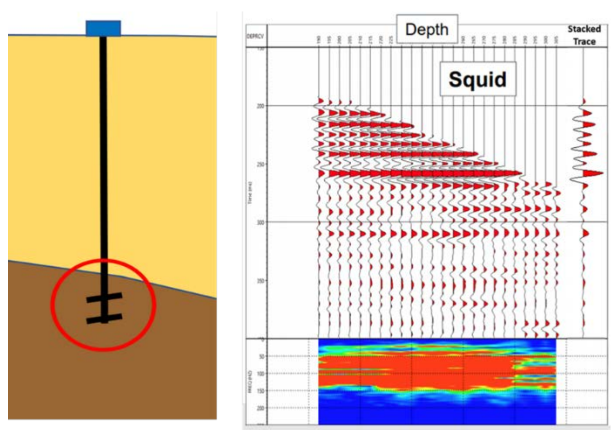

(a) (b)

FIG. 1. (a) Source coupling to bedrock through pedestal; (b) Pre-stack processed VSP gather and stack.

[1] CREWES, University of Calgary
[2] 3PTechnologies Inc
[3] CMC Research Institutes Inc.

Incorporating multiple a priori information for full waveform inversion

Da Li*, Michael P. Lamoureux, and Wenyuan Liao

ABSTRACT

Full waveform inversion (FWI) is a powerful data-fitting procedure for the seismic inversion problem. However, it suffers the local minimum problem when the accurate initial model is not available because of the nonlinear nonconvex structure of the objective function. Our initial idea in this work is that a better inverse result can be expected when more a priori information of the physical model is provided. We propose a numerical scheme which can incorporate multiple a priori information to the optimization problem. First, a scaled gradient projection method on adaptive constraint sets is provided which is compatible with the inexact projection algorithm. Next, we incorporate a priori information as convex constraint sets. Then, the FWI problem is solved as a constraint optimization problem on the intersection of the constraint sets as the feasible set. Numerical examples with box constraints, total variation constraints, and l^1 constraints on the cross-well model and the reflective seismic wave model are provided.

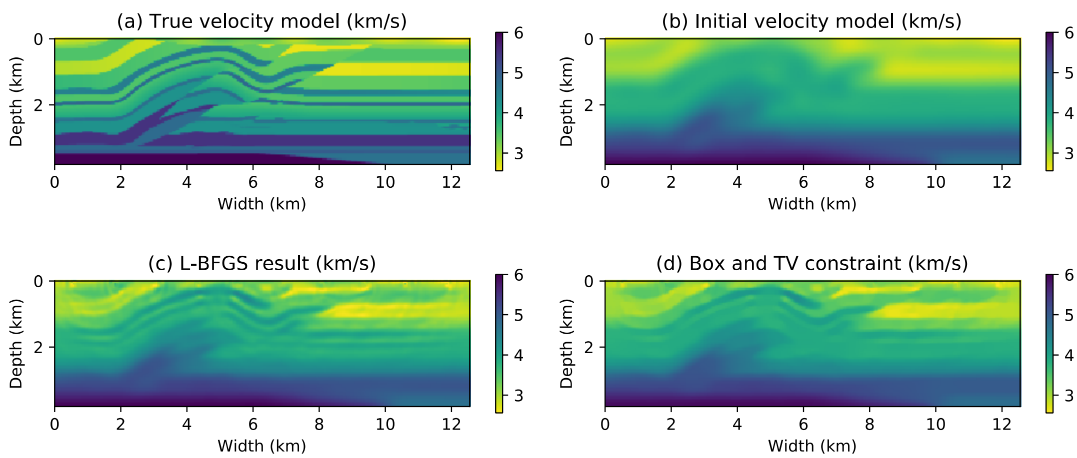

FIG. 1. demonstration of the FWI problem with box and total variation constraints. (a): true velocity model. (b) initial velocity model. (c): Inverse result of L-BFGS method. (d): Inverse result of proposed method with box and total variation constraints.

Acoustic full waveform inversion in time domain using blended data

He Liu*, Daniel Trad, and Kris Innanen

ABSTRACT

Cost is the primary factor that needs to be considered for the seismic data acquisition and processing. Super-shot or blended data strategy has been used in marine and land seismic surveys to reduce acquisition costs by reducing the number of recording times. Full waveform inversion (FWI) has been used to estimate high-resolution subsurface velocity models. However, it suffers from expensive computational cost for matching the synthetic and the observed data. Once the super-shots are acquired, conventional FWI methods would require a de-blending process for super-shots. To reduce the costs of both data acquisition and processing, FWI using blended data without the de-blending stage has been recognized very promising in future oil exploration. In this work, we accelerate the FWI process using different source-encoding strategies and compare their perfomance. The synthetic examples show that amplitude and random time delay encoding provide slow convergence rate and less satisfactory inversion results. The dynamic combined source-encoding strategy converges fast, providing updated velocity with ignorable artifacts. While the static combined source-encoding strategy provides the fast convergence rate as well as good estimation of velocity model. In addition, it requires the minimum computational effort cost since we can directly simulate the super-shots without the blending stage.

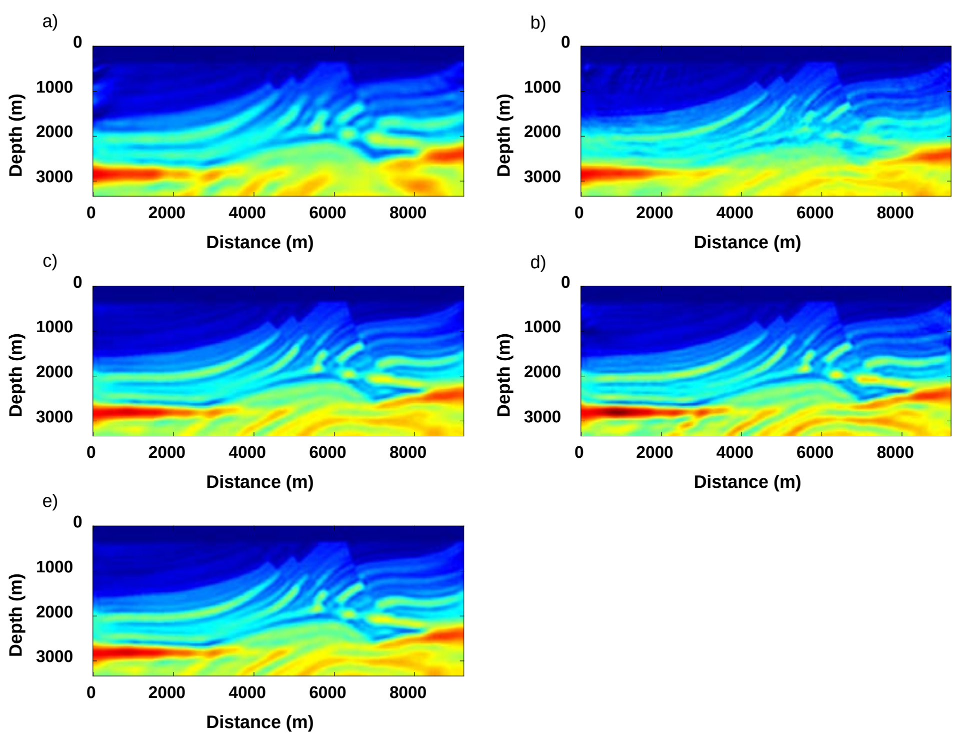

FIG. 1. Inversion results after 150 iterations: (a) amplitude encoding; (b) random time delay; (c) random polarity; (d) static encoding; (e) dynamic encoding.

A First-Order qP-Wave Propagator in 2D vertical transversely isotropic (VTI) media

He Liu* and Kris Innanen

ABSTRACT

In a vertical transversely isotropic (VTI) medium, quasi-P (qP) and quasi-SV (qSV) waves are intrinsically coupled as described in elastic wave equations. Therefore, when we perform elastic reverse time migration and imaging processes to qP-waves, qSV-wave energy will introduce crosstalk noise to the imaging results. Many authors have proposed to separate qP-waves from elastic waves for better imaging results. As an alternative way, some authors have proposed to directly simulate qP-waves with modified elastic wave equations. In this study, we develop a first-order wave propagator of pseudo-pure-qP-wave in 2D heterogeneous VTI media using staggered-grid scheme. We have performed this algorithm to simulate P-waves propagating in an isotropic medium, VTI media with weak/strong anisotropy and a two-layer VTI model, the synthetic results validate the feasibility of this algorithm. Also, we adopt the first-order Hybrid-PML in the simulation, which helps the simulation efficiency due to its better performance for anisotropic media.

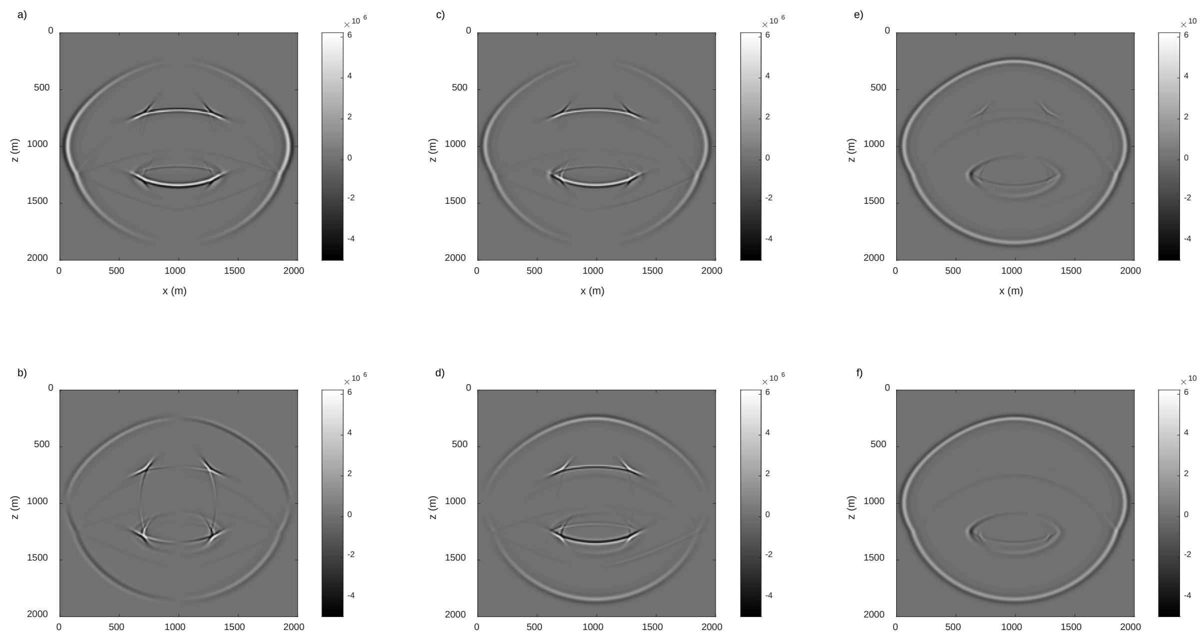

FIG. 1. Synthetic wavefields in a layered VTI model: a) x- and b) z-component simulated by original elastic wave equations; c) x- and d) z-component simulated by first-order pseudo-pure-qP-wave equations; e) summation of qP-wave components; f) separated scalar qP-wave.

Microseismicity detection and ambient noise correlation at the CaMI Field Research Station, Newell County, Alberta, Canada

Marie Macquet, Don Lawton, and J. Helen Isaac

ABSTRACT

We present the continuous seismic data recorded at the CaMI Field Research Station and present results obtained with various methods. We focus here on the microseismicity detection using the STA/LTA method, and on the ambient noise correlation method, applied to imaging and monitoring.

The STA/LTA method is applied on borehole continuous seismic data and detects 10's of thousands of events. The parameters chosen (STA, LTA and threshold) change the absolute number of detected events but the temporal distribution remains the same. We observe an increase in the number of detected events from February to end of March, and the number reduces after end of March. If some days of injection show a large number of detected events, some days without injection also show a large number of events. The frequent human activity (both at the site and in the surroundings) makes difficult to draw conclusions without a better discrimination between human produced events and injection related events.

The ambient noise correlation method is used to produce a near-surface V_S model which is compared with the one obtained with S-wave active source refraction analysis. Ambient noise correlation is also used to try to track the velocity change due to CO_2 injection trough the Moving-Window Cross Spectrum analysis applied on the reconstructed Green's function. A last application using this method is the attempt to reconstruct body waves, especially using the downhole continuous seismic data. Preliminary results show a good reconstruction of the body wave when correlating a surface station with downhole stations (Figure 1).

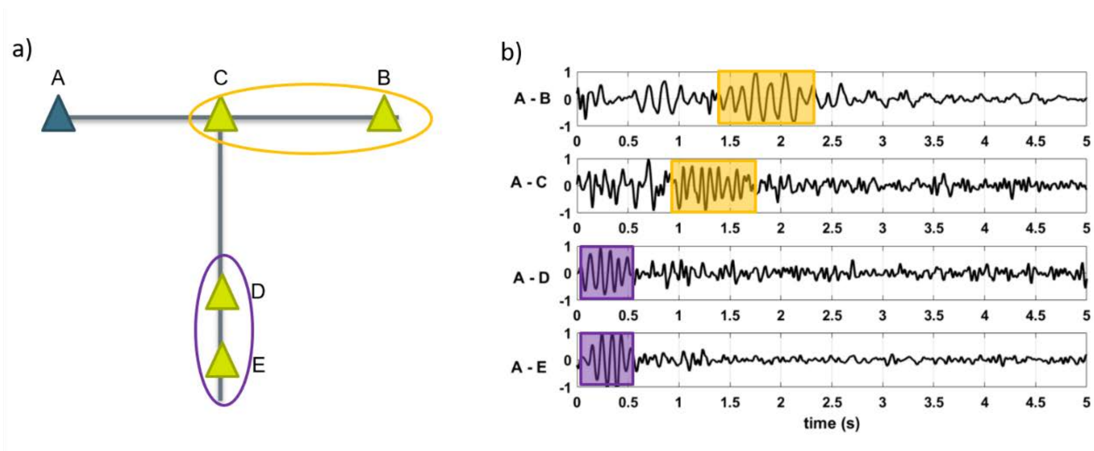

FIG. 1. Reconstructed Green's function using ambient noise correlation. a) Schematic location of the 5 stations used for the test. b) Reconstructed Green's function between A and the 4 other stations. Orange boxes highlight the surface wave, visible for the stations located at the surface, purple boxes highlight the body wave, visible for the station located in the observation well.

A comparative study of different DAS vendors data

Jorge E. Monsegny*, Daniel Trad, and Don Lawton

ABSTRACT

Distributed acoustic sensing is a technology with a high potential for seismic monitoring. Apart from the optical fibre, that is the sensing element and replaces the traditional geophone, the other part of this system is the interrogator that transforms the backscattered light from the fibre into a digital seismic signal. The fibre is usually installed permanently but the interrogator is interchangeable by newer and more sophisticated models but also by different vendors models. We compare distributed acoustic sensing data obtained at the same locations, with the same sources and optical fibre, and almost at the same frame time but generated by interrogators from three different vendors, at the Containment and Monitoring Institute Field Research Station in Alberta, Canada. We confront the DAS datasets before and after filtering and against vertically oriented geophone data. We confront the DAS datasets before and after filtering and against vertically oriented geophone data. We found that after some data conditioning, all vendors agree in wave character at the early times, however, at later times there are delays in the events arrivals that depend on the trace depth.

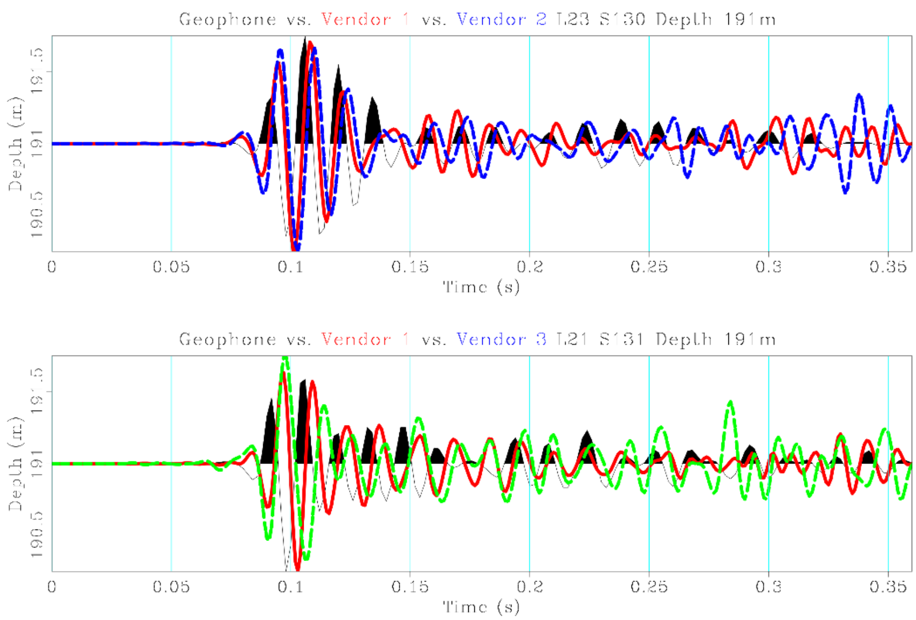

FIG. 1. Traces at 191m depth from geophone and DAS data. On the top the shot point is the 130 from line 23 and the DAS vendors are 1 and 2. On the bottom the shot point is the 131 from line 21 and the DAS vendors are 1 and 3. In the case of the first set, there is a small phase difference between Vendor 1 and Vendor 2 traces at the first arrivals. Then, the phase difference starts to increase with time. At the end both traces are totally out of phase. With respect to the relative amplitudes, they mostly agree in the first half, but towards the end the amplitudes of the Vendor 2 trace are noticeable higher than the vendor 1 trace. In the case of the second set, both DAS traces start at the same time but then they go out of phase and return to in phase three times. When they are out of phase it seems to be a small lag. The relative amplitudes coincide in the first arrival events but is different for some events towards the end of the traces.

Depth calibration of DAS VSP data at CaMI Field Research Station

Jorge E. Monsegny, Daniel Trad and Don Lawton

ABSTRACT

The correct localization of vertical seismic profile data in the surrounding geology is a very important step during processing and interpretation. Geophone data usually have very accurate positions along the well that help in this localization. In contrast, distributed acoustic sensing data positions are not as accurate because they do not have point locations like geophones and because of the imperfect knowledge of the fibre location in the well and surface. We test two methods to calibrate the depths of distributed acoustic sensing vertical data from the Containment and Monitoring Institute Field Research Station. The first method uses the frequency spectra but requires the presence of patterns related to the well casing. The second method correlates consistent scalars from the seismic data with the sonic log to obtain a vertical shift. Only the second method gave us values to calibrate the data with the geology.

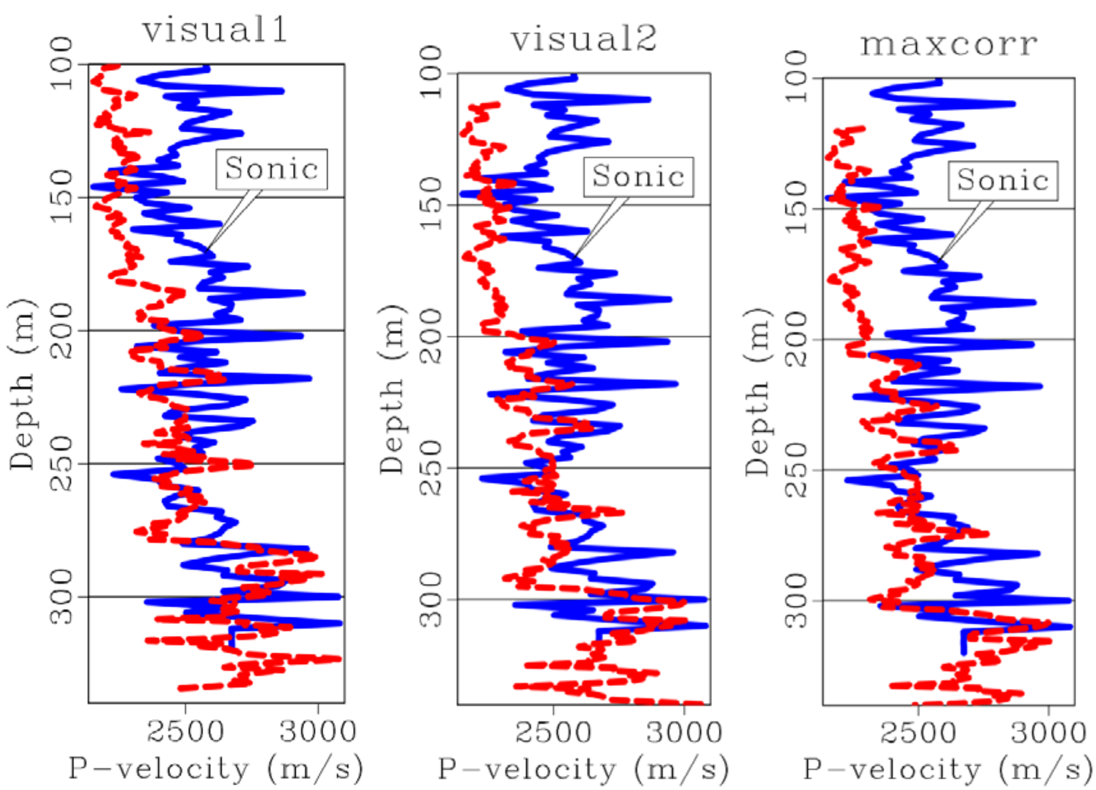

FIG. 1. Three different vertical shifts of the consistent scalars, in dashed lines, with respect to the sonic log. On the left, the vertical shift is 4.5m upward to line up the three peaks in "zone 1". On the center, the shift is 12m downward to align the two peaks in "zone 2". On the right, the shift is 19.5m upward, obtained from the lag of the cross-correlation maximum between the consistent scalars and the sonic log.

Least Squares DAS to geophone transform

Jorge E. Monsegny*, Kevin W. Hall, Daniel Trad, and Don Lawton

ABSTRACT

Distributed acoustic sensing uses optical fibre to measure strain or strain rate along the fibre direction. In contrast, geophones are equipped with a spring-mass system that measures the particle velocity in the direction of this spring-mass system. The strain rate estimated by distributed acoustic sensing is related to the total displacement of a section of the fibre called gauge length. By using this link between strain rate and displacement we propose a least squares inversion scheme to obtain particle velocity along the fibre from strain rate in a distributed acoustic sensing system. We test this least squares transformation with data from the Containment and Monitoring Institute Field Research Station in Alberta, Canada. We found that the transformed traces are very similar to a filtered version of the corresponding geophone ones, in particular at early times.

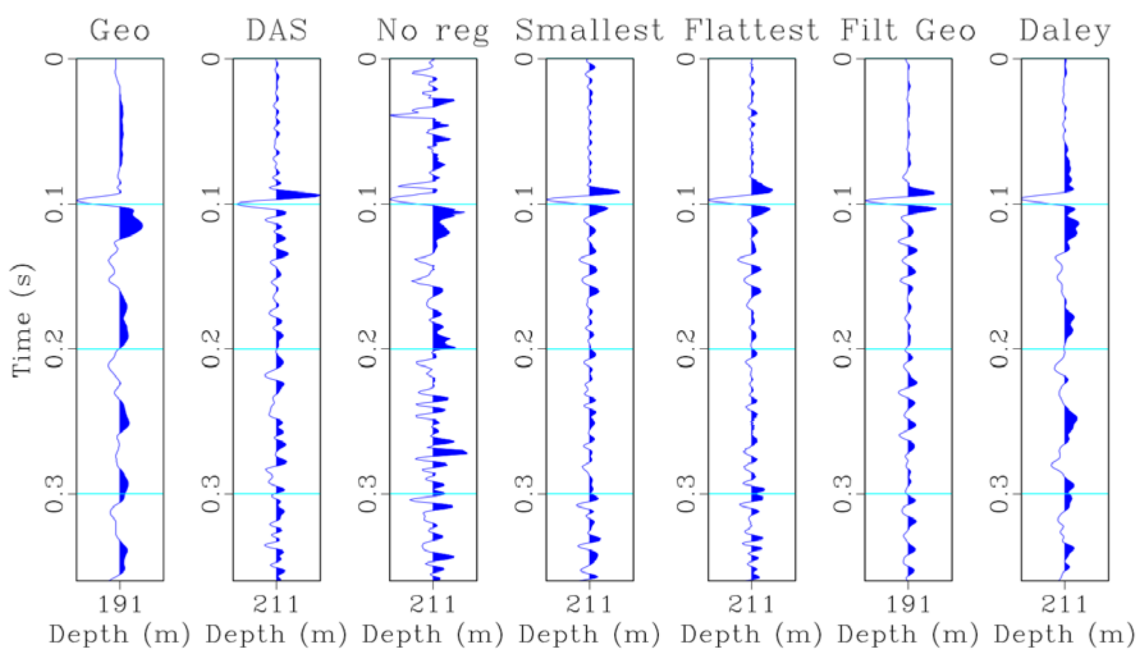

FIG. 1. Selected traces from the vertical geophone, DAS and inverted datasets. Geophone trace is at 191m depth in the well while DAS traces are at 211m along the fibre. From left to right, the first trace is the geophone response. The second is the DAS response. Without using regularization, the third is the inverted geophone response from the DAS data. Fourth uses smallest regularization. Five uses flattest regularization. Sixth is the high frequency part of the geophone response. Last is the Daley transform of the DAs trace.

Reverse time migration approaches for DAS VSP

Jorge E. Monsegny, Daniel Trad, and Don Lawton

ABSTRACT

Distributed acoustic sensing is a promising technology for seismic monitoring that uses optical fibre as a sensing element instead of geophones. In contrast to geophones, it produces a signal proportional to the strain, or strain rate depending on the vendor, instead of particle velocity. To apply processing techniques, like migration, this strain is usually transformed to particle velocity. We perform the migration directly in the strain domain and an associated pressure domain by modifying the wave equation. We compare their results on the reflectivity by using a synthetic model and compare the migration results with data from the Containment and Monitoring Institute Field Research Station. In the synthetic example we obtained a good match between the migrated amplitudes at the reflector depth and the theoretical reflection coefficients. The real data migrations showed a quality like the usual path of transforming to vertical particle velocity before migration.

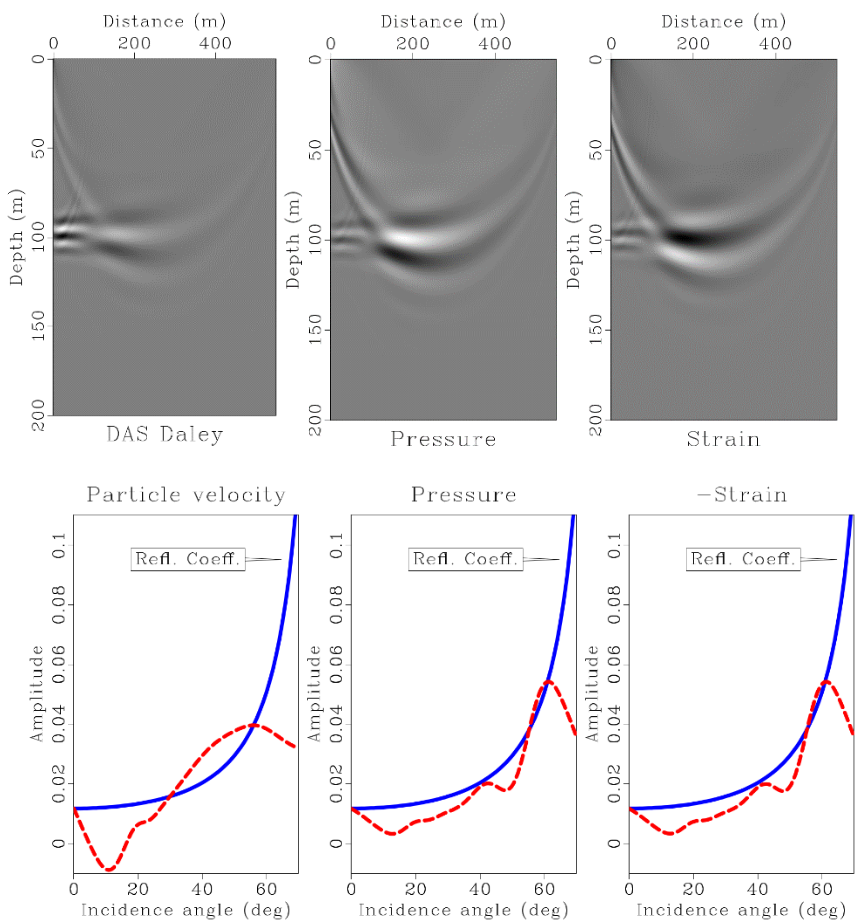

FIG. 1. Synthetic data RTM. On the left is the usual vertical particle velocity RTM. On the middle is the pressure RTM, while on the right is the strain RTM. Theoretical geophone reflectivity and amplitudes extracted at the reflector depth, 100m. The extracted amplitudes were stretched and shifted vertically to match the theoretical curve. Note that we are plotting the extracted amplitude strain with opposite polarity.

Experiments on constructing seismic using generative adversarial network

Zhan Niu* and Daniel Trad

ABSTRACT

Supervised machine learning attracts great attention in all areas of science. In Geophysics, however, supervised learning has the problem that available labelled data is often insufficient, limiting the chance of converging during training and harming model generality. As a solution, researchers explore ways to generate synthetic data for use in training. In this report, we explore the methodology of generating 1D data with a generative adversarial model. Both the generator and discriminator are convolutional, and the noise vectors are fed along the channel dimension to the generator. The networks are successfully trained via Wasserstein loss with gradient penalty and careful hypermeter tuning. We evaluate the trained networks quantitatively and qualitatively. We attempt to find the optimal stopping point for the training, however, the conclusion cannot be made during the training and part of it remains subjective.

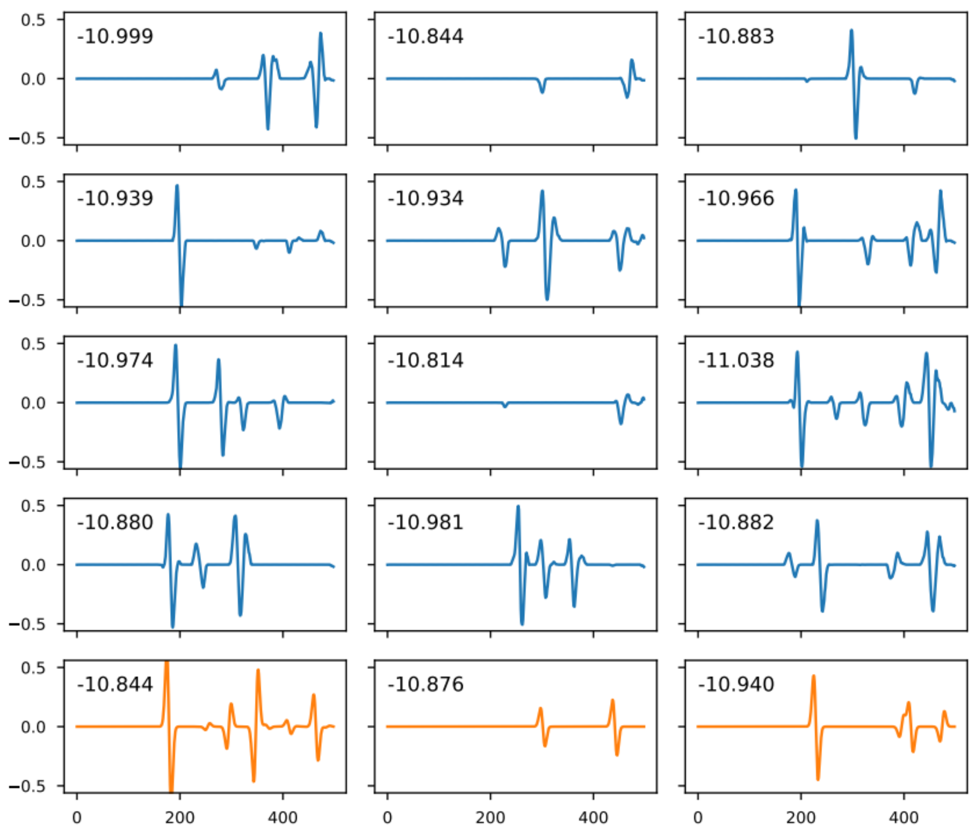

FIG. 2. The results from the trained generator. The blue curves refer to the generated traces while the orange traces are from the data. The numbers on the upper right in each subplot refers to the scores obtained from the discriminator. The higher the score, the better it looks from the perspective of the discriminator.

Sensitivity kernel analysis for time-domain viscoelastic full-waveform inversion based on the GSLS model

Wenyong Pan and Kris Innanen

ABSTRACT

Viscoelastic full-waveform inversion (FWI) is promising to build high-resolution sub-surface velocity and quality factor Q models. Based on the generalized standard linear solid model, the attenuation effects on propagating waves can be simulated with the superposition of parallel relaxation mechanisms. However, discrepancies exist between the frameworks for constructing the sensitivity kernels in viscoelastic FWI: (I) Charara derived the sensitivity kernels for unrelaxed moduli and attenuation parameters with a perturbation approach based on Born approximation; (II) Tromp proposed to construct the Q sensitivity kernels by introducing additional adjoint source based on the Kolsky-Futterman model and frequency domain Born scattering integral; (III) Fichtner derived the sensitivity kernels for relaxation functions and Q following the adjoint-state method. The Q sensitivity kernels were constructed with the strain memory variables. This study revisits the theories of these frameworks for constructing the viscoelastic FWI sensitivity kernels. In the numerical modeling section, we calculate the sensitivity kernels within these different frameworks for comparison. Synthetic experiments are carried out to evaluate their inversion performances. We have found that the Q sensitivity kernels constructed with memory variables can resolve the Q anomalies better suffering from fewer trade-off artifacts and uncertainties in the presence of velocity errors.

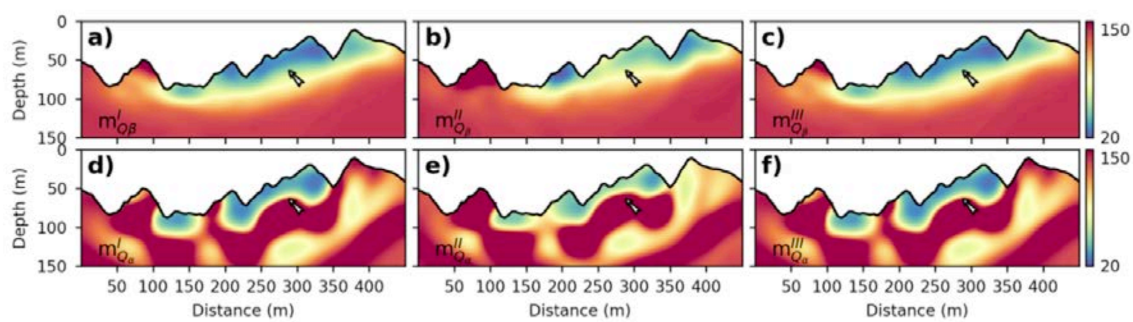

FIG. 1. (a-c) are the inverted Qβ models with the initial velocity models using SWs in framework-I, -II and -III, respectively; (d-f) are the inverted Qα models with the initial velocity models using BWs in different frameworks.

Waveform Q tomography with central-frequency shifts

Wenyong Pan

ABSTRACT

Subsurface Q (quality factor) structures can provide important constraints for characterizing hydrocarbon reservoirs and interpretating tectonic structures and evolution of Earth in exploration and earthquake seismology. The damping effects of attenuation on seismic amplitudes and phases can be modeled based on the generalized standard linear solid (GSLS) rheology. Compared to traditional ray-based methods, full-waveform adjoint tomography is promising to provide more accurate Q models by numerically solving the viscoelastodynamic wave equation. However, the progress of adjoint Q tomography is impeded by the difficulties of calculating Q sensitivity kernels and significant velocity-Q trade-offs. In this study, following the adjoint-state method, I derive the Q (P- and S-wave quality factors QP and QS) sensitivity kernels, which can be efficiently constructed with memory strain variables. A new central-frequency difference misfit function is designed to reduce the trade-off artifacts caused by velocity errors for adjoint Q tomography. Compared to traditional waveform-difference misfit function, this new misfit function is less sensitive to velocity variations and thus can invert for the Q models more stably suffering fewer trade-off uncertainties.

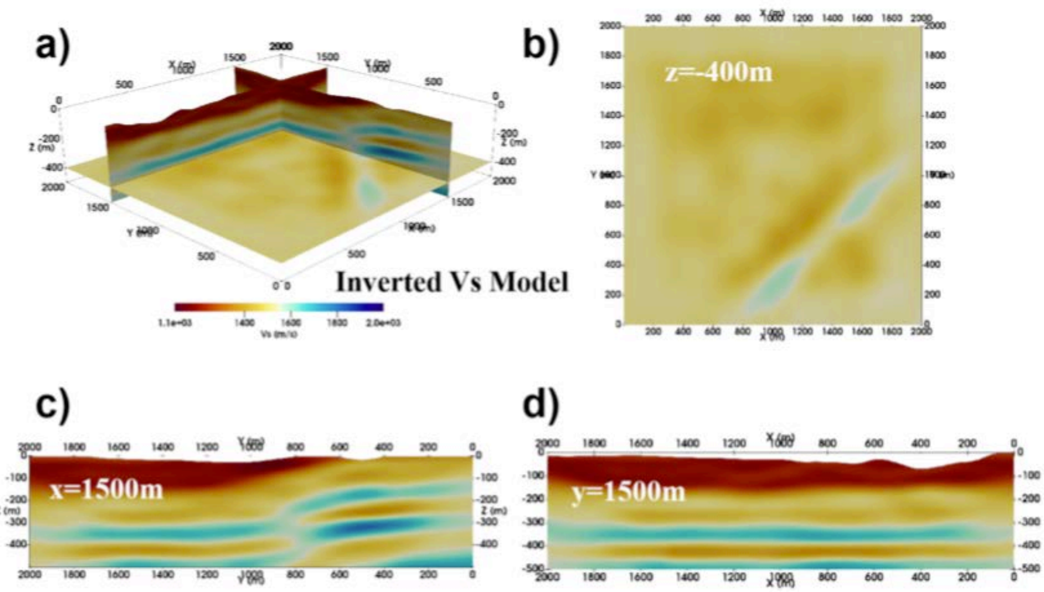

FIG. 1. Recovered VS (a), with depth and lateral slices (b-d).

2D surface wave inversion : Multioffset MASW vs FWI

Luping Qu*, Wenyong Pan, and Kris Innanen

ABSTRACT

Two major methods for 2D near-surface investigation are the Multi-offset MASW (MO-MASW) and surface-wave full waveform inversion. We test these two methods and analyze their limitations and advantages. MO-MASW can roughly detect and locate the abrupt lateral variation. However, it has difficulties in resolving irregular anomalous bodies or complex subsurface velocity structure. Full waveform inversion method overcomes these problems by providing a detailed subsurface shear-wave velocity structure, but easy to fall into local minimum since surface wave has a shorter wavelength. We test the surface wave full waveform inversion method on synthetic models containing high-velocity and low-velocity anomalous bodies. To avoid the cycle skipping, misfit function, combining waveform-difference and envelop-difference, is adopted, and a frequency-decreasing multi-scale approach is incorporated. From our synthetic tests, we find besides the negative and positive velocity anomalies, the nested velocity anomalies can be well recovered as well. At last, a preliminary test on surface-trenched DAS data is conducted using this multi-scale full waveform inversion process.

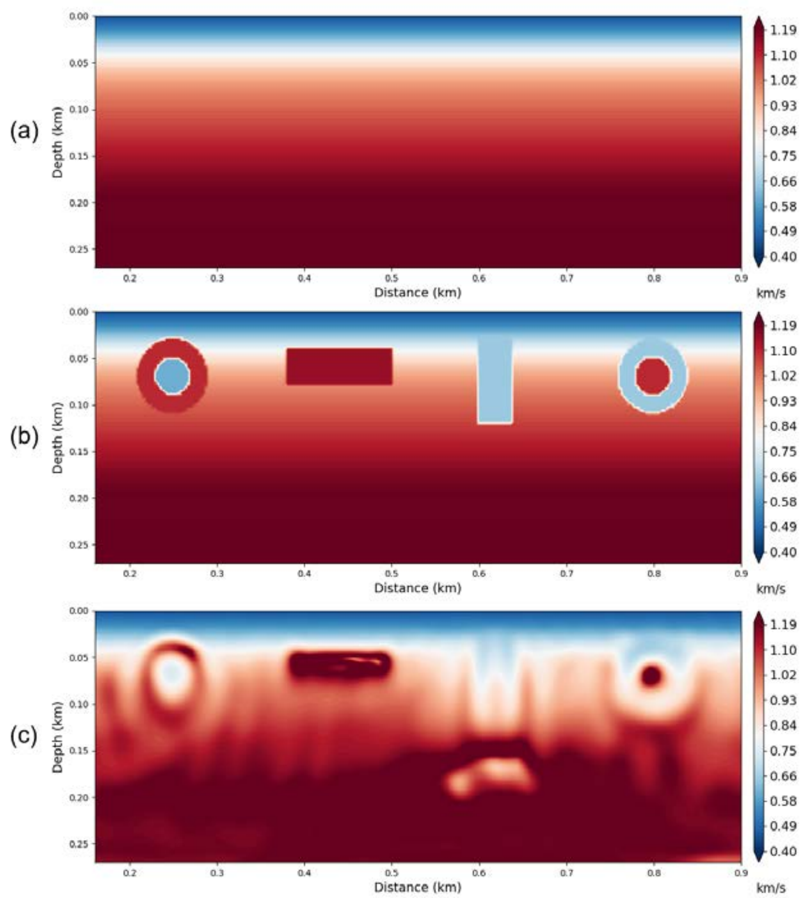

FIG. 1. Shear wave velocity model. (a) True Vs model. (b) Initial Vs model. (c) Inverted Vs model.

Sensitivity analysis of surface wave dispersion curves for various subsurface parameters

Luping Qu, Jan Dettmer, and Kris Innanen

ABSTRACT

The propagator matrix method is commonly used for inverting near-surface shear-wave velocity. An important precondition for its feasibility is the different sensitivity levels of dispersion curves with respect to shear-wave velocity, primary-wave velocity, layer thicknesses, and density. Here, we analyze the sensitivity of surface-wave dispersion-curves at different frequencies for various subsurface parameters. Not only the fundamental mode, higher-order modes extending to the fourth higher-order mode are all included in this study. From the analysis, higher modes are more sensitive to parameters in the deeper area. Besides, the sensitivity analysis is conducted on the phase-velocity, the group velocity, and their derivatives, respectively. Through comparing various types of observing data, the phase velocity derivative is more sensitive to parameter perturbations in the same wavelength range. However, its sensitivity shows simultaneously positivity and negativity at different depths. While the phase velocity shows positivity exclusively. At last, inversion stability and accuracy of different types of observing data are discussed.

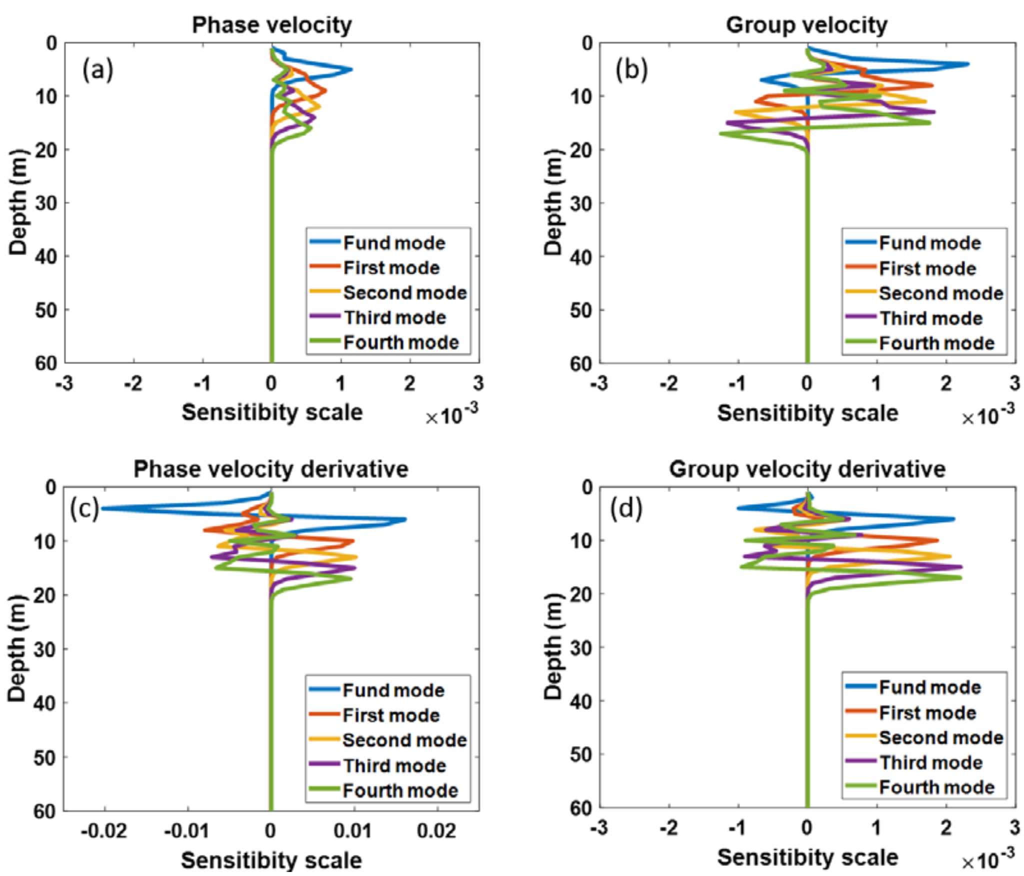

FIG. 1. Sensitivity of four types Rayleigh-wave data with respect to shear-wave velocity. (a) Phase velocity. (b) Group velocity. (c) Frequency derivative of phase velocity. (d) Frequency derivative of group velocity.

A numerical comparison of seismic inversion, multilayer and basis function neural networks

Brian Russell*[1]

ABSTRACT

In this presentation, a numerical example is used to illustrate the difference between geophysical inversion and several machine learning approaches to inversion. The results will show that, like inverse geophysical solutions, machine learning algorithms have a definite mathematical structure that can be written down and analyzed. The example used in this study is the extraction of the reflection coefficients from a synthetic created by convolving a dipole reflectivity with a symmetric three point wavelet. This simple example leads to the topics of deconvolution, recursive inversion, linear regression and nonlinear regression using several machine learning techniques. The first machine learning method discussed is the multi-layer feedforward neural network (MLFN) with a single hidden layer consisting of two neurons. The other two methods which are discussed are the radial basis function neural network (RBFN) and the generalized regression neural network (GRNN). As will be shown, all three of these networks involve different basis functions. In the MLFN the basis function is the sigmoidal logistic function and in both RBFN and GRNN the basis function is the Gaussian. However, for RBFN the weights are computed using a least-squares algorithm and in GRNN the weights are computed "on-the-fly" using the observed data. The MLFN algorithm is iterative and the key parameters are the initial random weights, the learning rate and the number of iterations. The RBFN and GRNN are not iterative and the key parameter in both methods is the width of the Gaussian, or sigma factor. Figures 1 (a) to (d) below show a comparison of the results of linear regression and the three machine learning algorithms. In all four figures, the horizontal axis represents the computed seismic amplitudes and the vertical axis represents the desired reflection coefficients. The black circles show the four training values, and the solid line shows the fitting function from the linear or nonlinear regressions. For the MLFN result, 10,000 iterations and a learning rate of 0.2 were used, and for both the RBFN and GRNN results a sigma factor of 0.5 was used.

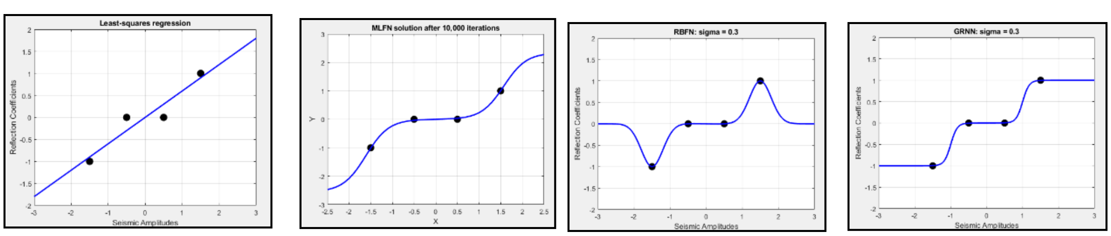

FIG. 1. The above figures show predicted reflection coefficient versus seismic amplitude for (a) linear regression, (b) the feed-forward neural network with 10,000 iterations and a learning rate of 0.2, (c) the radial-basis function neural network with sigma = 0.5 and (d) the generalized regression neural network with sigma = 0.5, where the black circles are the training points and the solid line is the fitting function.

[1] HampsonRussell, A CGG GeoSoftware Company, Calgary, Alberta, brian.russell@cgg.com

Deblending in common receiver and common angle gathers

Ziguang Su* and Daniel Trad

ABSTRACT

In specific seismic acquisition scenarios, such as ocean bottom node (OBN) surveys, there are more sources than receivers. This imbalance can be an issue since the efficiency of conventional deblending, and migration algorithms in common shot gathers (CSG) is related to the number of available traces (fold) in this gather. Therefore, we need to develop new deblending and migration algorithms that process data in domains other than CSG. Preferably, domains that have higher fold numbers than the CSG for these acquisition scenarios. Due to reciprocity, common receiver gathers (CRG) is equivalent to common shot gathers. Therefore, migration in the CRG domain is very similar to conventional migration in the CSG domain. Moreover, in the OBN case, reverse time migration (RTM) in the CRG domain saves significant memory and computational time compared to the CSG domain since the number of receivers is much smaller than the sources. Furthermore, blending interferences have an incoherence structure in CRG due to random time delays between sources, significantly improving deblending performance. This report investigates the efficiency of RTM and least-square RTM in the CRG domain as a deblending tool. Additionally, we investigate the suitability of other domains such as offset domain common image gather (ODCIG) and angle domain common image gather(ADCIG), as another domain for deblending using RTM.

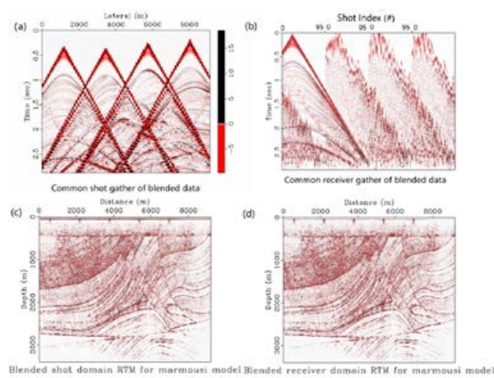

FIG. 1. a) The shot domain data, b) receiver domain data. c) shot domain RTM and d) receiver domain RTM

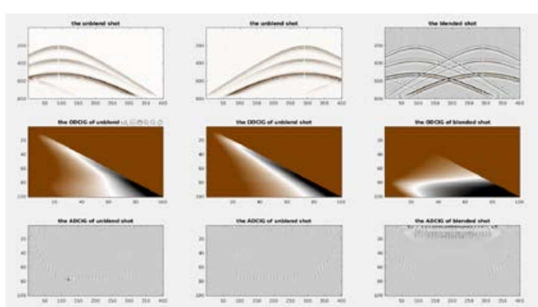

FIG. 2. The shots, ODCIG and ADCIG of unblend and blended data

Physics-guided deep learning for seismic inversion: hybrid training and uncertainty analysis

Jian Sun*, Kris Innanen, and Chao Huang

ABSTRCT

The determination of subsurface elastic property models is crucial in quantitative seismic data processing and interpretation. This problem is commonly solved by deterministic physical methods, such as tomography or full waveform inversion (FWI). However, these methods are entirely local, and require accurate initial models. *Deep learning* represents a plausible class of methods for seismic inversion, which may avoid some of the issues of purely descent-based approaches. However, any generic deep learning network capable of relating each elastic property cell value to each sample in a seismic dataset would require a very large number of degrees of freedom. We propose a hybrid network design, involving both deterministic, physics-based modelling and data-driven deep learning components. From an optimization standpoint, both a data-driven model misfit (i.e., standard deep learning), and now a physics-guided data residual (i.e., a wave propagation network), are simultaneously minimized during the training of the network. An experiment is carried out to analyze the trade-off between two types of losses. Synthetic velocity building is employed to examine the capacity of hybrid training.

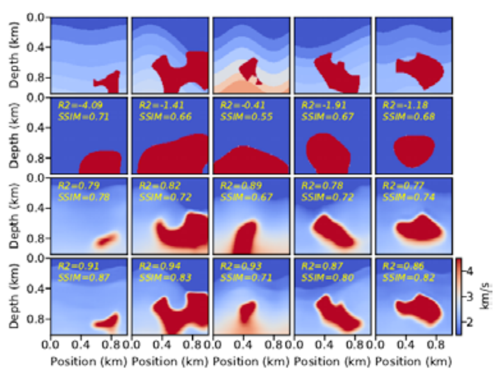

FIG. 10. Rows: ground-truth, CNN-2k, CNN-10k, and H-PGNN-2k.

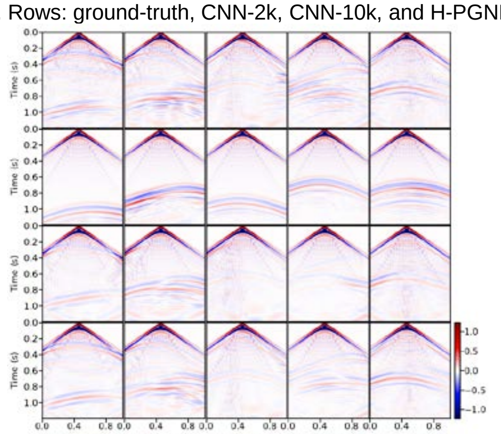

FIG. 12. Rows: ground-truth, CNN-2k, CNN-10k, and H-PGNN-2k.

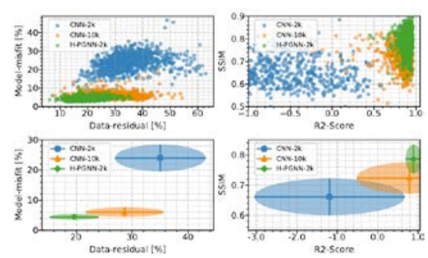

FIG. 14. Quantitative Error Analysis.

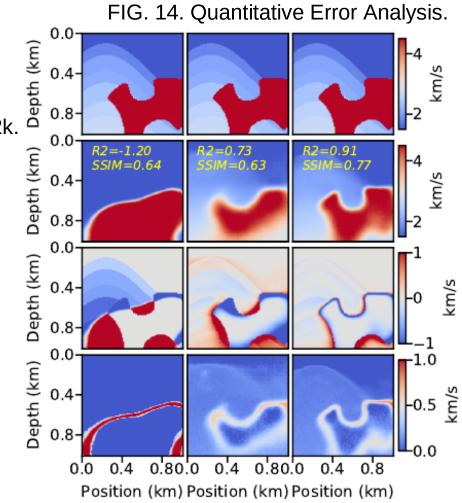

FIG. 19. The uncertainty analysis, from top to bottom, ground-truth, mean of 100 realizations, model misfits, standard deviations. Left to right: CNN-2k, CNN-10k, H-PGNN-2k.

A multigrid approach for time-domain Full Waveform Inversion

Daniel Trad*

ABSTRACT

Full Waveform inversion (FWI) is usually implemented in either time or frequency domains, and in some cases in a hybrid domain. The frequency domain (FD) formulation has some advantages: it is simple to understand in terms of matrices and permits the use of a multigrid approach consisting of bootstrapping from low to high frequencies where data bandwidth is gradually increased. A limitation of FD FWI, however, is that it becomes very expensive to calculate in 3 dimensions because a large system of equations must be solved at each frequency. The time-domain (TD) approach, however, seems to be more promising in terms of scalability. In this case, rather than solving one frequency of many shots at a time, all frequencies of one-shot are solved at a time. However, this statement is an oversimplification since parallelization and cycle skipping turn the algorithm into very different dataflow. In practice, the time domain algorithm permits to solve many shots simultaneously as well, by using parallelization in clusters with Graphics Processing Units (GPUs), leading to a very efficient implementation with coarse-grained parallelism across nodes and fine-grained parallelism across GPUs. On the other hand, additional complications arise to use a multigrid approach which is, in turn, easily done in the frequency-domain. In this report, we will discuss a multigrid time-domain implementation of Full Waveform Inversion which will also help to understand and attenuate inverse crime effects when working with synthetic data.

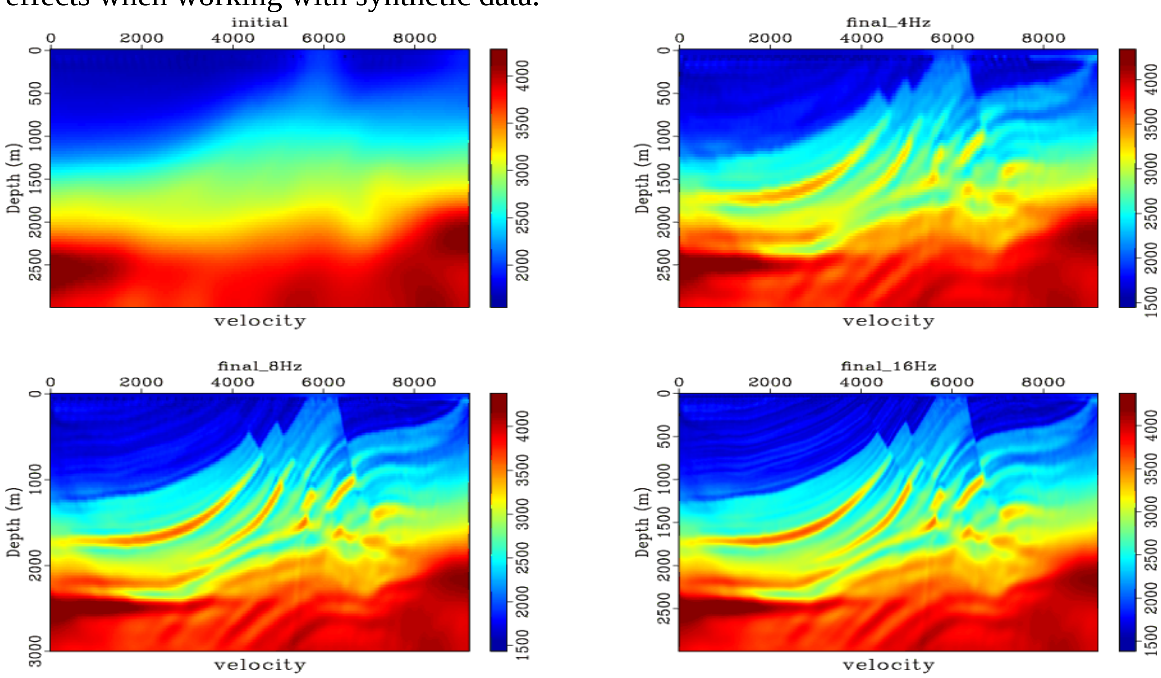

FIG. 1. Multigrid FWI for 40 shots with frequency bandwidth between 0-25Hz. a) Initial model, b) inverted model with filtered data using 4Hz dominant frequency wavelet and 32m cell size. c) Second stage starting from b) after interpolation to 16m cell size, reaching 8 Hz dominant frequency wavelet. d) Final stage starting from c) after interpolation to 8m cell size and reaching16 Hz dominant frequency wavelet. In each stage, 20 iterations were performed.

Enhanced source hardware and tank for physical modeling

Joe Wong, Kevin L. Bertram, Hongliang Zhang, Kevin W. Hall, and Kris Innanen

ABSTRACT

Enhancements made to the University of Calgary Seismic Physical Modeling System include: (1) hardware and software additions that produce arbitrary source waveforms for driving piezoelectric transducers; (2) an improved, larger water tank to support simulations of marine seismic surveys; and (3) data acquisition modules that expand the number of receiver channels to 24. This report describes (1) and (2) of these enhancements in detail. A companion report by Bertram and Wong (2020) discusses (3).

The ability to produce controlled source-waveforms increases the types of seismic physical-modeling experiments that are possible. Piezoelectric transducers driven by these controlled waveforms can be used in simulations of real-world seismic sources such as swept-frequency vibrators, impulsive sources with controlled delay times, and complex SWD signals produced by drill-bits interacting with subsurface rocks. For this purpose, we have designed and built a prototype Arbitrary Waveform Generator (AWG). The heart of the AWG is a Raspberry Pi 4B microcomputer driving an R2R resistor ladder for digital-to-analogue conversion.

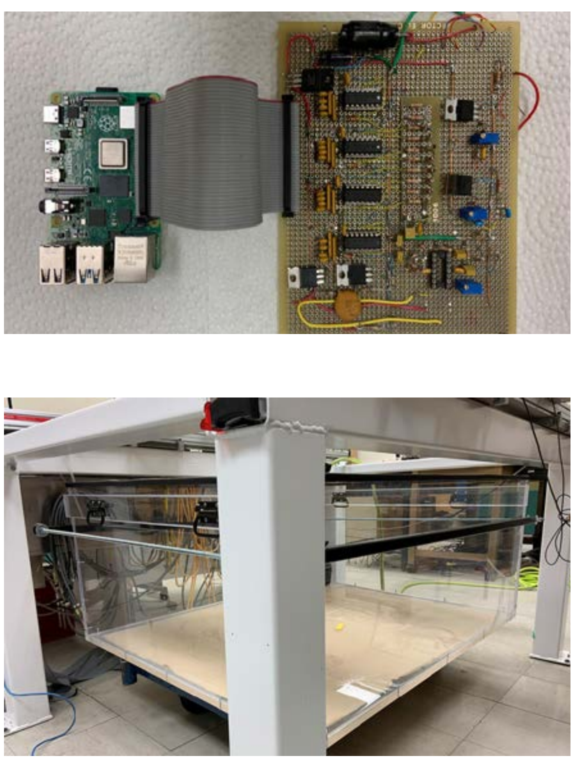

FIG. 1. **Top:** AWG showing Raspberry Pi 4B to the left and DAC circuitry to the right. **Bottom:** New acrylic water tank...

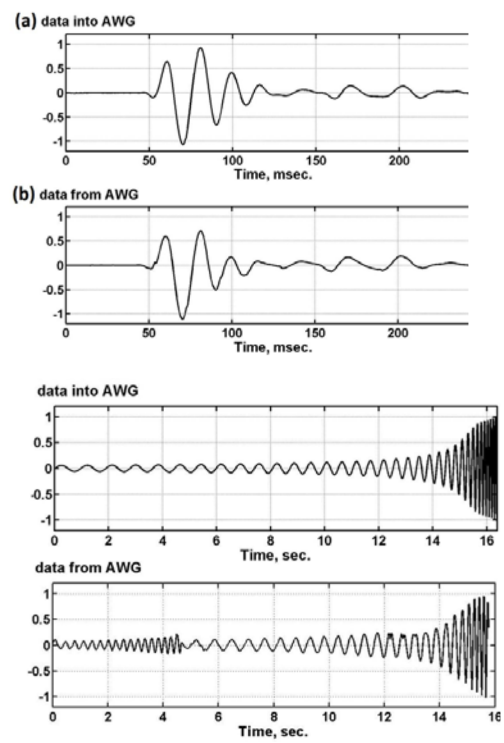

FIG. 2. AWG test results. **Top:** Input and output waveforms for a piezopin impulse response. **Bottom:** Input and output waveforms for a low-dwell Vibroseis pilot signal.

Fault Detection using Residual Neural Networks

Paulina Wozniakowska, Marcelo Guarido, Daniel Trad, David Emery, and David W. Eaton

ABSTRACT

This chapter presents an example of automated fault detection using Residual Neural Network. In this work, synthetic data set from the FORCE: Seismic fault Mapping competition was used. We present how the popular image segmentation technique can be used to identify faults on the 2D images exported from the 3D synthetic seismic cube.

a)

b)

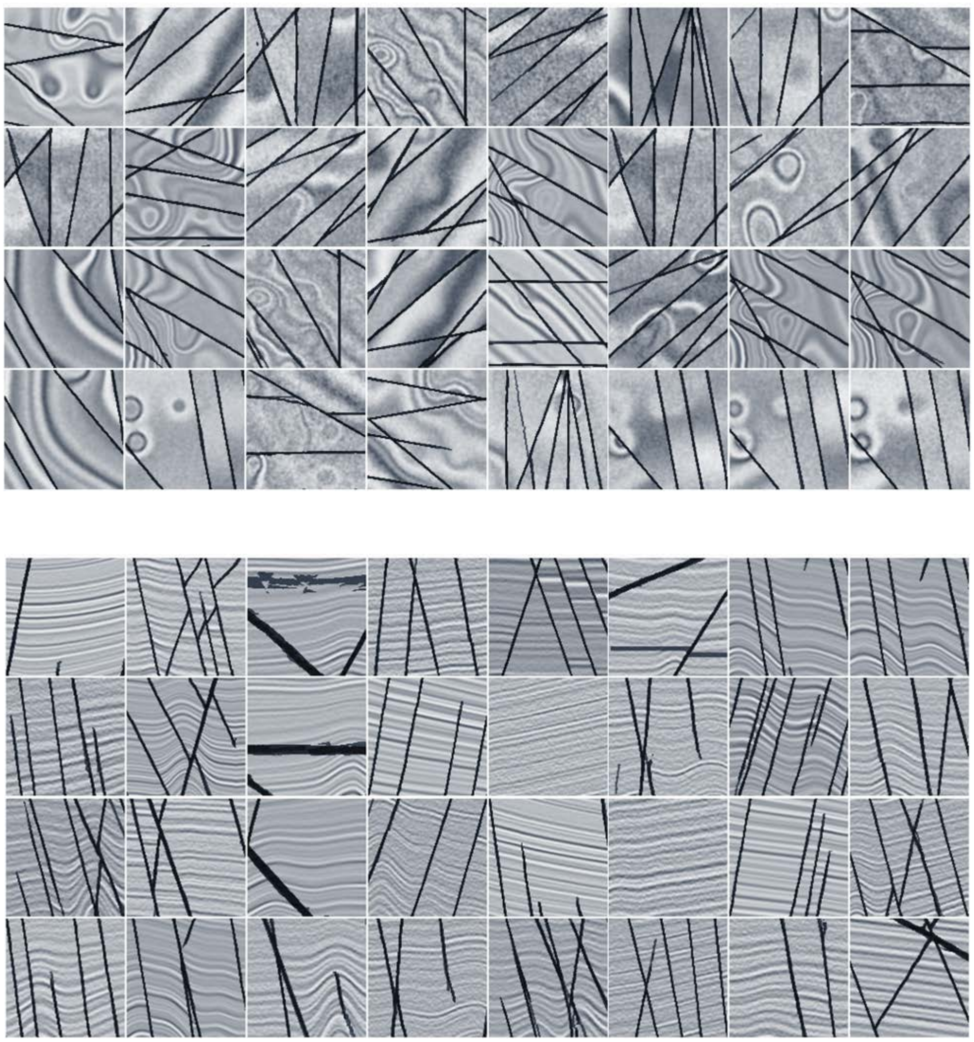

FIG. 1. Predictions obtained using ResNet models trained on inline and crossline (a) and time slice(b) sample images training sets. True fault locations and their predictions are indicated by the bluelines and red lines, respectively.

Fast Sweeping Method with Adaptive Finite Difference Scheme Eikonal Solver

Zhengsheng Yao

ABSTRACT

Whenever finite difference is used, a plane wavefront is implicitly assumed. When waves propagate in inhomogeneous media, the assumption of plane wave front may be invalid. The errors generated in the spots on the bending wave front will propagate to the entire calculation domain, resulting in inaccurate propagation times. In this report, an adaptive finite difference scheme is introduced to improve the accuracy of the Eikonal solver in the Fast Sweeping Method.

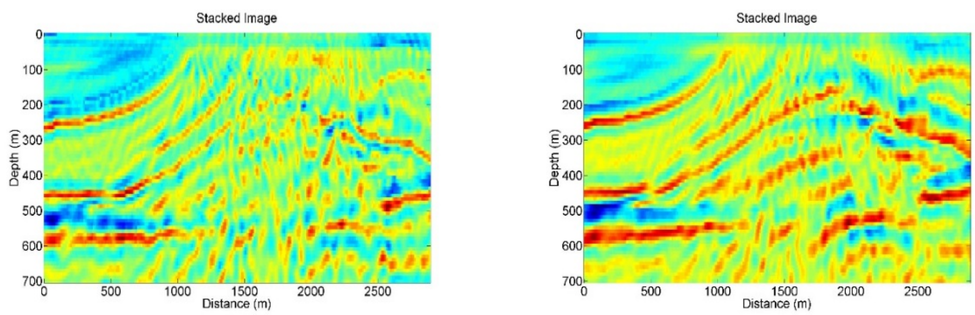

(a) (b)

FIG. 1. Stacked of all single shot migrated results with Fast Sweeping traveltime (a) and (b) is same as (a) but with Modified Fast Sweeping traveltime.

Bayesian inversion for source mechanisms of microearthquakes

Hongliang Zhang and Kris Innanen

ABSTRACT

We develop a Bayesian approach to simultaneously estimate source mechanisms for a set of microearthquakes, in which uncertainties of model parameters are vigorously quantified. To overcome limitations associated with the use of conventional moment-tensor inversion for low-magnitude events, we use a physically based shear-tensile crack model to characterize the seismic source in the inversion. The shear-tensile model consists of four parameters, strike, dip, rake and slope, to represent a superposition of a shear slip along the fault and a crack opening/closure. In the inversion, normalized displacement amplitudes of direct P-wave are used as observations. The Bayesian inference is employed via Markov-chain Monte Carlo (McMC) sampling with parallel tempering, and the principal component diminishing adaption is also used to ensure efficient sampling. In addition, to reduce the number of modes in 2D posterior marginals and avoid one-side distributed marginals for strike, new prior bounds are applied for strike (0° - 180°) and dip (0° - 180°). We apply the Bayesian inversion to a passive seismic dataset acquired during a four-well hydraulic-fracture completion program. For three representative events, uncertainties are quantified through posterior distributions of shear-tensile model parameters. The resulting source mechanisms are highly consistent results with a previous study, indicative of the effectiveness of the proposed algorithm.

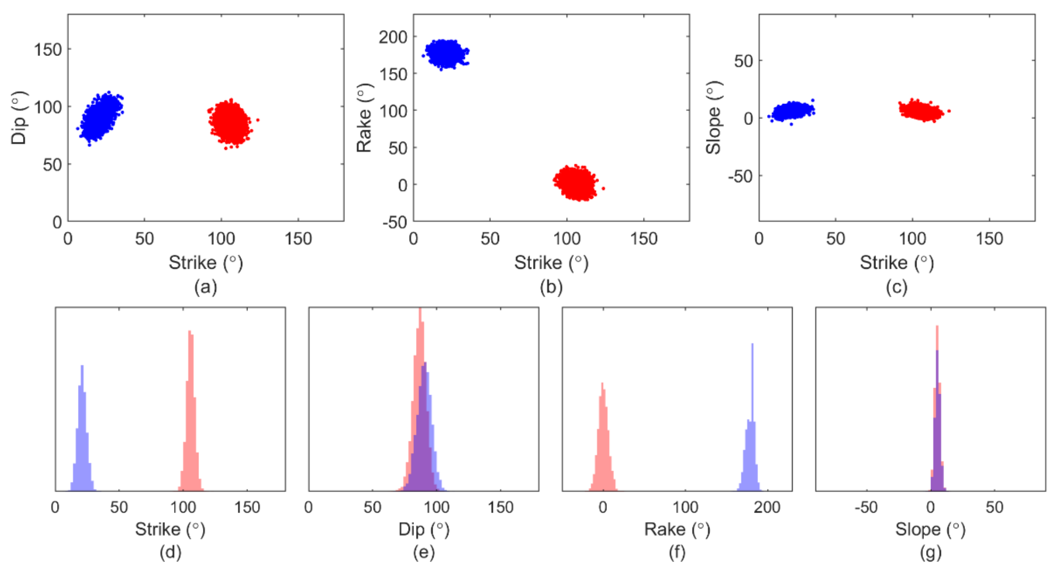

FIG. 1. Source-mechanism inversion results for a representative event. (a-c) Scatter plots between strike and the other three model parameters (dip, rake and slope). (d-g) Posterior marginals of model parameters for shear-tensile source mechanism. Red and blue colors represent the results associated with two nodal planes.

Inversion for shear-tensile focal mechanisms using an unsupervised physics-guided neural network

Hongliang Zhang, Kris Innanen, and David W. Eaton

ABSTRACT

We present a novel physics-guided neural network to estimate shear-tensile focal mechanisms for microearthquakes using displacement amplitudes of direct P-wave. Compared with conventional data-driven fully connected (FC) neural networks, our physics-guided neural network is implemented in an unsupervised fashion and avoids the use of training data, which may be incomplete or unavailable. We incorporate three FC layers and a scaling & shifting layer to estimate shear-tensile focal mechanisms for multiple events. Then, a forward modeling layer is added, which generates synthetic amplitude data based on the source mechanisms emerging from the previous layer. The neural network weights are iteratively updated to minimize the mean squared error between observed and modeled normalized P-wave amplitudes. We apply this machine-learning approach to a set of 530 induced events recorded during hydraulic fracture simulation of Duvernay Shale west of Fox Creek, Alberta, yielding results that are consistent with previously reported source mechanisms for the same dataset. A distinct cluster characterized by more complex mechanisms exhibits relatively large Kagan angles ($10^\circ - 25^\circ$) compared with the previously reported best double-couple solutions, mainly due to model simplification of the shear-tensile focal mechanism. Uncertainty tests demonstrate the robustness of the inversion results and high tolerance of our neural network to errors in event locations, velocity model and P-wave amplitudes. Compared with a single-event grid-search algorithm to estimate shear-tensile focal mechanisms, the proposed neural network approach exhibits significantly higher computational efficiency.

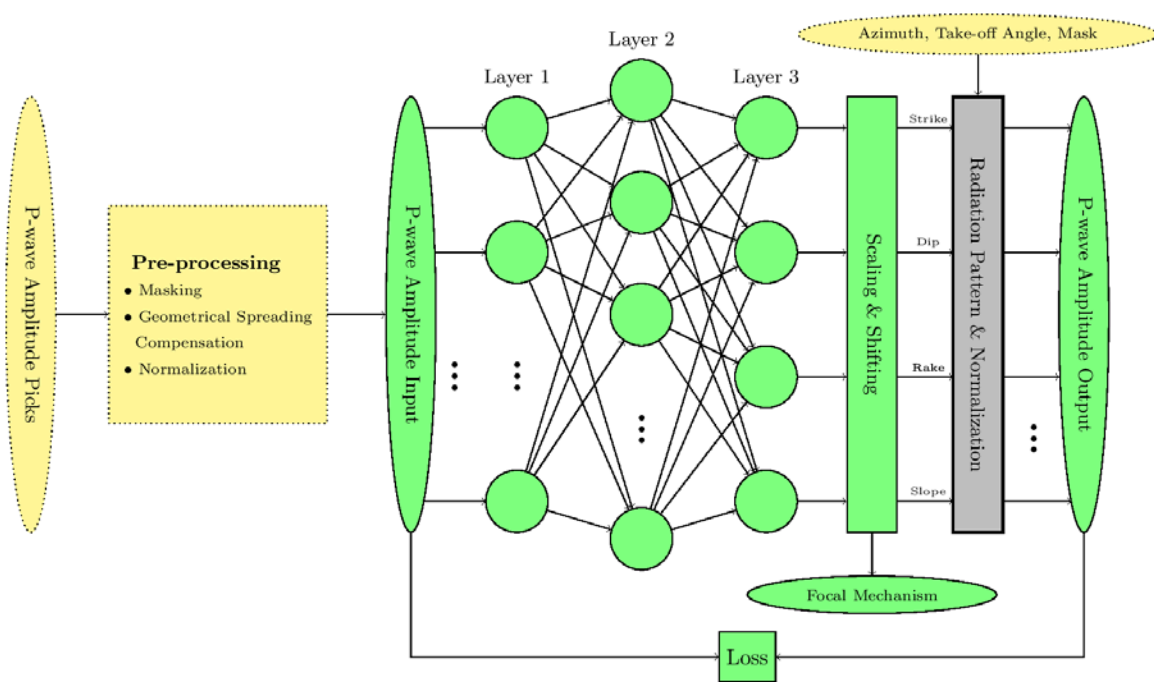

FIG. 1. Architecture of the physics-guided neural network.

Physics-guided neural network for velocity calibration using downhole microseismic data

Hongliang Zhang*, Jubran Akram, and Kris Innanen

ABSTRACT

We present an unsupervised physics-guided neural network to calibrate the simplified 1D layered velocity model based on downhole recordings of perforation shots. This novel neural network incorporates five fully connected layers, a Scaling & Shifting layer as well as a forward modeling layer that generates theoretical travel times of P- and S-waves. Due to the inclusion of the forward modeling layer, our network eliminates the need for labeled data which is unavailable or limited in many cases. In addition, compared with conventional theory-based inversion, the neural network can solve the velocity optimization problem without explicit programming. To yield better constraint for both velocity-calibration and event-location problems, a hybrid objective function is used, which combines misfits of both arrival times and arrival-time difference between P- and S-waves. We apply the proposed neural network to a numerical example with six simulated perforation shots, yielding robust inversion results for layer velocities in the presence of noise. This neural network will be further examined with field data in the future research.

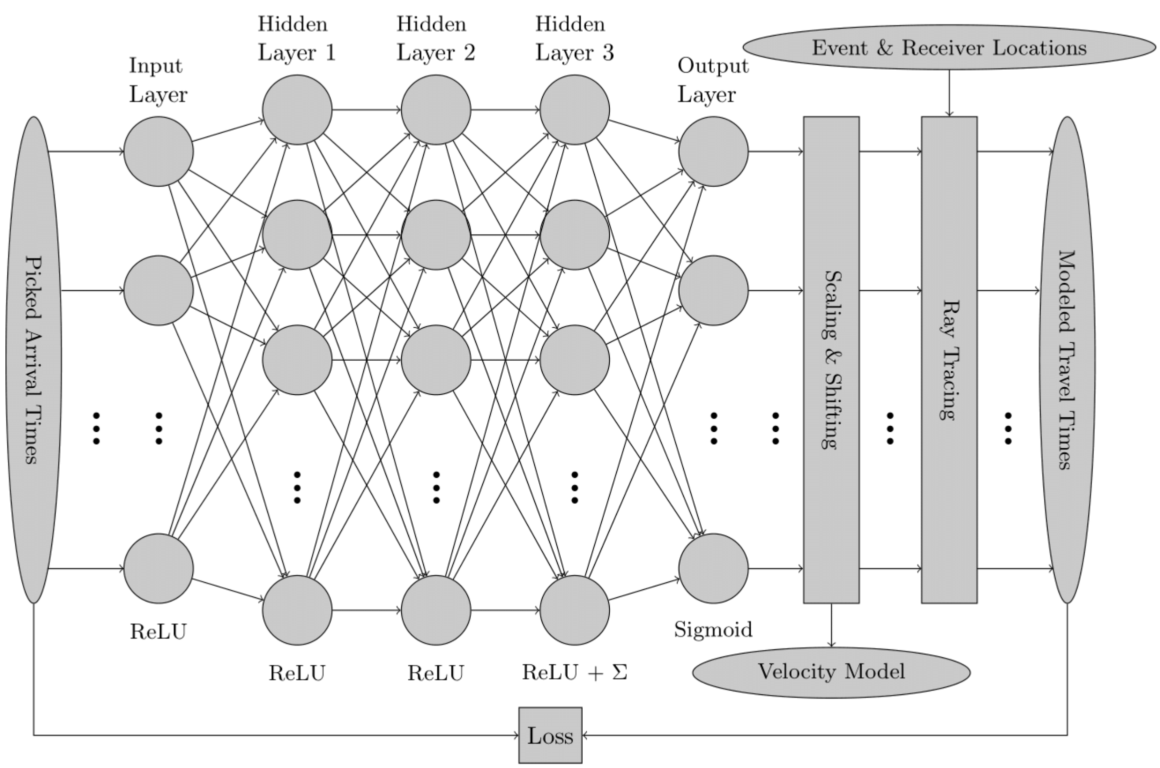

FIG. 1. Architecture of the physics-guided neural network. Activation functions and extra operations are indicated at the bottom of FC layers. Inputs and outputs of the network are represented by ellipses.

Simultaneous Bayesian inversion for effective anisotropic parameters and microseismic event locations: a physical modelling study

Hongliang Zhang, Jan Dettmer, Joe Wong, and Kris Innanen

ABSTRACT

To account for anisotropy caused by the presence of a set of aligned vertical fractures in a finely horizontally layered background medium, we present an inversion procedure to simultaneously estimate microseismic event locations and the parameters of an orthorhombic (ORT) anisotropic medium property model. The procedure employs Bayesian inference via Markov-chain Monte Carlo (McMC) sampling with parallel tempering, and principal component diminishing adaptation, to ensure efficient sampling of the parameter space. This approach provides a nonlinear uncertainty quantification, by approximating the posterior probability density with an ensemble of model-parameter sets for effective anisotropic parameters, microseismic event locations and horizontal locations of perforation shots. The noise standard deviation is also treated as an extra unknown in the inversion. To investigate the effects of model simplification, e.g., neglect of horizontal-layering induced vertical transverse isotropy (VTI), we also consider a simpler, horizontal transverse isotropic (HTI), parametrization. The inversion is carried out for simulated data and data from a seismic physical laboratory model. Results suggest that, for field microseismic data processing, neglect of VTI signal caused by horizontal layering in fractured reservoirs may lead to systematic errors in microseismic event locations. Synthetic experiments further demonstrate that the acquisition geometry significantly impacts the resolution of event origin times, event depths, and effective velocity parameters. In addition, resolving these parameters requires an aperture size which may not be practical for field monitoring. Finally, we demonstrate that precise perforation-shot timing information and the incorporation of a vertical downhole array into the small-aperture surface array both reduce the requirement for large array apertures.

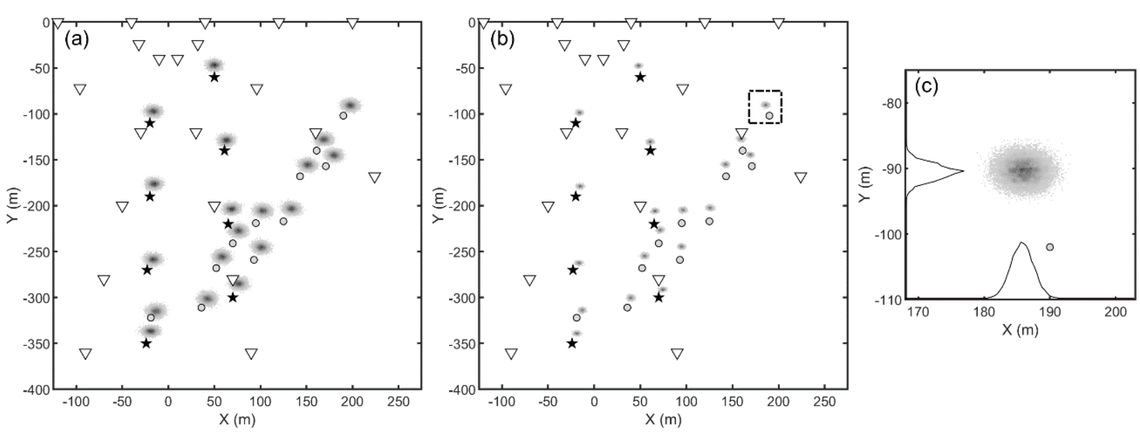

FIG. 1. Epicentre marginal distributions for (a) HTI-model inversion and (b) ORT-model inversion. (c) An enlargement of the red box in (b) with 1D marginals along the X and Y axes.

Recurrent neural network formulation of viscoelastic VTI full waveform inversion

Tianze Zhang*, Jian Sun, Kris Innanen, and Daniel Trad

ABSTRACT

In this study, we use the recurrent neural network (RNN) to achieve viscoelastic VTI full waveform inversion. Eight parameters are simultaneously inverted, which are elastic parameters C_{11}, C_{13} , C_{33}, C_{44}nd their corresponding attenuation parameters QC_{11}, QC_{13} , QC_{33}, QC_{44} The recurrent neural network is built according to the stress velocity VTI viscoelastic wave equation. We also study the acquisition influence on the inversion results. Numerical inversion results show that the combination of cross well data and the surface data can help to better recover the elastic parameters compared with only surface acquisition in which the receivers and shots are all on the surface of the model. To mitigate the cross-talk between the parameters, we also use the high order total variation (TV) to mitigate the cross-talk. The simple structure model and complex part of the overthrust model proves the validation of this method.

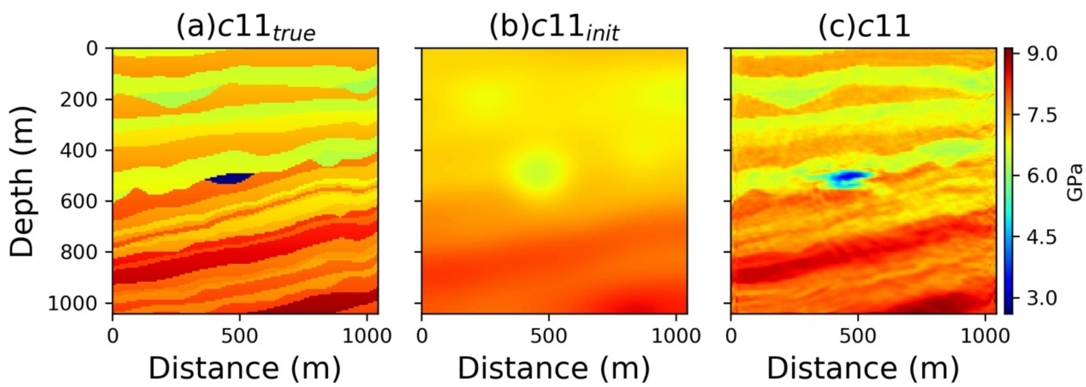

FIG. 1. C_{11} Inversion result. (a) True model. (b) Initial model. (c) Inversion result.

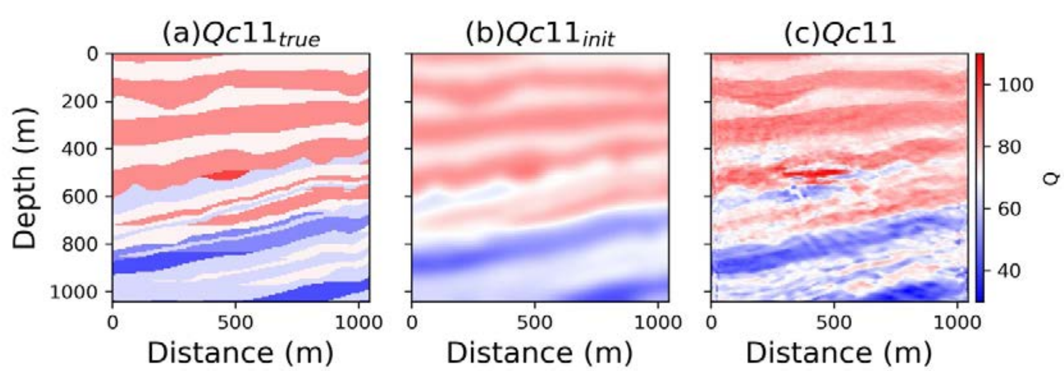

FIG. 2. QC_{11} Inversion result. (a) True model. (b) Initial model. (c) Inversion result.

Theory based machine learning TTI full waveform inversion based on recurrent neural network with the estimating of title angle*.*

Tianze Zhang, Jian Sun, Kris Innanen, and Daniel Trad

ABSTRACT

In this study, we use the recurrent neural network (RNN) to achieve TTI elastic full waveform inversion. The motivation for building such a network is that in real media full waveform inversion, the physics of wave propagation is very complex, and implementing insufficient accurate wave equations in such complex media would lead modeling errors. Most fractures are not vertically but with certain dips and azimuths, thus estimating the title angles along with the elastic parameters are important for accurately invert the parameters. The recurrent neural network (RNN) is a typical type of neural network that is consisted of several RNN cells. In this study, each RNN cell is designed according to the staggered grid stress velocity TTI wave equation and the Voigt stiffness parameters and the title angles are considered as the parameters in this inversion. Based on the forward computational graph, the gradients with respect to each parameter are given by the backpropagation of the forward computational graph. In order to mitigate the cross talk, we use high order total variation (TV) regularization to mitigate the cross-talk in the inversion, Numerical inversions using simple models and complex models prove the validation of this method.

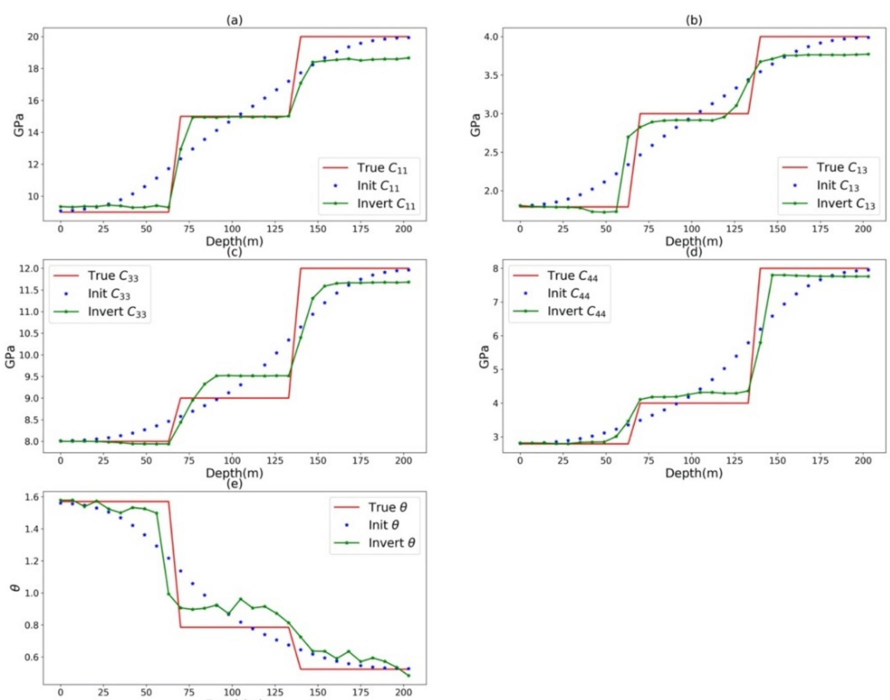

FIG. 1. RNN based TTI Full wave form inversion results. (a) C_{11} inversion result. (b) C_{13} inversion result. (c) C_{33} inversion result. (d) C_{44} inversion result. (e) Title angle inversion result.

Comparison of high performance computing methods for high resolution Radon transform and deblending

Kai Zhuang* and Daniel Trad

ABSTRACT

We implemented both a sparse Radon transform and a least-squares deblending algorithm in C++ using different parallel processing methods. In this paper, we compare three different Application Programming Interfaces (APIs) to perform parallel computing on large datasets, using openMP, openMPI, and CUDA. Our goal is to understand the scaling of different parallel processing methods with our codes and explore the advantages and drawbacks of each API. For our comparison, we will be utilizing the sparse Radon transform and least squares deblending as our focus algorithms that will benefit from parallelization. The sparse Radon transform is easily parallelizable as each Radon frame is calculated independently from each other, which results in greatly reduced calculation time proportional to the resources given. On the other hand, the least-squares deblending algorithm is not efficient when implemented with openMPI as the least-squares gradient requires the application of the blending forward and adjoint operators that involve resorting the data from the entire dataset at each iteration. Therefore, the openMPI implementation of least-squares deblending requires collecting all the data in a single main node at every iteration, thus adding a significant overhead because of data transfer that often outweigh the computing performance gain. By implementing the deblending in CUDA on a single local machine, we then significantly reduce data copying overhead and increase the computational speed of the gradient calculation. Most likely a CUDA implementation with distributed GPUs (GPU clusters) would suffer from similar issues as the openMPI version for inversion but is not tested for this report.

Processor (API)	Radon Transform Time (s)	LS Deblending Time (s)
i7 8750H 6-core (openMP)	3026	1625
i7 9800x 8-core (openMP)	3630	1973
TR 3960x 24-core (openMP)	997	570
GTX 1080 (CUDA)	789	458
RTX 2060 MAX-Q (CUDA)	1273	786
RTX 2060 Super (CUDA)	1010	588
TR 3960x (openMPI)	420	—

Table 1. Table of average runtimes for Radon and Least squares deblending on different machines.